MINISTÉRIO DA EDUCAÇÃO

UNIVERSIDADE FEDERAL DO RIO GRANDE DO SUL

PROGRAMA DE PÓS-GRADUAÇÃO EM ENGENHARIA MECÂNICA

EVALUATION OF THE WSGG AND SLW MODELS FOR THE RADIATIVE TRANSFER PREDICTION IN NON-ISOTHERMAL HOMOGENEOUS AND NON-HOMOGENEOUS MEDIA

por

Roger Mazurek da Silva

Dissertação para obtenção do Título de

Mestre em Engenharia

Porto Alegre, Março de 2019

AVALIAÇÃO DOS MODELOS WSGG E SLW PARA A PREDIÇÃO DA TRANSFERÊNCIA RADIATIVA EM MEIOS NÃO ISOTÉRMICOS HOMOGÊNEOS E NÃO HOMOGÊNEOS

por

Roger Mazurek da Silva
Engenheiro Mecânico

Dissertação submetida ao Corpo Docente do Programa de Pós-Graduação em Engenharia Mecânica, PROMEC, da Escola de Engenharia da Universidade Federal do Rio Grande do Sul, como parte dos requisitos necessários para a obtenção do Título de

Mestre em Engenharia

Área de Concentração: Fenômenos de Transporte

Orientador: Prof. Dr. Francis Henrique Ramos França

Aprovada por:

Prof. Dr. Antônio José da Silva Neto ....PPGMC/UERJ

Prof. Dr. Felipe Roman Centeno ....PROMEC/UFRGS

Prof. Dr. Fernando Marcelo Pereira ....PROMEC/UFRGS

Prof. Dr. Fernando Marcelo Pareira
Coordenador do PROMEC

Porto Alegre, 29 de Março de 2019

AGRADECIMENTOS

Agradeço àqueles amigos e colegas de mestrado que foram companheiros, ato de extrema importância, principalmente ao longo do primeiro ano.

Agradecimento especial ao meus amigos e colegas do Laboratório de Radiação Térmica por toda ajuda, apoio e conhecimento compartilhado durante este período.

Agradeço também ao Prof. Francis França pela orientação e suporte ao longo da pesquisa.

À banca avaliadora por todas as contribuições ao trabalho.

Por fim, agradeço à Coordenação de Aperfeiçoamento de Pessoal de Nível Superior (CAPES) pela bolsa de mestrado.

RESUMO

Em sistemas de combustão tais como fornos para tratamento térmico, geradores de vapor, câmaras de motores e *flares* na indústria de petróleo, a radiação térmica é o mecanismo de transferência de calor predominante devido à presença de gases, fuligem e partículas em altas temperaturas. O cálculo da radiação térmica em gases participantes, tais como H_2O e CO_2, é uma tarefa complexa devido à forte dependência de suas propriedades radiativas com o número de onda. A solução 'exata' linha-por-linha (LBL) é a alternativa mais precisa. No entanto, esta metodologia requer um alto esforço computacional, o qual não é factível para soluções de problemas práticos de engenharia. Modelos Globais tais como a Soma-Ponderada-de-Gases-Cinza (WSGG) e a Soma-Ponderada-de-Gases-Cinza baseada em linhas espectrais (SLW) são alternativas promissoras. O modelo WSGG, apesar de sua formulação relativamente simples, fornece resultados próximos à integração LBL, assim como o modelo SLW, normalmente reconhecido como uma evolução do modelo WSGG. Desse modo, neste trabalho foi realizada a comparação entre a precisão do modelo WSGG e a do SLW. Para tanto, foram obtidas soluções para H_2O, CO_2 e misturas de H_2O/CO_2 em meios não isotérmicos homogêneos e não homogêneos. Para misturas, no modelo WSGG também foi utilizado o método da sobreposição, o qual faz parte da modelagem de misturas do modelo SLW. A abordagem da sobreposição surge como uma alternativa para o tratamento de meios não homogêneos. No entanto, o desafio deste método é a combinação de espécies participantes uma vez que isto requer um aumento no esforço computacional com o aumento do número de componentes. A partir disto, este trabalho propõe e aplica um método da sobreposição reduzido para o modelo WSGG, com o intuito de reduzir o tempo computacional. Além disso, é verificada a consistência desta proposta em chamas difusivas. Os resultados mostram que o modelo WSGG pode levar a resultados tão bons quanto os do modelo SLW dependendo do problema analisado. Ainda, o método da sobreposição reduzido forneceu uma precisão muito próxima à do método da sobreposição padrão.

Palavras-chave: Radiação Térmica; Modelo WSGG; Modelo SLW; LBL; Método da Sobreposição.

ABSTRACT

In combustion systems such as gas furnaces for thermal processing, steam generators, engine chambers and flares in the petroleum industry, the thermal radiation is the dominant heat transfer mechanism due to the presence of participating gases, soot and particulates at high temperatures. The thermal radiation computation in participating gases, such as H_2O and CO_2, is a complex task due to the strong dependence of its radiative properties on the wavenumber. The 'exact' Line-by-Line (LBL) calculation is the most accurate alternative. However, this methodology requires a very expensive computational effort, which is not feasible for practical engineering problems solution. Global Models such as the Weighted-Sum-of-Gray-Gases (WSGG) and the Spectral-Line Weighted-Sum-of-Gray-Gases (SLW) are promising alternatives. The WSGG model, despite its relatively simple formulation, has provided results near to LBL integration as well as the SLW model, often recognized as a WSGG model improvement. Thus, in this work a comparison between the accuracy of the WSGG and SLW models was made. Therefore, were obtained solutions for H_2O, CO_2, and H_2O/CO_2 mixtures in non-isothermal homogeneous and non-homogeneous media. For mixtures, in the WSGG model was also used the superposition method, which makes part of SLW mixture modeling. The superposition approach arises as an alternative to non-homogeneous media treatment. However, the challenge of this approach is the combination of participating gases since it requires increasing computational effort as the components number increase. Thereby, this work proposes and applies a reduced superposition method for the WSGG model aiming for computational time reduction. In addition, the consistency of this proposition is also verified in diffusion flames. The results show that the WSGG model can lead to results as good as those of SLW depending on the problem under analysis. Further, the reduced superposition method provided accuracy very near to that of the standard superposition method.

Keywords: Thermal Radiation; WSGG Model; SLW Model; LBL; Superposition Method.

INDEX

LIST OF FIGURES

LIST OF TABLES

LIST OF ACRONYMS AND ABBREVIATIONS

ADF	Absorption distribution function model
ADFFG	Absorption distribution function with fictitious gases model
ALBDF	Absorption line blackbody distribution function
BM	Band models
CK	Correlated-k methodology
CW	Cumulative wavenumber model
DOM	Discrete ordinates method
EWB	Exponential wide band model
FSK	Full-spectrum k-distribution model
GG	Gray gas model
HITEMP	High temperature molecular spectroscopic database
HITRAN	High resolution transmission molecular spectroscopic database
LBL	Line-by-line integration
MCW	Modified cumulative wavenumber model
NB	Narrow band models
RTE	Radiative transfer equation
RC-SLW	Rank Correlated SLW model
SLW	Spectral line weighted-sum-of-gray-gases model
SLW-1	SLW model for 1 gray gas
SNB	Statistical narrow band
SNBCK	Statistical narrow band model based on CK
WB	Wide band models
WBCK	Wide band model based on CK
WSGG	Weighted-sum-of-gray-gases model

LIST OF SYMBOLS

A	Area [m^2]
c	Speed of the light in the vacuum [m/s]
a_0	Weighting factor of the transparent window
$a_{c,k}$	Weighting factor for the kth gray gas of CO_2
$a_{w,j}$	Weighting factor for the jth gray gas of H_2O
$a_{m,i}$	Weighting factor for the ith gray gas of mixture
a_j	Weighting factor of each gray gas
$b_{j,k}$	Polynomial coefficient of order k^{th} for the jth gray gas
C	Prescribed absorption cross section [cm^2/molecule]
C_1	Fist Planck's constant [W.μm^4/(m^2.sr)]
C_2	Second Planck's constant [μm]
C_η	Spectral absorption cross section [cm^2/molecule]
$\tilde{C}_j$	Supplemental absorption cross section [cm^2/molecule]
D	Diameter of the atoms or molecules [m]
E_b	Total emissive power of the blackbody [W/m^2]
$E_{\eta b}$	Spectral emissive power of the blackbody [W/(m^2.μm)]
E_p	Photon radiative energy transition [J]
E_i	Photon energy associated to level i [J]
E_j	Photon energy associated to level j [J]
F	Absorption line blackbody distribution function
h	Planck's constant [J.s]
I_η	Spectral radiation intensity [W/(m^2.μm.sr)]
$I_{\eta b}$	Blackbody spectral radiation intensity [W/(m^2.μm.sr)]
$I_{\eta,l}^+$	Spectral radiation intensity in the forward direction [W/(m^2.μm.sr)]
$I_{\eta,l}^-$	Spectral radiation intensity in the backward direction [W/(m^2.μm.sr)]
$I_{j,l}^+$	Gray gas radiation intensity in the forward direction [W/(m^2.sr)]
$I_{j,l}^-$	Gray gas radiation intensity in the backward direction [W/(m^2.sr)]
I_b	Blackbody radiation intensity [W/(m^2.sr)]

I_j	Gray gas radiation intensity [W/(m².sr)]
K	Boltzmann's constant [J/K]
L	Distance between the parallel black surfaces [m]
LBL	Line-by-line spectral integration
M	Mass [Kg]
$\max \left| q^{"}_{R,LBL} \right|$	Maximum absolute value of the LBL radiative heat flux [W/(m²)]
$\max \left| \frac{-dq^{"}_{R,LBL}}{dx} \right|$	Maximum absolute value of the LBL radiative heat source [W/(m³)]
n	Temperature dependence coefficient
n_d	Number of directions
n_g	Number of gray gases
N	Gas molar density [molecule/m³]
N_A	Avogadro's number [molecule/mol]
p	Gas pressure [atm]
p_c	Partial pressure of CO_2 [atm]
p_i	Partial pressure of the chemical specie i [atm]
p_w	Partial pressure of H_2O [atm]
P	Sum of partial pressure of the individual species of the gaseous mixture [atm]
P_T	Gas total pressure [atm]
Q	Total intern partition sum
$q^{"}_R$	Radiative heat flux [W/m²]
$-dq^{"}_R/dx$	Radiative heat source [W/m³]
R	Sphere radius [m]
R_u	Gases universal constant [J/mol.K]
r	Local partial pressure ratio
$\overline{r}$	Average partial pressure ratio
S_i	Integrated intensity of the line i [cm⁻¹/molecule.cm⁻²]
S_{ij}	Spectral line intensity where occurs the transition energy between the levels i and j [cm⁻¹/molecule.cm⁻²]
s	Path traveled by radiation [m]
T	Temperature [K]
T_0	Database reference temperature[K]
T_b	Blackbody temperature [K]

T_g	Gas temperature [K]
x	Local position in the domain [m]
x^*	Dimensionless distance

Greek Symbols

α	$(p_w + p_c)T^4$
α_η	Spectral absortance
ε	Total emittance
ε_η	Spectral emittance
δ	Radiative heat flux local deviation [%]
ζ	Radiative heat source local deviation [%]
$\gamma_{air,i}$	Air-broadened half-width $[(\text{cm.atm})^{-1}]$
γ	Spectral line half-width $[(\text{cm.atm})^{-1}]$
γ_i	Line half-width $[(\text{cm.atm})^{-1}]$
$\gamma_{self,i}$	Self-broadened half-width $[(\text{cm.atm})^{-1}]$
λ	Wavelength $[\mu\text{m}]$
μ_l	Cosine diretor of the angle θ_l []
η	Wavenumber $[\text{cm}^{-1}]$
η_i	Line location in the spectrum $[\text{cm}^{-1}]$
σ	Stefan-Boltzmann constant $[\text{W}/(\text{m}^2.\text{K}^4)]$
θ	Angle [rad]
θ_l	Angle formed with direction l [rad]
$\kappa_{p,\eta}$	Spectral pressure absorption coefficient $[\text{atm.m}^{-1}]$
κ_j	Gray gas absorption coefficient $[\text{m}^{-1}]$
$\kappa_{p,j}$	Gray gas pressure absorption coefficient $[\text{atm.m}^{-1}]$
$\Delta\eta$	Spectral interval $[\text{cm}^{-1}]$
$\Delta\eta_i$	Spectral interval i $[\text{cm}^{-1}]$
ϕ	Spatial dependence of the absorption cross section
ψ	Spectral dependence of the absorption cross section
ν_{ij}	Frequency of the photon energy where occurs the transition energy between the levels i and j [Hz]
ν_i	Energy difference between the initial and final state $[\text{cm}^{-1}]$

ω	Solid angle [sr]
ω_l	Factors of the quadrature scheme

Subscripts

avg	Average value
c	Condition referent to carbon dioxide molecule
C	Collision broadening
CO_2	Condition referent to carbon dioxide molecule
D	Doppler broadening
H_2O	Condition referent to water vapor molecule
i	i^{th} gray gas of mixture
j	j^{th} gray gas of H_2O
k	k^{th} gray gas of CO_2
L	Lorentz broadening
loc	Local condition
m	Reference to the mixture
max	Maximum value
η	Spectral condition
ref	Reference condition
w	Condition referent to water vapor molecule

1   INTRODUCTION

Several engineering processes need to operate in elevated temperatures. In combustion systems, for instance, the participating gases temperature may reach above 2500 K. In such conditions, the thermal radiation is the prevalent heat transfer mechanism. Despite this fact, the accurate thermal radiation modeling in combustion systems has being ignored in many cases and treated with simplistic optically thin and gray models [Modest and Haworth, 2016]. The main reason for that may be the difficulty of including accurate radiative transfer calculation in problems already complex. However, simply neglecting the thermal radiation in atmospheric pressure combustion systems may overpredict the temperature up to 200 °C, while using the optically thin or gray radiation models underpredict up to 100 °C [Modest and Haworth, 2016]. Due to this, many works have been developed presenting different methodologies for the thermal radiation modeling in participating gases, as will be described in Chapter 2.

In participating media, when a gas molecule absorbs or emits radiative energy, the vibrational and/or rotational energies of the molecule are raised or lowered. These energy levels lead to many thousands of discrete spectral lines, forming so-called vibration–rotation bands. The photon energy needed to the transition levels are affected by some physical mechanisms which makes the line to be broadened. The main mechanisms are the molecular collisions and the molecular movement (Doppler effect). In a certain spectral location, a spectral line is described by its strength and its line width. These informations are found in conceited databases, such as HITRAN and HITEMP. In these databases is also found the information of how to calculate the resulting absorption coefficient, necessary in the radiative transfer equation (RTE) solution. The absorption coefficient is characterized by thousands of absorption lines having a very erratic behavior with wavenumber, which makes the analysis complicated. Such behavior is illustrated in Figure 1.1, where the spectral absorption coefficient, κ_η, is plotted against the wavenumber η for a small concentration of H_2O ($Y_{H_2O} = 0.01$), at a temperature of 1500 K and total pressure of 1 atm. There are some approaches focused on capturing this spectral dependence of the absorption coefficient. The Line-by-Line (LBL) spectral integration solve the RTE for wavenumber intervals small enough to capture the data exactly. The challenge of this method is the high computational time needed in this calculation. On the

other hand, the gray approach removes the spectral dependence of the absorption coefficient by calculating an average value for all wavenumbers. Despite the less computational effort required, this approach lead to elevated errors.
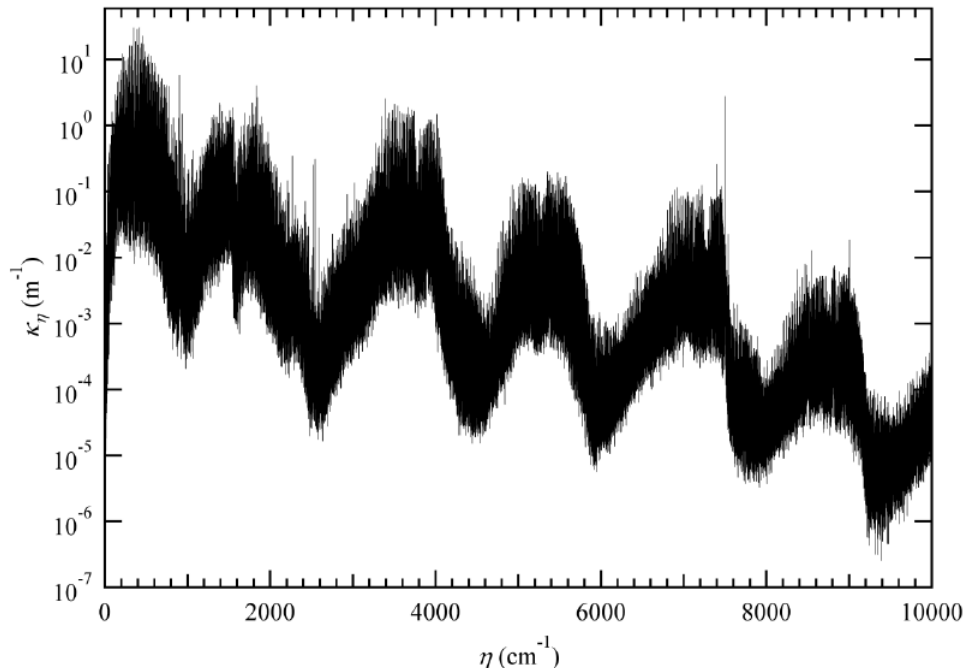
Figure 1.1 – The absorption coefficient, κ_η, as a function of wavenumber η, for H_2O at T = 1500 K, p = 1 atm, Y_{H_2O} = 0.01, and for wavenumbers ranging from 0 to 10,000 cm^{-1} [Pearson, 2013].

Between these two extremists approaches there are the Global Models. These methods propose a integration scheme over the absorption coefficient rather than wavenumber. Thus, it renders fewer than 20 RTE integrations with an accuracy near to that of LBL. The WSGG and the SLW models are among the most promising Global Models. The WSGG model, initially developed by Hottel and Sarofim, 1967, in despite of its simple formulation yields satisfactory accuracy, solving the RTE with a summation over just 3 or 4 gray gases instead of spectral integration. While the SLW model [Denison and Webb, 1993b] was developed in 1990's, and has received several improvements since its initial proposition for the treatment of non-isothermal and/or non-homogeneous media. Therefore, this model is more sophisticated than WSGG, utilizing 10 or even 20 gray gases. For participating gases mixtures, the limitation of WSGG is that its correlations are given for constant partial pressure ratio between the species in non-homogeneous media. This problem is removed with the superposition method [Cassol et al., 2014], based

on individual gases correlations, which also makes part of SLW mixture formulation. Even though the SLW model be considered an improvement of WSGG, the difference between the solutions of these models may not be substantial depending on the case under analysis. Furthermore, one important issue of the superposition method is that the number of times that the RTE must be solved increases significantly as the species number also increases.

1.1   Objectives of the study

The general objective of this study is to apply the WSGG and SLW models for radiative transfer prediction in participating media. From that, the following specific objectives can be defined:

- Compute the thermal radiation in non-isothermal homogeneous and non-homogeneous media using both WSGG and SLW models. The results will be compared against LBL benchmark solutions in order to verify the accuracy of these models. The problems will be solved for H_2O and CO_2 individually, and for H_2O/CO_2 mixtures, considering different profiles of temperature and molar concentration of the species. For mixtures, the superposition method will be applied to the WSGG to do an adequate comparison with SLW solution;

- Proposition and application of a reduced superposition method in the WSGG model, aiming at a computational time reduction. In the superposition method the number of times that the RTE must be solved is expressively raised as the participating species number increases. In combustion systems where the radiative transfer calculation is only part of a complex problem, which includes chemical kinetic and turbulence modeling, any computational time reduction is very important.

- Verify the consistency of the reduced superposition method in diffusion flames.

1.2   Organization of the Work

Chapter 2 will present a literature review for the main methods developed for spectral integration of the RTE. Chapter 3 will provide a description of the thermal radiation fundamental relevant for this work, focusing on those important for the definition

and solution of the RTE. The detailed description of the spectral integration methods used in this study will be shown in Chapter 4. A new approach for the superposition method applied to the WSGG model will be described in Chapter 5. This proposition aims at the computational effort reduction. Chapter 6 will show the application of WSGG and SLW models for the radiative transfer prediction in participating media. The validation of the new approach for the superposition method will also be presented. Chapter 7 will give conclusions and perspectives for future works. Some results of the radiative transfer from participating gases are also included in the appendices.

2 BIBLIOGRAPHY SURVEY

At high temperatures, thermal radiation can significantly affect the heat transfer characteristics in media involving combustion products. However, the prediction of the radiative heat transfer is still a challenging task due to the strong spectral variation of the absorption coefficient of gases with the wavenumber. The line-by-line (LBL) integration can provide a solution with high level of accuracy for this kind of problem, but, due to the many thousands of absorption lines present in gases spectra, LBL calculations are computationally expensive [Denison and Webb, 1995a], which often makes the solution impracticable. As an alternative to overcome this difficulty, some gas models have been developed.

2.1 Radiative Transfer Modeling

The Gray Gas (GG) model is the simplest method to predict the radiative heat transfer in combustion systems and atmosphere processes. This approach consists in considering the radiative properties, as the absorption coefficient, to be independent of the wavenumber. Despite this unrealistic approximation for gases, the GG model is yet used in modern engineering problem solution [Xue et al., 2001; Al-Omari, 2006; Narayanan and Trouvé, 2009; Crnomarkovic et al., 2013] since it is of quite simple implementation if compared to other spectral models. Besides that, studies have shown that the GG model leads to pool accuracy when the media is dominated by participating gases, and becomes more accurate as the soot concentration increases [Mossi et al., 2012; Cassol et al., 2015].

When there is a non-gray media, the Radiative Transfer Equation (RTE) solution can be found by three groups of methods : Band Models, Global Models, and Line-by-line (LBL) method. In the LBL method the RTE integration is performed over the entire radiation spectrum taking into account the contribution of each spectral line. This procedure requires about 10^6 resolution of the RTE [Modest, 2003b], involving a lot of computational effort that is not feasible for practical applications [Demarco, 2012]. However, this method is useful for providing benchmark solutions, and it has been used in a few works which solve two-dimensional problems [Mazumder and Modest, 2002; Modest and Zhang, 2002; Zhang and Modest, 2002, 2003; Pal and Modest, 2010; Chu et al., 2012; Consalvi and Liu, 2014; Centeno et al., 2016].

The Band Models (BM) consist of dividing the radiation spectrum into spectral intervals in which the radiative properties are considered constant, and are classified in Narrow Band (NB) and Wide Band (WB) models. With the NB models is possible to replace the actual absorption coefficient behavior by average values over narrow wavenumber intervals. In the WB models the integration is realized over larger wavenumber intervals considering that blackbody intensities do not vary substantially across bands. Despite being less computationally expansive, WB models does not achieve the same level of accuracy as the NB models [Modest, 2003b]. The disadvantaged of Band Models is the difficulty to be used in an arbitrary solution technique of the RTE, as the discrete ordinates method (DOM), since they yield gas transmissivity (NB model) or absorptance (WB model) instead of absorption coefficient. One alternative to overcome such issue is to implement the band models through the correlated-k (CK) methodology to acquire absorption coefficients [Liu and Smallwood, 2004]. In the BM are included the Statistical Narrow Band (SNB) [Goody, 1952], SNB based on CK (SNBCK) [Liu and Smallwood, 2004], Exponential Wide Band (EWB) [Edwards and Balakrishnan, 1973], and Wide Band based on CK (WBCK) [Çayan and Selçuk, 2007] models. In the absence of the LBL calculation due to its excessive computing time, the SNB model is used as benchmark solution for gas radiation transfer problems [Bressloff, 1999; Goutiere et al., 2000; Coelho, 2002; Demarco et al., 2011].

Global Models propose an integration scheme over the absorption coefficient rather than wavenumber. This engineering approach typically renders fewer than 20 integrations of the RTE for prediction of total quantities such as radiative flux and net flux divergence, while the LBL method requires millions of times, which is prohibitively expensive. One popular Global Model is the Weighted-Sum-of-Gray-Gases (WSGG), initially developed by Hottel and Sarofim, 1967. The approach of this model replaces the integration of spectral properties with a summation over a small set of gray gases (often three or four) plus the spectral window to simulate the properties of the non-gray gas. These gray gases replace the real spectrum behavior, and it is considered that each of them has uniform absorption coefficient and a temperature coefficient which correspond to the fraction of blackbody energy emitted in the spectral region that represent each gray gas location. The coefficients of such gray gases in the WSGG model can be determined from fitting data of total emittance computed, for instance, from LBL calculations of high-resolution

spectral absorption coefficient. Smith et al., 1982 present these coefficients obtained from interpolation of experimental data. However, such coefficients are limited to H_2O/CO_2 mixture with uniform concentration, and they can generate elevated errors in the solution when compared to problems that use modern spectral data [Maurente et al., 2008; Mossi et al., 2012]. Despite this, such correlations are still used in contemporary studies [Trivic, 2014] and in commercial software of computational fluid dynamics as the ANSYS/Fluent [Fluent, 2018].

Nonetheless, few studies have focused on generate new WSGG correlations for H_2O/CO_2 mixtures [Kangwanpongpan et al., 2012; Dorigon et al., 2013], and for individual species such as carbon monoxide (CO) [Ziemniczak et al., 2015; Brittes et al., 2017]. Although the correlations are, often, obtained for a wide temperature range, the partial pressure ratio between the species is maintained constant. For this reason, Johansson et al., 2011 proposed a WSGG modification to consider partial pressure ratio between H_2O and CO_2 varying from 0.125 to 2.

Besides having a relatively simple formulation, the WSGG model does not require the knowledge of spectral data banks, and was demonstrated by Modest, 1991 that this model can be applied with arbitrary RTE methods of solution since the media is non-scattering with a black-walled enclosure. However, Modest and Zhang, 2000 showed that these restrictions can be disregarded. Thereby, the WSGG methodology is adopted in several problems solution as those of oxi-combustion [Becher et al., 2012; Rajhi et al., 2014; Garten et al., 2015], one-dimensional [Dorigon et al., 2013; Fonseca and França, 2015; Ziemniczak et al., 2015; Brittes et al., 2017; Fonseca et al., 2018], two-dimensional [Silva et al., 2007; Centeno et al., 2013; Crnomarkovic et al., 2013; Centeno et al., 2014; Garten et al., 2015; Centeno et al., 2016], and three-dimensional problems [Coelho, 2002; Trivic, 2014; Bhuiyan and Naser, 2015; G.Clements et al., 2015; Zhang et al., 2015; Fraga et al., 2017], as well as in the Turbulence-Radiation-Iterations (TRI) modeling [Silva et al., 2007; Krishnamoorthy, 2010; Coelho, 2012; Centeno et al., 2014; Shiehnejadhesar et al., 2014; Centeno et al., 2016; Fraga et al., 2017].

Although the standard WSGG model be widely used in engineering computations of radiative heat transfer in participating media, it is limited to the gas mixtures where the mole ratio between the species is constant. As a way to eliminate this restriction, Cassol et al., 2014 applied the superposition methodology [Smith et al., 1987] to the WSGG

model for H_2O, CO_2, and soot mixtures . This approach consists on first setting up independent correlations for each species, which are then superposed to form the WSGG correlations for the mixture. Thus, it is possible to compute the radiative heat transfer in mixtures with arbitrary concentrations, allowing for local variations in the mole ratios, and the inclusion of any number of participating species.

Based on these advantages, a few works have been done on which is used the WSGG model with the superposition approach. Centeno et al., 2016 studied the effect of soot on the radiative heat transfer in a turbulent, non-premixed methane–air flame inside a combustion chamber. It was shown that the superposition of the correlations of H_2O/CO_2 mixtures and soot in the WSGG model provides results of good agreement with the LBL benchmark solution. The TRI phenomena in the context of a non-reactive 3-D channel flow of a high temperature homogeneous participating gas was successfully modeled using the WSGG model with the superposition method [Fraga et al., 2017]. Another recent paper also explored this approaching in the computation of the radiative heat transfer in an axisymmetric gas system composed of H_2O, CO_2, and soot [Centeno et al., 2018]. This study showed that the superposition method between the coefficients of the individual species led to the least accurate results, while the WSGG model considering the superposition between the H_2O/CO_2 mixture and soot coefficients proved the best alternative for both moderate and high concentrations of soot.

Another prominent Global Model that also uses the superposition method is the Spectral-Line Weighted-Sum-of-Gray-Gases (SLW) first introduced by Denison and Webb, 1993b. The fundamental component of this model is the absorption line blackbody distribution function (ALBDF). For a given gas temperature, the ALBDF is the fraction of the blackbody energy in the portions of the spectrum where the spectral absorption cross-section of the gas is less than a prescribed value. The ALBDF is used for temperature coefficient calculation of each gray gas in the RTE solution. This function is generated with a detailed spectral data available in databases as the HITRAN and HITEMP. Since this procedure spend much computational time, empirical correlations for ALBDF of H_2O [Denison and Webb, 1993a], and CO_2 [Denison and Webb, 1995a] were developed in a form of a hyperbolic tangent function. Radiative transfer model parameters for carbon monoxide (CO) were also proposed [Solovjov and Webb, 1998].

New ALBDF correlations for H_2O, CO_2, and CO based on the updated HITEMP

2010 database were generated by Pearson et al., 2014b. In this study were considered variable temperature, mole fraction, and total pressure. The LBL ALBDF was also computed and tabulated for discrete temperature, mole fractions, and total pressure ranging from 300 K to 3000 K, 0 to 1, and 0.1 atm to 50 atm, respectively. The correlation showed an accuracy that is quite adequate for engineering applications but considerably less accurate than the tabulated ALBDF. In spite of having an initial computational cost to read the data, the inaccuracy of the tabulated ALBDF is only caused by interpolations used to obtain its values at specified conditions [Pearson, 2013]. The effect of total pressure on the ALBDF and radiative transfer in H_2O, CO_2, and CO was also recently analyzed [Pearson et al., 2014a].

In the non-isothermal and/or non-homogeneous media treatment, the Liebnitz rule leads to appearance of additional terms in the spectral integration of the RTE. This renders the analysis complicated, especially for multidimensional media, and alter the RTE standard form of solution [Denison and Webb, 1993b]. As an alternative, two approaches have been adopted to treat these terms in the SLW model. The first is the reference approach which allows the Liebnitz terms to be canceled using a reference state [Denison and Webb, 1995c]. Since this method require the implicit calculation of a set of parameters, the computational time can be expensive. The second approach suggests the simple neglect of these terms from the RTE [Solovjov and Webb, 2000], however this procedure can yield significant errors and less accuracy if compared with the reference approach [Pearson, 2013].

For the case of gas mixtures, some approaches have also been proposed. The double integration and the convolution approaches were applied to radiative heat transfer calculation in H_2O/CO_2 mixtures [Denison and Webb, 1995b]. The extension to multi-component gas mixtures with the superposition and multiplication approaches, along with a hybrid of the two, were also introduced [Solovjov and Webb, 2000]. The soot inclusion as a gas in the multiplication method was studied by Solovjov and Webb, 2001. A new model, named SLW-1, was introduced by Solovjov et al., 2011a for individual species and latter for non-isothermal non-homogeneous gaseous mixture with soot [Solovjov et al., 2011b]. In this methodology, the problem is reduced to the simplest case of the SLW model with a single gray gas and a clear gas, providing the accuracy near that of the SLW method with a large number of gray gases.

As the SLW model, the Full-Spectrum k-Distribution model (FSK) can be viewed as an improvement of the WSGG [Demarco, 2012]. In the FSK model, The RTE solution is given by a integration over a distribution function virtually identical to the ALBDF developed by Denison and Webb, 1993a [Pearson, 2013]. Proposed by Modest e Zhang [Modest and Zhang, 2000, 2002], th FSK model has been implemented with both correlated-k and scaled-k distribution methods. These methods are an approach developed for non-homogeneous media treatment, while for homogeneous medium (i.e., the absorption coefficient is not a function of spatial coordinate) with narrow spectral intervals (i.e., range over which the Planck's function is nearly constant) the absorption coefficient may be reordered into a monotonic k-distribution, which produces exact results in a small fraction of the time required for LBL calculations [Modest, 2003a; Modest and Riazzi, 2005]. The correlated-k method is based on the fact that inside a spectral band, which is sufficiently narrow to assume a constant Planck's function, the precise position of a spectral line is not important for spectral integration. In the scaled-k distribution the spectral and spatial dependence of the absorption coefficient are separately treated.

Thereby, the FSK model has been applied to radiative transfer prediction in non-homogeneous gas mixtures [Modest and Zhang, 2002; Wang and Modest, 2005; Pal et al., 2008], nonhomogeneous gas-soot mixtures [Pal and Modest, 2010], and in multidimensional media [Modest and Zhang, 2002; Mazumder and Modest, 2002; Modest and Riazzi, 2005; Ma et al., 2014]. Its relation with the SLW model is discussed by Solovjov and Webb, 2009, showing that these two models are equivalent when the number of gray gases tends to infinity.

The concept of correlated spectrum [Modest, 2013], initially refereed as ideal spectrum by Denison and Webb, 1995c, has been recently applied to the SLW model. It establishes a relation between absorption coefficient at an arbitrary state and the absorption coefficient at some chosen reference state. An extension of this approach is the novel Rank Correlated SLW (RC-SLW) model of gas radiation in non-uniform media developed by Solovjov et al., 2017. The approach of this model is remarkable by the fact that it does not require the specification of a reference gas thermodynamic state, and it preserves the emission term in the spectrally integrated RTE. Studies have shown that the RC-SLW model provides more accurate results than the original SLW model based on a reference state [Solovjov et al., 2017; Andre et al., 2017]. The range of the ALBDF database has

also been studied for the accurate radiative prediction in this model [Webb et al., 2018], and it is shown that good accuracy may be achieved by using the RC-SLW model with as few as 3–5 gray gases. A more general assumption of rank correlated spectrum is given by the scaled spectrum assumption used for the Scaled SLW model proposition [Solovjov et al., 2017, 2018].

The Absorption Distribution Function (ADF) model is another distinguished Global Model. Developed in the 1990's [Rivière et al., 1996], the ADF model is quite similar to the SLW [Modest and Zhang, 2002; Pierrot et al., 1999a], differing only in the calculation of the gray gas temperature coefficients. This method was extended to non-isothermal media by means of the absorption distribution function model proposition with fictitious gases (ADFFG) [Pierrot et al., 1999a]. For a non-isothermal medium, it was shown that the ADF and SLW models lead to resemblant accuracy, and the ADFFG model proved to be more accurate than these latest models, but requires greater computing time [Pierrot et al., 1999b].

Instead of the full-spectrum correlation techniques traditionally used (i.e., ideal behavior of the spectrum), a new model, called Cumulative Wavenumber (CW), proposes a local-spectrum correlation for the solution of the RTE in non-uniform media at high temperature [Solovjov and Webb, 2002]. By means of the cumulative wavenumber (a new gas absorption spectral distribution function), this model introduces a local correction factor to consider the spatial variation of species concentration and gas temperature calculated independently in each fixed spectral interval. Thus, there is no Leibniz terms production in the RTE solution. This approach is an attempt to replace the scale approximation. Despite providing good results for radiative heat transfer calculation, the CW model formulation do not satisfy the energy balance, presenting considerable error in the radiative heat flux prediction, as shown by Galarça et al., 2011. For this reason, the Modified CW (MCW) model was developed [Galarça et al., 2011] to satisfy the energy balance while keeping the same value of the radiative volumetric heat source. The MCW model demonstrated to be more accurate than CW, however, spends much computational time, that can not be practical to be coupled with combustion problems.

Some CW model applications for radiative transfer calculation in participating gases have been accomplished. This model has been extended to non-uniform gas mixtures with soot [Solovjov and Webb, 2005], and to account for non-gray walls [Solovjov et al.,

2013]. A fast approach was applied to reduce the computational cost [Salinas, 2008], and two-dimensional problems were also studied [Ismail and Salinas, 2005; Salinas, 2008]. The multilayer approach was used to modeling non-isothermal gaseous medium by SLW and CW models [Solovjov and Webb, 2008]. In this methodology the non-isothermal media is modeled by a system of isotherm layers, and, thus, the intervals of spectral integration do not vary with spatial coordinate within the layers. Hence, the Leibnitz terms are eliminated in the spectral integration of the RTE, but the spectral integration in the interface between the layers requires special consideration for the consistency of the model radiation intensities in different layers.

As demonstrated in the literature, even more simple gas models such as the WSGG can provide satisfactory results for the radiative transfer prediction in combustion gases. The superposition method applied to the WSGG has shown to be a good alternative for radiative transfer computation in non-homogeneous mixtures, and recently has been applied in some works [Centeno et al., 2016; Fraga et al., 2017; Centeno et al., 2018]. Even though in these works have been used the WSGG model based on the superposition method, it was carried out for complex and multidimensional problems. However, the application of the superposition approach in the WSGG model needs to be better understood in fundamental problems. Since this method is also used in the SLW mixture modeling, the solution of this model can be adequately compared with that of the WSGG. In this work, the WSGG and SLW model solutions are investigated in one-dimensional problems, for H_2O, CO_2, and H_2O/CO_2 mixture gas layers, exploring different profiles of temperature and concentration of the participating species. Moreover, the main challenge in the radiative transfer prediction using the superposition method is the combination of participating gases since it requires increasing computational effort as the components number increase. Thereby, it is fundamental to develop a methodology capable of reduce the computational time in such cases. Performing this study with the WSGG model is another objective of this work.

2.2 Summary

The LBL method provides the higher level of accuracy in radiative transfer predictions in participating media. However, it spends a computational time that can be prohibitively high for practical applications. The Band Models become a restrictive alter-

native since it provides the gas transmissivity or the absorptance, which can not be used with arbitrary RTE solution methods. Such difficulty is removed by the Global Models that yield the absorption coefficient. The WSGG is the simplest Global Model, but can provide satisfactory results for the radiative transfer prediction in combustion gases. The SLW model has received several improvements in the last years. The formulation of this model is based on the superposition method, which has also been recently explored in the WSGG model. The superposition method furnishes some new possibilities to the WSGG model, such as the treatment of mixtures with arbitrary concentrations, local variable mole ratios, and with any number of participating species. However, the WSGG model, employing this approach, need to be better investigated in fundamental problems, comparing the solution with that of SLW model, and searching for ways to reduce the computational effort which significantly increases as the number of participating gases also increases. Such investigations are made in this work.

3 FUNDAMENTALS OF THERMAL RADIATION

The thermal radiation propagation can be described by two viewpoints: quantum mechanics and classical electromagnetic wave theory. With the first, the thermal radiation energy is described as quanta of particles, or photons. A statistical mechanism is used to approximate their propagation in a medium and interaction with matter. Thermal radiation also can be viewed as consisting of electromagnetic waves. In general, radiative properties of liquids and solids are more easily predicted using electromagnetic wave theory, while radiative properties of gases are more conveniently obtained from quantum mechanics [Modest, 2013]. For practical engineering applications, the thermal radiation regions of interest is in the wavelength range of 0.1 μm to 100 μm, including the ultraviolet and visible ($\lambda = 0.1$ to 0.7 μm), near-infrared ($\lambda = 0.7$ to 10 μm), and far-infrared ($\lambda = 10$ to 100 μm) spectra [Howell et al., 2010].

Unlike conduction and convection, the thermal radiation can be transferred over a long distance without interacting with a medium. Because of this, it is of great importance in vacuum, space applications, and combustion processes. Another distinguishing feature which differ these three heat transfer mechanisms is that conductive and convective heat transfer rates are linearly proportional to temperature differences, and, on the other hand, radiative heat transfer rates are generally proportional to differences in temperature to the fourth power. Therefore, thermal radiation becomes more important than conduction and convection in high temperatures, as in combustion applications (fires, furnaces, rocket nozzles, engines, etc.). Since the modern technologies have as priority higher efficiencies, it will require higher temperatures, making thermal radiation even more important [Modest, 2013]. This chapter will show same fundamentals concepts of thermal radiation, which are important to the development of this work.

3.1 Blackbody

The concept of a blackbody is basic to the study of radiative transfer. The black-body is called an ideal body, and it allows all the incident radiation pass into it (no reflected energy) and internally absorbs all the incident radiation (no energy transmitted through the body). This behavior happens for all wavenumbers and for all angles of incidence [Howell and Siegel, 2002]. Hence, the blackbody is a perfect absorber for all

incident radiation, and it serves as a standard with which real absorbers can be compared to. The blackbody also emits the maximum total amount of energy at each wavenumber and at each direction.

Considering a blackbody at temperature T enveloped by a hemispherical detector that captures thermal radiation with a wavenumber η within a wavenumber interval $d\eta$, as shown in Figure 3.1, the hemispherical spectral emissive power, $E_{\eta b}$, in W/(m^2.μm), is the energy emitted by a black surface per unit time per unit area and per unit wavenumber interval around η. This quantity is given by Planck's spectral distribution of emissive power:

$$E_{\eta b}(\eta, T) = \frac{2C_1 \pi \eta^3}{e^{C_2 \eta / T} - 1} \tag{3.1}$$

where, C_1 and C_2 are constants for which the values are, respectively, 0.59552137×10^8 W.μm^4/(m^2.sr) and $1.4387752 \times 10^4 \mu$m; T (K) is the temperature, and η (cm^{-1}) is the wavenumber.

Integrating Equation 3.1 over all the spectrum, results the mathematic expression called Stefan-Boltzmann law:

$$E_b = \sigma T^4 \tag{3.2}$$

in which E_b is the emitted blackbody energy flux (W/m^2), and $\sigma = 5.670400 \times 10^{-8}$ W/(m^2.K^4) is the Stefan-Boltzmann constant. Through this expression it is possible to calculate the radiation emission quantity in all directions and all wavenumbers only knowing the blackbody temperature.
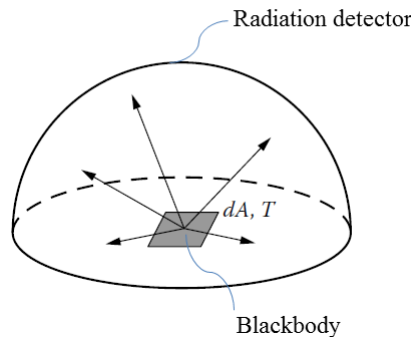
Figure 3.1 – Blackbody enveloped by a hemispherical radiation detector [adapted from Howell et al., 2010].

3.2   Thermal Radiation Intensity

The intensity is an important quantity for studying radiative transfer in absorbing, emitting, and scattering media due to certain invariance properties. The emitted spectral intensity is defined as the energy emitted per unit time per unit small wavenumber interval around the wavenumber η, per unit elemental projected surface area normal to the direction and into a unit elemental solid angle centered around the direction given by the polar angle θ. For an elemental area dA within participating media shown in Fig. 3.2, the spectral radiation intensity is:

$$I_\eta = \frac{d^3 Q_R}{dA \cos \theta d\omega d\eta} \tag{3.3}$$

where I_η is expressed in $W/(m^2.\mu m.sr)$. For a non-attenuating and non-emitting medium with constant properties, the intensity in a given direction is independent of position along that direction.
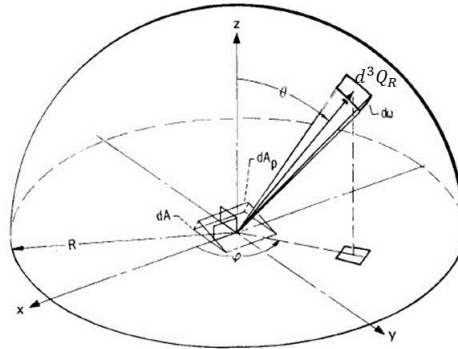
Figure 3.2 – Spectral intensity emitted by an elemental area dA [adapted from Siegel and Howell, 1993].

Another feature is that the radiation emitted by the blackbody depends on the wavenumber and on the temperature, and it is independent of direction, being, thus, a diffuse emitter [Howell and Siegel, 2002]. The blackbody radiation intensity has its relation with the spectral emissive power according to:

$$I_{\eta b}(\eta, T) = \frac{E_{\eta b}}{\pi} = \frac{2C_1 \eta^3}{e^{C_2 \eta / T} - 1} \tag{3.4}$$

in which $I_{\eta b}$ is the spectral radiation intensity emitted by blackbody, in $W/(m^2.\mu m.sr)$.

For a participating media, such as a mixture of water vapor and carbon dioxide,

the radiative intensity is a function of the distance along a path. It happens due to absorption, emission and the scattering effects of the medium.

3.2.1 Attenuation of Intensity by Absorption

The spectral radiation of intensity I_η incident normally on a volume element of thickness ds which absorbs radiation, can be analyzed in Fig. 3.3. As radiation passes through ds, its intensity is reduced by absorption. This change in the intensity is proportional to the magnitude of the local intensity, as has been found experimentally [Howell and Siegel, 2002]. If the media is non-scattering, the coefficient of proportionality will be the absorption coefficient (κ_η). Thus, the decrease is:

$$dI_\eta = -\kappa_\eta I_\eta ds \tag{3.5}$$
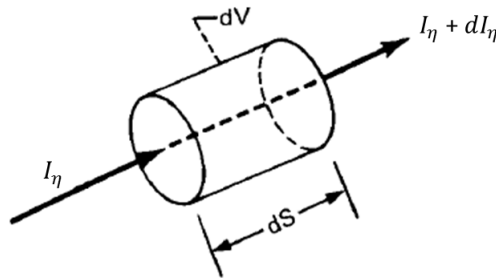
Figure 3.3 – Intensity incident normally on absorbing volume element dV [adapted from Siegel and Howell, 1993)].

3.2.2 The Increase of Intensity by Emission

For emission of energy within the medium, it is considered an elemental volume dV (Figure. 3.4) at the center of a large black hollow sphere of radius R at uniform temperature T. The elemental volume dV limits a participating medium with absorption coefficient κ_η, and the space between dV and the sphere is filled with non-participating material. The spectral intensity incident at the elemental area dA_s, from element dA is $I_\eta(s = 0) = I_{\eta b}(\eta, T)$, where $I_{\eta b}$ is the blackbody spectral intensity. Because of the

absorption, the change of the intensity in dV is [Howell and Siegel, 2002]:

$$- I_\eta(0)\kappa_\eta ds = -I_{\eta b}(\eta, T)\kappa_\eta ds \qquad (3.6)$$

The energy absorbed by the differential volume $dSdA_s$ is $I_{\eta b}(\eta, T)\kappa_\eta dSdA_s d_\eta d\omega$, where $d\omega = dA/R^2$ and dA_s is the projected area normal to $I_\eta(0)$. The energy emitted by dA and absorbed by all of dV is $\kappa_\eta I_{\eta b}(\eta, T)dV d_\eta d\omega$ (result from integration over all $dA_s dS$ elements), where $d\omega$ is the solid angle defined by dA when viewed from dV. The energy incident upon dV from the entire spherical enclosure, is obtained by integration over all solid angles, which gives $4\pi\kappa_\eta I_{\eta b}(\eta, T)dV d_\eta$.
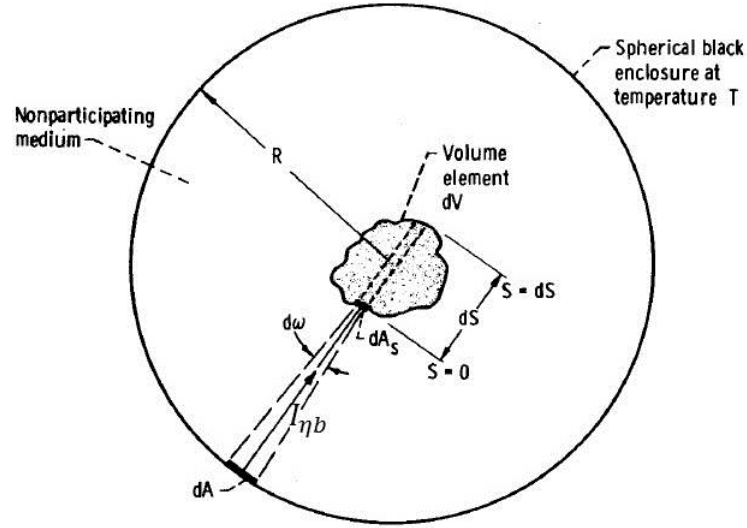
Figure 3.4 − Geometry for derivation of emission from elemental volume[Siegel and Howell, 1993].

The elemental volume dV must emit energy equal to that absorbed to maintain equilibrium in the enclosure. Hence, for a isothermal volume, the spectral emissivity is given by the expression:

$$4\pi\kappa_\eta I_{\eta b}(\eta, T)I_{\eta b}(\eta, T)dV d_\eta = 4\kappa_\eta I_{\eta b}(\eta, T)E_{\eta b}(\eta, T)dV d_\eta \qquad (3.7)$$

where $E_{\eta b}$ is the blackbody spectral emissive power. Finally, considering that the thermal emission is uniform over all directions, the spectral intensity emitted by an elemental volume into any direction is:

$$dI_\eta = \kappa_\eta I_{\eta b} ds \qquad (3.8)$$

3.3   Spectral Line Broadening

It is convenient to discuss the radiation process by utilizing a photon or quantum point of view. Since the photon is the basic unit of radiative energy, the emission releases photons, and absorption is the capture of photons. When a photon is emitted or absorbed, the energy is correspondingly decreased or increased. However, a photon can also transfer part of its energy by the scattering process which is of minor engineering relevance [Howell and Siegel, 2002]. The magnitude of the radiative energy transition is related to the frequency of the emitted or absorbed radiation according to:

$$E_p = E_j - E_i = h\nu_{ij} \tag{3.9}$$

in which h is Planck's constant and ν is the frequency of the photon energy; E_i and E_j are the energy that a photon can present in the levels i and j, respectively.

A fixed frequency is associated with the transition from a specific energy level to another. Thus, in the absence of other effects, the spectrum of the emitted radiation is a spectral line at that frequency. For a photon to be absorbed, the frequency of the photon energy must have one of certain discrete values. According to Equation 3.9, very little energy could be absorbed from the entire incident spectrum by an absorption line, since only those having a single wavenumber could be absorbed. However, other effects cause the line to be broadened and consequently to have a finite wavenumber span around the transition wavenumber η_{ij}. Some important effects are the physical mechanisms such as natural, Doppler, collision, and Stark broadening. Each one of these mechanisms contribute to a certain shape of the spectral lines, as shown in Figure 3.5, where γ_D and γ_L are the spectral line half-width for Doppler and Lorentz broadening, respectively, measured in the middle of the height.

The line intensity can be obtained with the integration of the absorption coefficient over all the wavenumber range according to the following expression:

$$S_{ij} = \int_0^\infty \kappa_{\eta,ij}(\eta)d\eta = \int_{-\infty}^\infty \kappa_{\eta,ij}(\eta)d(\eta - \eta_{ij}) \tag{3.10}$$

where S_{ij} and $\kappa_{\eta,ij}$ depend on the number of molecules in transition between the levels i and j, and on the gas density. The effect of the density on magnitude is seen taking the ratio κ_η/S_{ij}. Thus, it shows the effect of density in changing the line shape. In the

subsections that follow are shown the mechanisms of line broadening.
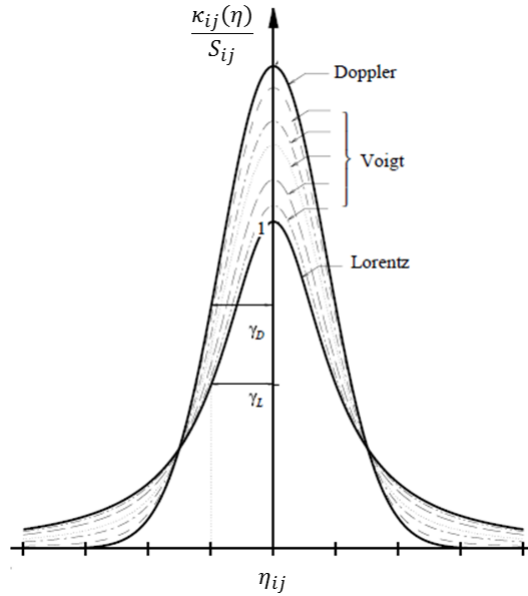
Figure 3.5 – Spectral line shape for different line broadening mechanisms [adapted from Modest, 2013].

3.3.1 Natural Broadening

This mechanism happens when a stationary emitter not perturbed by any external effects emits energy over a finite spectral interval about each transition wavenumber. This natural line broadening arises from the uncertainty in the exact levels E_i and E_j of the transition energy states, and is given by the Lorentz profile [Howell et al., 2010]:

$$\frac{\kappa_{ij}(\eta)}{S_{ij}} = \frac{\gamma_\eta/\pi}{\gamma_\eta^2 + (\eta - \eta_{ij})^2} \tag{3.11}$$

where γ_η is the half-width. In engineering applications the half-width for natural broadening is usually small compared with that for other line broadening phenomena, and, thus, this mechanism is neglected.

3.3.2 Doppler Broadening

Since the atoms or molecules of an absorbing or emitting gas are not stationary, it has a distribution of velocities associated with its thermal energy. If the gas molecules are in thermal equilibrium, it has a Maxwell-Boltzmann distribution of velocities which

results in a spectral line shape with a Gaussian distribution [Howell et al., 2010]:

$$\frac{\kappa_{ij}(\eta)}{S_{ij}} = \frac{1}{\gamma_D}\sqrt{\frac{\ln 2}{\pi}}exp\left[-(\eta-\eta_{ij})^2\frac{\ln 2}{\gamma_D^2}\right] \tag{3.12}$$

in which γ_D is the line half-width for Doppler broadening,

$$\gamma_D = \frac{\eta_{ij}}{c}\left(\frac{2KT}{M}\ln 2\right)^{1/2} \tag{3.13}$$

Here, c is the speed of light in the vacuum ($c = 2.998 \times 10^8$m/s), K is Boltzmann's constant ($K = 1.3806 \times 10^{-23}$J/K), T is the temperature in K, and M is the molecules mass, in kg. Since γ_D depends on $T^{1/2}$, the Doppler broadening becomes important at high temperatures, more specifically above those found in combustion systems.

3.3.3 Collision Broadening

The collision rate by an atom or molecule increases when the gas pressure gas is increased, and it perturbs the energy states of atoms or molecules, resulting in collision broadening of spectral lines. The line shape has a Lorentz profile, as the natural broadening [Howell et al., 2010]:

$$\frac{\kappa_{ij}(\eta)}{S_{ij}} = \frac{\gamma_c/\pi}{\gamma_c^2 + (\eta-\eta_{ij})^2} \tag{3.14}$$

where the collision half-width γ_c is determined by the collision rate,

$$\gamma_c = \frac{1}{2\pi c}\frac{4\sqrt{\pi}D^2 p_i}{(MKT)^{1/2}} \tag{3.15}$$

in which D is the diameter of the atoms or molecules and p_i is the gas pressure for the single component gas. With this equation, it is shown that collision broadening become important at high pressures and low temperatures. For engineering infrared conditions, the collision broadening is often the mean contributor to line broadening, and the other line broadening mechanisms can usually be neglected.

3.3.4 Stark Broadening

When the Stark effect happens, the energy levels of the radiating gas particles can be greatly perturbed due to the presence of strong electric fields. This kind of physical mechanism can produce very large line broadening. The Stark broadening is observed

in ionized gases due to the interactions of radiating particles with electrons and protons. The line shapes must be calculated by quantum mechanisms, and are quite unsymmetrical and complicated.

3.4   Absorption Coefficient

As already discussed, the absorption coefficient of participating gases has a strong variation with the wavenumber. The determination of this coefficient is given by means of the computation of the absorption cross section, which, according to Howell et al., 2010, is obtained with the Lorentz collision profile:

$$C_\eta = \sum_i \frac{S_i}{\pi} \frac{\gamma_i}{\gamma_i^2 + (\eta - \eta_i)^2} \qquad (3.16)$$

In this equation η is the wavenumber, C_η is the absorption cross section, in $cm^2/molecule$, S_i is the integrated intensity of the line i, η_i is the line location in the spectrum (found in spectral databases), and γ_i is the line half-width. In Equation 3.16 the summation includes all the lines that are within an interval $\Delta\eta$, for which the contribution of C_η is significant.

In the work of Wang and Modest, 2004, it is shown that, for both H_2O and CO_2, the Lorentz profile is adequate for total pressure of 1 atm or higher and temperatures above 2500 K. The integrated intensity of a spectral line, S_i, for a given temperature T (K), is calculated with the following expression [Rothman et al., 2010]:

$$S_i(T) = S_i(T_0)\frac{Q(T_0)}{Q(T)}\frac{exp(-C_2 E_i/T)}{exp(-C_2 E_i/T_0)}\frac{1 - exp(-C_2\nu_i T)}{1 - exp(-C_2\nu_i T_0)} \qquad (3.17)$$

where T_0 is the database reference temperature ($T_0 = 296$ K in the HITEMP), Q is the total intern partition sum (which depends on the molecule structure, its isotope and temperature) [Fischer et al., 2003], and represents the summation of all energy states (electronic, vibrational, rotational, torsional, etc.); E_i is the energy of the lower state (cm^{-1}), and ν_i is the energy difference between the initial and final state (given as vacuum wavenumber, cm^{-1}, in the database). The constant C_2 is the second Planck's constant ($C_2 = 1.43877$ cm.K).

The quantities $S_i(T_0)$, E_i, and ν_i are provided in the HITRAN compilation, and the value of Q is obtained with a Fortran routine [Fischer et al., 2003] available in the databases. The line half-width γ_i (p, T) for a gas at pressure p (atm), temperature T (K),

and partial pressure p_i (atm), is calculated as [Rothman et al., 1998]:

$$\gamma_i(p,T) = \left(\frac{T_0}{T}\right)^n \left[\gamma_{air,i}(p_0,T_0)(p-p_i) + \gamma_{self,i}(p_0,T_0)p_i\right] \tag{3.18}$$

in which n is the temperature dependence coefficient, p_0 is the reference pressure, $\gamma_{air,i}$ is the air-broadened half-width, and $\gamma_{self,i}$ is the self-broadened half-width. Since the databases only provides $\gamma_{air,i}$, Rothman et al., 1998 proposes that $n = \gamma_{air,i} = \gamma_{self,i}$.

After defining the spectral line intensity $S_i(T)$, the line half-wight γ_i (p,T), and the absorption cross section C_η, then the absorption coefficient can be expressed as:

$$\kappa_\eta(p,T,Y) = N(p,T)YC_\eta(p,T,Y) \tag{3.19}$$

Here, $Y = p_i/p$ is the gas molar fraction, $N(p,T) = pN_A/R_uT$ is the gas molar density, being $N_A = 6.022\times10^{-23}$ molecules/mol the Avogadro's number, and $R_u = 8.314$ J/mol.K the gases universal constant.

3.5   Spectral Databases

The advances in the spectroscopy of high resolution in the last decades have been very important in the thermal radiation field. It allowed the detailed compilation of parameters of those molecules that are the mean constituents of the terrestrial atmosphere. McClatchey et al., 1973 published a technical report containing spectral data of molecules of water vapor, carbon dioxide, ozone, nitrous oxide, carbon dioxide, methane, and oxygen. Some of the parameters included were the frequency, intensity, half-width and the energy of the lower state of transition. Posteriorly, this study gave rise to the HITRAN database [Rothman et al., 1987] which has been periodically updated. The HITRAN2012 [Rothman et al., 2013] encompassing spectral information of 47 molecules. This database has its origins in applications for conditions of the terrestrial atmosphere. The last update is the HITRAN2016 [Gordon et al., 2017].

For combustion applications arises the need of molecules spectra at high temperatures (> 1000 K). This requirement was attended by Rothman et al., 1995 with the HITEMP1995 spectroscopic database. Hence, it contains many more spectral lines than HITRAN for participating species. The last version, the HITEMP2010, has the spectral data of the absorbers H_2O, CO_2, CO, NO, and OH [Rothman et al., 2010]. One interesting point to note is that in the HITEMP2010 there is an amount of spectral lines for

H$_2$O and CO$_2$ much greater than for the others species, as can be seen in Table 3.1.

Table 3.1 – Number of spectral lines for molecules of the HITEMP 2010 [Rothman et al., 2010].

Molecule	Spectral Coverage (cm^{-1})	Number of Spectral Lines
H$_2$O	0 - 30,000	111,377,777
CO$_2$	258 - 9,648	11,167,618
CO	0 - 8,465	115,218
NO	0 - 9,274	105,633
OH	0 - 19,268	40,055

3.6   Radiative Transfer Equation

When it is considered a participating media, such as a H$_2$O/CO$_2$ mixtures at high temperatures, the particles emits and absorbs radiation, and the scattering of this quantity can be neglected. To take into account the emission and absorption effects it is necessary to do the radiative energy balance over the enclosure. Thus, it results in the radiative transfer equation (RTE) which, for a non-scattering media, accounts for the spectral intensity variation along a given path x [Modest, 2013]:

$$\frac{dI_\eta}{dx} = -\kappa_\eta(x)I_\eta(x) + \kappa_\eta(x)I_{\eta b}(x) \tag{3.20}$$

where, in the right-side, the first term represents the intensity attenuation due to absorption, and the second is the intensity increasing due to emission; κ_η is the spectral absorption coefficient and $I_{\eta b}$ is the blackbody spectral radiation intensity, which were discussed in the previous sections. This equation needs to be solved for all directions and wavenumbers.

3.7   Summary

Unlike conduction and convection, the thermal radiation can be transferred along a distance without interacting with the medium. Since this mechanism is proportional to differences in temperature to the fourth power, it is very important in high temperatures such as those of combustion process. In this kind of problems, the blackbody, as a perfect absorber for all incident thermal radiation, serves as a standard with which real absorbers

can be compared. Another fundamental definition in the radiation field is the spectral intensity. As the radiation passes through a participating media, the intensity can be attenuated by absorption, and increased by emission. The concepts of line broadening also must be considered. For engineering applications, the effect of the collision broadening is the most important. However, the Doppler broadening can become also relevant at elevated temperatures. To solve the RTE, besides to calculate the radiation intensity, it is needed to know the absorption coefficient of the gases. This coefficient depends on the absorption cross section, which can be obtained from the spectral databases.

4 AVAILABLE METHODS FOR SPECTRAL INTEGRATION OF THE RTE AND A NEW PROPOSITION

After presenting the spectral form of the RTE, which needS to be solved for all direction and all wavenumbers, some methods for its spectral integration will be described. In this chapter, only the methods relevant to this work will be shown. The LBL integration may require a high computational time depending on the problem under analysis. It happens due to the highly irregular behavior of the absorption coefficient with the wavenumber. One common alternative is to apply the gas models such as the WSGG and the SLW for the radiative transfer computation.

4.1 The Line-by-Line Integration

As already discussed, the absorption coefficient of the participating gases presents a strong variation with the wavenumber. This behavior is characterized by hundreds of thousands of spectral lines forming the gases spectra. In the Line-by-Line (LBL) solution of the RTE it is considered each one of these spectral lines individually. Because of this approach, the LBL method is taken as a benchmark solution with which the accuracy of the gases models is verified.

In Figure 4.1 there is a representation of an one-dimensional participating medium bounded by two parallel surfaces separated by a distance L. The spectral intensities in the forward and backward direction, $I_{\eta,l}^+(x)$ and $I_{\eta,l}^-(x)$, in a non-scattering participating media, are determined from the RTE equation as follow, according to the discrete ordinates method (DOM)[Cassol et al., 2014; Modest, 2013]:

$$\mu_l \frac{dI_{\eta,l}^+(x)}{dx} = -\kappa_\eta(x)I_{\eta,l}^+(x) + \kappa_\eta(x)I_{\eta b}(x) \tag{4.1}$$

$$-\mu_l \frac{dI_{\eta,l}^-(x)}{dx} = -\kappa_\eta(x)I_{\eta,l}^-(x) + \kappa_\eta(x)I_{\eta b}(x) \tag{4.2}$$

in which μ_l is the the cosine of the polar angle θ_l in l direction, $I_{\eta,l}^+$ and $I_{\eta,l}^-$ are the spectral radiation intensities for $\mu_l > 0$ and $\mu_l < 0$, respectively; x is the spatial position. Considering that the walls are black with known temperatures, the boundary conditions for Equations 4.1 and 4.2 at positions $x = 0$ and $x = L$ are, respectively, $I_{\eta,l}^+(0) = I_{\eta b}(0)$ and $I_{\eta,l}^-(L) = I_{\eta b}(L)$.
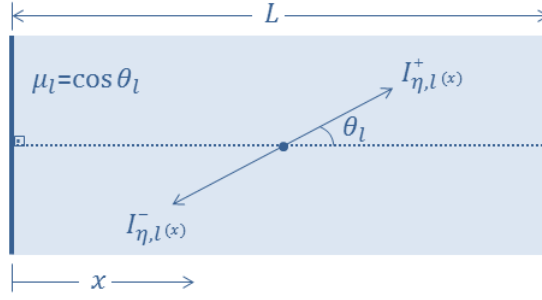
Figure 4.1 – Schematic representation of the one-dimensional domain studied.

If Equation 4.1 and 4.2 are solved for all directions and wavenumbers, the radiative heat flux and the heat source, $q_R^{''}$ and $\dot{q_R}$, respectively, at position x, can be calculated by [Cassol et al., 2014]:

$$q_R^{''}(x) = \sum_{l=1}^{n_d} \int_\eta 2\pi\mu_l\omega_l \left[I_{\eta,l}^+(x) - I_{\eta,l}^-(x)\right]d\eta \qquad (4.3)$$

$$\dot{q_R}(x) = \sum_{l=1}^{n_d} \int_\eta 2\pi\omega_l\kappa_\eta \left\{\left[I_{\eta,l}^+(x) + I_{\eta,l}^-(x)\right] - 2I_{\eta b}(x)\right\}d\eta \qquad (4.4)$$

where, for n_d directions, the μ_l and the weights ω_l of the quadrature scheme are defined within the interval [0,1]. To solve the radiative transfer equation, in this work was used the Gauss Legendre quadrature.

Usually the RTE must be solved for a mixture of gases such as those found in combustion systems. Thus, the spectral absorption coefficient in Equations 4.1 and 4.2 has to be modified. For a mixture of H_2O and CO_2 this coefficient is written then as:

$$\kappa_\eta = \kappa_{\eta,w} + \kappa_{\eta,c} \qquad (4.5)$$

in which $\kappa_{\eta,w}$ and $\kappa_{\eta,c}$ are the spectral absorption coefficients for H_2O and CO_2, respectively.

4.2   Weighted-Sum-of-Gray-Gases

Since the LBL integration solves the RTE for each spectral line, it requires a high computational time which may be not feasible for practical applications. Based on this, the Weighted-Sum-of-Gray-Gases (WSGG) model comes to overcome this difficult with a good accuracy. Initially proposed by Hottel and Sarofim, 1967, this model replaces the

spectrum by a set of gray gases with uniform pressure absorption coefficient, as shown in Figure 4.2. Thus, it is assumed that each gray gas covers a fixed portion $\Delta\eta_j$ in the spectrum. Moreover, each pressure absorption coefficient $\kappa_{p,j}$ is assumed to be independent of the temperature and partial pressure of the participating gases.
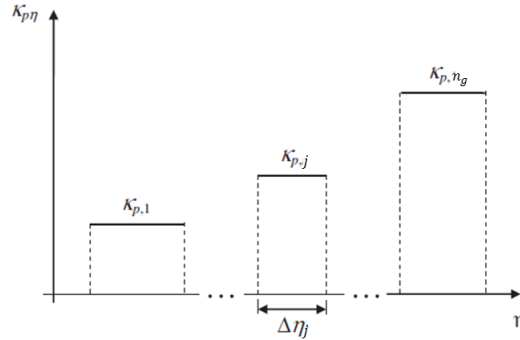
Figure 4.2 – Pressure absorption coefficient representation using n_g gray gases [adapted from Dorigon et al., 2013].

One parameter of great importance for the WSGG model is the total emittance along a certain path s in a medium at a given temperature and composition. This quantity accounts for the amount of energy emitted by a participating media compared with the energy emitted by a blackbody. Thereby, the total emittance is expressed as [Howell et al., 2010]:

$$\varepsilon(s) = \frac{\pi \int_\eta I_{\eta b}\varepsilon_\eta(s)d\eta}{\int_\eta I_{\eta b}d\eta} \tag{4.6}$$

The Kirchhoff's law states that the absorbed and emitted energies must be equal: $\varepsilon_\eta = \alpha_\eta$, where ε_η is the spectral emittance, and α_η the spectral absorptance which is defined by the expression:

$$\alpha_\eta(s) = 1 - e^{-\kappa_{p\eta}Ps} \tag{4.7}$$

This equation expresses the fraction of spectral intensity that has been absorbed along a path s, where $\kappa_{p\eta} = \kappa_\eta/P$ is the absorption coefficient based on pressure, being P the sum of the partial pressures of the individual species of the gaseous mixture. Thus, Equation 4.6 can be rewritten as follows:

$$\varepsilon(s) = \frac{\pi \int_\eta I_{\eta b}\big[1 - e^{-\kappa_{p\eta}Ps}\big]d\eta}{\sigma T^4} \tag{4.8}$$

For the WSGG model, the total emittance is evaluated according to the following

relation [Smith et al., 1982]:

$$\varepsilon(s) = \sum_{j=0}^{n_g} a_j(T) \left[1 - e^{-\kappa_{p,j} Ps} \right] \tag{4.9}$$

where $a_j(T)$ is the weighting factor for each gray gas, based on the gas temperature; $j = 0$ represents the spectral windows for which the absorption coefficient is null, and n_g indicates the number of gray gases. The weighting factor, $a_j(T)$, may be physically interpreted as the fraction of the blackbody energy in the range of the spectrum in which the gray gas has a pressure absorption coefficient $\kappa_{p,j}$. Another interpretation for $a_j(T)$ and $\kappa_{p,j}$ is that they are the numerical values that yield the better fit of Equation 4.9. The coefficients $a_j(T)$ can be represented by polynomial functions [Smith et al., 1982]:

$$a_j(T) = \sum_{k=0}^{K} b_{j,k} T^k \tag{4.10}$$

in which $b_{j,k}$ is the polynomial coefficient of kth order for the jth gray gas. Despite the transparent window having a null absorption coefficient, the weighting factor must be different from zero to assure that radiation energy is conserved:

$$a_0 = 1 - \sum_{j=1}^{n_g} a_j \tag{4.11}$$

To solve Equation 4.9 - 4.11 the $\kappa_{p,j}$ and $b_{j,k}$ coefficients for H_2O/CO_2 mixtures have been proposed in the last years [Galarça et al., 2008; Kangwanpongpan et al., 2012; Dorigon et al., 2013]. In this work was adopted the Dorigon et al., 2013 correlations for a partial pressure ratio between H_2O and CO_2 (p_w/p_c) equal to 2, as shown in Table 4.1. Such correlations are valid for a temperature range from 400 K to 2500 K, and for the pressure path lengths Ps of Equations 4.7 - 4.9 between 0.001 atm.m and 10 atm.m.

Table 4.1 – WSGG coefficients for H_2O/CO_2 mixtures for $p_w/p_c = 2$ [Dorigon et al., 2013].

j	$\kappa_{p,j}(\text{atm.m})^{-1}$	$b_{j,0}$	$b_{j,1}(\text{K})^{-1}$	$b_{j,2}(\text{K})^{-2}$	$b_{j,3}(\text{K})^{-3}$	$b_{j,4}(\text{K})^{-4}$
1	1.921E-01	5.617E-02	7.844E-04	-8.563E-07	4.246E-10	-7.440E-14
2	1.719E+00	1.426E-01	1.795E-04	-1.077E-08	-6.971E-11	1.774E-14
3	1.137E+01	1.362E-01	2.574E-04	-3.711E-07	1.575E-10	-2.267E-14
4	1.110E+02	1.222E-01	-2.492E-05	-7.272E-08	4.275E-11	-6.608E-15

It was shown by Modest, 1991 that the WSGG model can be used with any method of solution of the RTE, which assumes the following form:

$$\frac{dI_j(x)}{dx} = -\kappa_j(x)I_j(x) + \kappa_j(x)a_j(x)I_b(x) \tag{4.12}$$

In this equation, I_j and κ_j are the intensity and the absorption coefficient associated with the jth gray gas; $I_b = \sigma T^4/\pi$ is the blackbody intensity, which is the Planck's distribution law. For a H_2O/CO_2 mixture, the coefficient κ_j can be rewritten as $\kappa_{m,i}$ to have the contribution of each participating gas: $\kappa_{m,i} = \kappa_{w,j} + \kappa_{c,k}$, being $k_{w,j}$ and $k_{c,k}$ the gray gas absorption coefficient for H_2O and CO_2, respectively. Considering a gaseous mixture confined between two parallel surfaces, Equation 4.12 can be written for positive and negative directions, according to the discrete ordinates method [Cassol et al., 2014; Modest, 2013]:

$$\mu_l \frac{dI_{j,l}^+(x)}{dx} = -\kappa_j(x)I_{j,l}^+(x) + \kappa_j(x)a_j(x)I_b(x) \tag{4.13}$$

$$-\mu_l \frac{dI_{j,l}^-(x)}{dx} = -\kappa_j(x)I_{j,l}^-(x) + \kappa_j(x)a_j(x)I_b(x) \tag{4.14}$$

in which μ_l is the cosine of the polar angle θ_l in the l direction, $I_{j,l}^+$ and $I_{j,l}^-$ are the radiation intensities of the gray gas j for $\mu_l > 0$ and $\mu_l < 0$, respectively. Whereas the walls are black with known temperatures, the boundary conditions for Equations 4.13 and Equation 4.14 at positions $x = 0$ and $x = L$ are, respectively, $I_{j,l}^+(0) = a_j(0)I_b(0)$ and $I_{j,l}^-(L) = a_j(L)I_b(L)$.

Solving Equations 4.13 and 4.14, the radiative heat flux and heat source, $q_R^{"}$ and $\dot{q}_R$, respectively, at a position x, can be determined as [Cassol et al., 2014; Dorigon et al., 2013]:

$$q_R^{"}(x) = \sum_{j=0}^{n_g} \sum_{l=1}^{n_d} 2\pi \mu_l \omega_l \left[I_{j,l}^+(x) - I_{j,l}^-(x) \right] \tag{4.15}$$

$$\dot{q}_R(x) = \sum_{j=1}^{n_g} \sum_{l=1}^{n_d} 2\pi \omega_l \kappa_j \left\{ \left[I_{j,l}^+(x) + I_{j,l}^-(x) \right] - 2a_j(x)I_b(x) \right\} \tag{4.16}$$

where the summation over all gray gases (n_g) represent the spectral integration in the WSGG model.

4.2.1 Superposition Method

The correlations obtained for the standard WSGG model usually are for a constant partial pressure ratio between the participating species or when this ratio presents a little variation. Cassol et al., 2014 applied the superposition method as a way to eliminate this restriction. This approach consists of first setting up independent correlations for each species, which are then superposed to form the WSGG correlations for the mixture. Thus, it is possible to compute the radiative heat transfer in mixtures with arbitrary concentrations, allowing for local variations in the mole ratios, and the inclusion of any number of participating species.

According to the superposition method, for a mixture of water vapor and carbon dioxide, the gray gas absorption coefficient is a sum of a given combination of gray gases absorption coefficient of the components, and the weighting factor will be the product of their respective weighting factors. These definitions are represented by the expressions:

$$\kappa_{m,i} = \kappa_{w,j} + \kappa_{c,k} \tag{4.17}$$

$$a_{m,i}(T) = a_{w,j}(T) \times a_{c,k}(T) \tag{4.18}$$

where $\kappa_{w,j}$ and $\kappa_{c,k}$ are the local absorption coefficients for the jth and the kth gray gas of H_2O and CO_2, respectively; $a_{w,j}(T)$ and $a_{c,k}(T)$ are the corresponding weighting factors. Such method is similar to the implementation realized by Smith et al., 1987 for the WSGG model combining H_2O and CO_2 with soot, and was also applied to the SLW model development for H_2O/CO_2 mixtures [Denison and Webb, 1995b].

Since this methodology requires the correlations of the individuals species, in this work it is adopted those found by Cassol et al., 2014 for H_2O and CO_2. These correlations, described in Tables 4.2 and 4.3, are valid for temperatures between 400 K and 2500 K, and 0.001 atm.m to 10 atm.m.

Table 4.2 – WSGG coefficients for H_2O [Cassol et al., 2014].

j	$\kappa_{p,j}(\text{atm.m})^{-1}$	$b_{j,0}$	$b_{j,1}(\text{K})^{-1}$	$b_{j,2}(\text{K})^{-2}$	$b_{j,3}(\text{K})^{-3}$	$b_{j,4}(\text{K})^{-4}$
1	0.171	0.06617	55.48E-05	-48.41E-08	22.27E-11	-40.17E-15
2	1.551	0.11045	0.576E-05	24.00E-08	-17.01E-11	30.96E-15
3	5.562	-0.04915	70.63E-05	-70.12E-08	26.07E-11	-34.94E-15
4	49.159	0.23675	-18.91E-05	-0.907E-08	4.082E-11	-8.778E-15

Table 4.3 – WSGG coefficients for CO_2 [Cassol et al., 2014].

j	$\kappa_{p,j}(\text{atm.m})^{-1}$	$b_{j,0}$	$b_{j,1}(\text{K})^{-1}$	$b_{j,2}(\text{K})^{-2}$	$b_{j,3}(\text{K})^{-3}$	$b_{j,4}(\text{K})^{-4}$
1	0.138	0.09990	64.41E-05	-86.94E-08	41.27E-11	-67.74E-15
2	1.895	0.00942	10.36E-05	2.277E-08	-2.134E-11	6.497E-15
3	13.301	0.14511	-3073E-05	-37.65E-08	-18.41E-11	30.16E-15
4	340.811	-0.02915	25.23E-05	-26.10E-08	9.965E-11	-13.26E-15

4.2.2 Proposition of a Reduced Superposition Method

The superposition method applied to the WSGG has proved to be a good alternative for radiative transfer prediction in participating media, and has been applied recently in some works [Centeno et al., 2016, 2018; Fraga et al., 2017]. However, this approach needs to be better investigated when used for the radiative transfer prediction in combustion gases. In this case, the main challenge is the combination of participating species since it requires increasing computational effort as the components number increase. For combustion problems modeling, the thermal radiation calculation needs to be coupled with other complex phenomena such as chemical kinetic and turbulence. Thereby, any computational cost improvement in the thermal radiation prediction is of great relevance.

Considering a H_2O/CO_2 mixture, the present proposition is based on the absorption coefficient of each specie. Let $\kappa_{w,j}$ and $\kappa_{c,k}$ be the absorption coefficient of the H_2O and CO_2, respectively, and j and k varying from 0 (transparent window) to n_g (number of gray gaes). Thus, the main assumption for the reduced superposition method can be written as:

$$\begin{cases} \kappa_{w,j} >> \kappa_{c,k}, & \text{if } j > k \\ \kappa_{w,j} << \kappa_{c,k}, & \text{if } j < k \end{cases} \qquad (4.19)$$

This assumption can be obtained from the analysis of the WSGG correlations [Cassol et al., 2014], observing that the $\kappa_{w,j}$ and $\kappa_{c,j}$ coefficients are given as follows:

$$\begin{cases} \kappa_{w,j} = p_w \kappa_{p,j} \\ \kappa_{c,k} = p_c \kappa_{p,k} \end{cases} \qquad (4.20)$$

where p_w and p_c are the partial pressures of H_2O and CO_2, respectively; $\kappa_{p,j}$ and $\kappa_{p,k}$ are accordingly the pressure absorption coefficient which are found in the literature [Cassol

et al., 2014], and as shown in Tables 4.2 and 4.3, they are arranged in order of magnitude that makes the assumption of Equation 4.19 possible.

It is fundamental to emphasize the relevance of the partial pressure of the participating species (p_w and p_c). The assumption of the Equation 4.19 is valid when the partial pressure ratio (p_w/p_c), from Equation 4.20, is on scale with 1 ($p_w/p_c \sim 1$). Otherwise, if p_w/p_c ratio is much larger or much smaller, the proposed reduced superposition method may not accurately predict the radiative transfer. In such a case it is necessary to evaluate if the regions where this happens are important or not to the thermal radiation.

In Figure 4.3 there is a representation of the proposed reduced superposition method. The combination of two absorption coefficients of H_2O ($\kappa_{w,j}$) with those of CO_2 ($\kappa_{c,k}$) is shown in Figure 4.3(a), where the subscripts j and k are varying from 0 (transparent window) to 4 (number of gray gases). In the case where $j = k$ the absorption coefficient of the two species has the same magnitude, and, then, the absorption coefficient i of the mixture, $\kappa_{m,i}$, will have the contribution of both the H_2O and the CO_2 absorption coefficients. The same happens for the weighting factor of the mixture, $a_{m,i}(T)$, forming then one gray gas. This assumption can be summarized by the following expression:

$$\text{if } j = k \begin{cases} \kappa_{m,i} = \kappa_{w,j} + \kappa_{c,k} \\ a_{m,i}(T) = a_{w,j}(T) \times a_{c,k}(T) \end{cases} \tag{4.21}$$
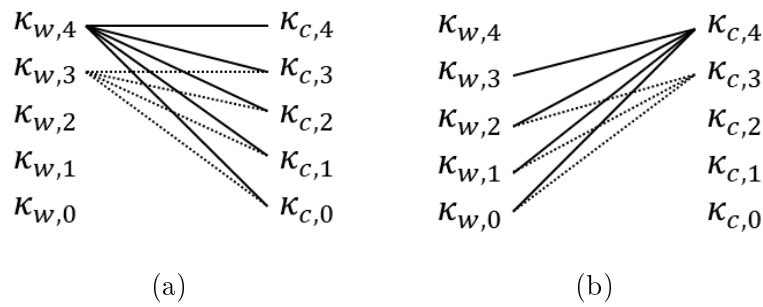
Figure 4.3 – Reduced superposition approach for the arrangement of (a) H_2O coefficients with those of CO_2, and for the arrangement of (b) CO_2 coefficients with those of H_2O.

Each of the combinations for which $j > k$ will also form one gray gas. However, these gray gases will have the same absorption coefficient, which is $\kappa_{w,j}$. This happens because the H_2O absorption coefficients will be much larger than those of CO_2, and, then, will predominate. Since all combinations have the same absorption coefficient, it will

generate one unique gray gas i of the mixture, with absorption coefficient $\kappa_{w,j}$. Thus, for this gray gas i, the absorption coefficient, $\kappa_{m,i}$, and the weighting factor, $a_{m,i}(T)$, are given as:

$$\text{if } j > k \begin{cases} \kappa_{m,i} = \kappa_{w,j} \\ a_{m,i}(T) = a_{w,j}(T) \times \left[1 - \sum_{k+1}^{4} a_{c,k}(T)\right] \end{cases} \quad (4.22)$$

In Equation 4.22, for CO_2, all the arrangements together will form a fraction of the blackbody energy, represented by the term $[1 - \sum_{k+1}^{4} a_{c,k}(T)]$, in the range of the spectrum where the gray gas of the mixture has the absorption coefficient $\kappa_{w,j}$. Thereby, considering, for instance, all the possible arrangements of the absorption coefficient $\kappa_{w,4}$ of H_2O with those of CO_2 in Figure 4.3, it will be formed only two gray gases of the mixture.

For the combinations of the CO_2 absorption coefficient with those of H_2O, remains the scheme of the Figure 4.3(b) showed for two CO_2 absorption coefficients. As can be seen, there are only the combinations for $j < k$ since those for $j = k$ have already been accounted in the arrangement of Figure 4.3(a). Observing this, the absorption coefficient and the weighting factor for the H_2O/CO_2 mixture, $\kappa_{m,i}$ and $a_{m,i}(T)$, are expressed as follows:

$$\text{if } j < k \begin{cases} \kappa_{m,i} = \kappa_{c,k} \\ a_{m,i}(T) = a_{c,k}(T) \times \left[1 - \sum_{j+1}^{4} a_{w,j}(T)\right] \end{cases} \quad (4.23)$$

Considering the application of the standard superposition method for a mixture of H_2O/CO_2, the number of gray gases, adding the transparent windows, will be $i = (j+1) \times (k+1)$. In this relation, the correlations adopted for H_2O and CO_2 leads to $j = k = 4$, then $i = 25$. However, if the proposed reduced superposition is adopted i is reduced to 13. This result is of great relevance when concerning computational effort. The radiative transfer equation (RTE) is solved approximately only half of the time needed to obtain the solution by means of the standard superposition method. Moreover, it gains even more importance when it is working with more than two participating species. In the case of three components, the RTE should be solved 125 times applying the standard superposition method. Since the combustion system modeling requires the consideration of even more components, the computational time increases significantly for the solution the RTE. Because of it, it is important the development of methodologies like the one presented in this work, which are capable of decreasing the computational effort.

4.3   Spectral-Line Weighted-Sum-of-Gray-Gases

Derived from the formulation of the WSGG model proposed by Modest, 1991, the Spectral-Line Weighted-Sum-of-Gray-Gases (SLW) model allows for a further detailing in the treatment of the radiation spectrum, gases mixtures, and non-isothermal and non-homogeneous media. This model, first introduced by Denison and Webb, 1993b, replaces the traditional LBL spectral integration over the wavenumber with an integration over the spectral absorption cross-section. Numerically, it means a discretization of the spectral absorption cross-section. The RTE has the same form as that of the WSGG model, differing only in the way of calculating the gray gases absorption coefficient and the correspondent weighting factors, which are obtained with the absorption line blackbody distribution function (ALBDF). For a non-scattering media, the RTE becomes, then:

$$\frac{dI_j(x)}{dx} = -\kappa_j(x)I_j(x) + \kappa_j(x)a_j(x)I_b(x) \tag{4.24}$$

where κ_j and a_j are the absorption coefficient and the weighting factor for each gray gas, respectively.

The ALBDF is defined as the fraction of the blackbody energy in the portions of the spectrum where the high-resolution spectral absorption cross-section of the gas C_η is less than the prescribed value C, as illustrated in Figure 4.4. The dark-gray hatches represent the portions of the spectrum where the Planck's function ($E_{b\eta}$) is integrated. The ALBDF can be expressed as [Denison and Webb, 1995c]:

$$F(C, T_b, T_g, P_T, Y) = \frac{1}{\sigma T_b^4} \sum_i \int_{\Delta \eta_i} E_{b\eta}(\eta, T_b)d\eta \tag{4.25}$$

in which σ is the Stephan-Boltzmann constant and $E_{b\eta}$ is Planck's function evaluated at the wavenumber η and blackbody temperature T_b. The subscript i refers to the ith spectral segment and the summation is performed over the all segments for which $C_\eta < C$, covering the entire spectrum. The dependence of the ALBDF on the spectrum is given by the spectral intervals $\Delta \eta_i$, which are dependent on the absorption cross-section, gas temperature T_g, the total pressure P_T, and the species concentration Y. This distribution function monotonically increases from 0 to 1 with increasing absorption cross section.

The discretization of C_η results in the called supplemental absorption cross sections, whose values are logarithmically spaced between the minimum and maximum values of
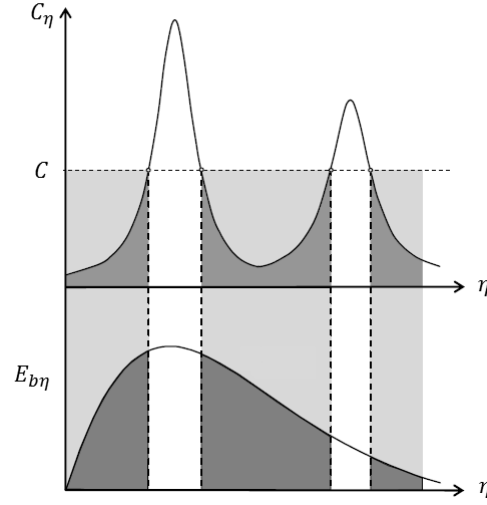
Figure 4.4 – Representation of part of the spectrum in which the ALBDF is calculated [adapted from Solovjov et al., 2016].

C_η. Each discrete increment of C_η is represented by a single absorption cross section C_j or a single gray gas. Thus, for each gray gas, the fraction of blackbody energy, a_j, for a given source temperature, is computed as the difference of two distribution functions evaluated at the supplementals absorption cross sections $\tilde{C}_j$ and $\tilde{C}_{j+1}$:

$$a_j = F(\tilde{C}_{j+1}, T_b, T_g, P_T, Y) - F(\tilde{C}_j, T_b, T_g, P_T, Y) \tag{4.26}$$

The application of the SLW model to non-isothermal and/or non-homogeneous media is made through scaling approximations, wherein a non-isothermal and/or non-homogeneous gas is replaced with an equivalently absorbing isothermal homogeneous gas. The most known is the Curtis-Godson approximation [Godson, 1953]. Goody and Yung, 1989 showed that the scaling approximations are exact if the high-resolution absorption cross section can be expressed as the product of two functions [Denison and Webb, 1995c]:

$$C_\eta(T_g, P_T, Y) = \phi(T_g, P_T, Y)\psi(\eta) \tag{4.27}$$

where ϕ and ψ define the spatial and the spectral dependence of the absorption cross section, respectively. For non-isotherm and/or non-homogeneous problems, the spectral integration of the RTE leads to the appearance of the additional so-called Liebnitz terms [Denison and Webb, 1993b], which makes the analysis complicated . However, employing the scaling approximation, these terms vanish, and, therefore, the RTE can be solved with

arbitrary solution methods.

The employment of the scaling approximation can be analyzed through Figure 4.5. In this figure there is a high-resolution portion of an ideal spectrum of a gas described by Equation 4.27 at two different thermodynamic states. The spectrum at the state 1 is represented by temperature T_{g1}, total pressure P_{T1}, and molar fraction Y_1. For this state, the ALBDF may be calculated by integrating Planck's function over all spectral segments where $C_\eta(T_{g1}, P_{T1}, Y_1)$ is less than the prescribed value $C_j(T_{g1}, P_{T1}, Y_1)$. The stated 2 is described by temperature T_{g2}, total pressure P_{T2}, and molar fraction Y_2. Then, if the Equation 4.27 is valid, the absorption cross section of the state 2, $C_j(T_{g2}, P_{T2}, Y_2)$, is given as [Denison and Webb, 1995c]:

$$C_j(T_{g2}, P_{T2}, Y_2) = C_j(T_{g1}, P_{T1}, Y_1) \frac{\phi(T_{g2}, P_{T2}, Y_2)}{\phi(T_{g1}, P_{T1}, Y_1)} \qquad (4.28)$$

This result is due to function $\psi(\eta)$ be independent of the gas state, according to Equation 4.27.
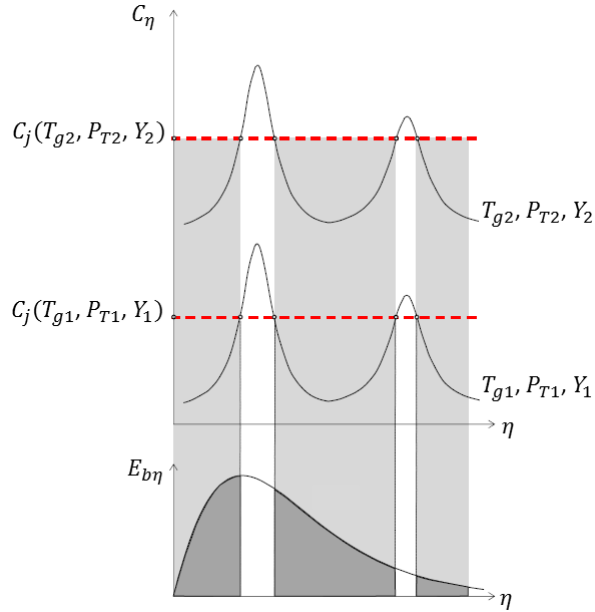
Figure 4.5 – Idealized dependence of high resolution spectrum on two different thermodynamics states, resulting in equivalent blackbody energy fractions [adapted from Solovjov et al., 2017].

As can be observed in Figure 4.5, the spectral segments defined where $C_\eta(T_{g1}, P_{T1}, Y_1)$ is less than the prescribed value $C_j(T_{g1}, P_{T1}, Y_1)$ are identical to those spectral segments where $C_\eta(T_{g2}, P_{T2}, Y_2)$ is less than $C_j(T_{g2}, P_{T2}, Y_2)$. Thereby, from the definition of the

ALBDF, there is an equality between the ALBDFs of the two thermodynamic states for a given blackbody temperature, established by the following expression:

$$F\big[C_j(T_{g2}, P_{T2}, Y_2); T_b = T_{ref}; T_g = T_{g2}; Y = Y_2; P_T = P_{T2}\big]$$
$$= F\big[C_j(T_{g1}, P_{T1}, Y_1); T_b = T_{ref}; T_g = T_{g1}; Y = Y_1; P_T = P_{T1}\big]$$
(4.29)

where T_{ref} is a reference temperature. This equation provides an implicit dependence of C_j on the local gas state. Thus, the local absorption cross section C_j is determined from the following implicit equation, which is the Equation 4.29 written for equivalent absorption-line blackbody functions at the reference and the local states [Denison and Webb, 1995c]:

$$F\big[C_j; T_b = T_{ref}; T_g = T_{loc}; Y = Y_{loc}; P_T = P_{loc}\big]$$
$$= F\big[C_{j,ref}; T_b = T_{ref}; T_g = T_{ref}; Y = Y_{ref}; P_T = P_{ref}\big]$$
(4.30)

in which the "ref" and "loc" terms means the reference and the local values, respectively, of each variable. Equation 4.30 is known as the reference approach [Solovjov and Webb, 2000; Solovjov et al., 2014, 2017] which assumes an ideal spectrum producing scaling of the spectrum in non-uniform media. Under this assumption, the intervals of integration can then be fixed for each spatial position, eliminating the Leibnitz terms. Since Equation 4.30 is implicit, C_j must be determined at each spatial location from an iterative technique such as bisection (adopted in this work) or Newton-Raphson [Denison and Webb, 1995c]. For Solovjov and Webb, 2010 the reference approach provides satisfactory results when the spatial temperature gradients are not too high.

According to Denison and Webb, 1995c the reference state can be determined as the spatial average of the temperature, total pressure, and composition fields. The reference absorption cross section, $C_{j,ref}$ in Equation 4.30, is an appropriate value between the supplemental absorption cross sections $\tilde{C}_j$ and $\tilde{C}_{j+1}$, which are logarithmically spaced. Thus, if sufficient gray gases (20 or more) are used, $C_{j,ref}$ may be determined as the logarithmic mean of $\tilde{C}_j$ and $\tilde{C}_{j+1}$:

$$C_{j,ref} = exp\left[\frac{\ln(\tilde{C}_j) + \ln(\tilde{C}_{j+1})}{2}\right]$$
(4.31)

The local gray gas absorption coefficient κ_j is a function of the local molar density N, determined from an appropriate equation of state, and the local gray gas absorption

cross section C_j:

$$\kappa_j = NYC_j \tag{4.32}$$

where Y is the local molar fraction of each participating specie.

Since the fraction of blackbody energy of each gray gas, a_j, has already been defined in Equation 4.26, remains to set the appropriated values of the gas temperature, total pressure, and mole fraction to calculate a_j. Denison and Webb, 1995c recommend that the fraction of blackbody energy of each gray gas be calculated as follow:

$$
\begin{aligned}
a_j = F(\tilde{C}_{j+1}, T_b = T_{loc}, T_g = T_{ref}, P_T = P_{ref}, Y = Y_{ref}) \\
-F(\tilde{C}_j, T_b = T_{loc}, T_g = T_{ref}, P_T = P_{ref}, Y = Y_{ref})
\end{aligned}
\tag{4.33}
$$

For a participating media bounded by two parallel surfaces, Equation 4.24 can be written for positive and negative directions, according to the discrete ordinates method [Cassol et al., 2014; Modest, 2013]:

$$\mu_l \frac{dI_{j,l}^+(x)}{dx} = -\kappa_j(x)I_{j,l}^+(x) + \kappa_j(x)a_j(x)I_b(x) \tag{4.34}$$

$$-\mu_l \frac{dI_{j,l}^-(x)}{dx} = -\kappa_j(x)I_{j,l}^-(x) + \kappa_j(x)a_j(x)I_b(x) \tag{4.35}$$

in which μ_l is the the cosine of the angle θ_l in l direction, $I_{j,l}^+$ and $I_{j,l}^-$ are the radiation intensities for the gray gas j for $\mu_l > 0$ and $\mu_l < 0$, respectively. Considering that the walls are black with known temperatures, the boundary conditions for Equation 4.34 and Equation 4.35 at the positions $x = 0$ and $x = L$ are, respectively, $I_{j,l}^+(0) = a_j(0)I_b(0)$ and $I_{j,l}^-(L) = a_j(L)I_b(L)$.

Solving Equations 4.34 and 4.35, the radiative heat flux and the heat source, $q_R^{''}$ and $\dot{q}_R$, respectively, at position x, can be determined as [Cassol et al., 2014; Dorigon et al., 2013]:

$$q_R^{''}(x) = \sum_{j=0}^{n_g} \sum_{l=1}^{n_d} 2\pi\mu_l\omega_l \left[I_{j,l}^+(x) - I_{j,l}^-(x) \right] \tag{4.36}$$

$$\dot{q}_R(x) = \sum_{j=1}^{n_g} \sum_{l=1}^{n_d} 2\pi\omega_l\kappa_j \left\{ \left[I_{j,l}^+(x) + I_{j,l}^-(x) \right] - 2a_j(x)I_b(x) \right\} \tag{4.37}$$

where the summation over all gray gases (n_g) represent the spectral integration in the SLW model.

4.3.1 SLW Modeling of Gas Mixture

In the SLW model, when it is considered more than one participating specie Equations 4.30 - 4.33 must be solved for each specie. Thereby, for a mixture of H_2O and CO_2, the absorption coefficient is given as:

$$\kappa_{m,i} = \kappa_{w,j} + \kappa_{c,k} \tag{4.38}$$

where $\kappa_{w,j}$ and $\kappa_{c,k}$ are the local absorption coefficients for the jth and the kth gray gas of H_2O and CO_2, respectively. The value of $\kappa_{w,j}$ and $\kappa_{c,k}$ is calculated using Equation 4.32.

The direct method is considered to be the most accurate approach for treatment of mixtures in the SLW model [Solovjov et al., 2011b]. This method was developed by Denison and Webb, 1995b for binary mixtures, and later extended to multicomponent gas mixtures [Solovjov and Webb, 2000, 2001]. This approach consists of obtaining the ALBDF separately for each specie. Thus, the weighting factor of H_2O and CO_2 can be written as follow, respectively:

$$a_{w,j} = F_w(\tilde{C}_{j+1}, T_b, T_g, P_T, Y) - F_w(\tilde{C}_j, T_b, T_g, P_T, Y) \tag{4.39}$$

$$a_{c,k} = F_c(\tilde{C}_{j+1}, T_b, T_g, P_T, Y) - F_c(\tilde{C}_j, T_b, T_g, P_T, Y) \tag{4.40}$$

in which F_w and F_c are the ALBDFs for H_2O and CO_2, respectively. The values of the ALBDF are calculated for each local mole concentration and temperature.

Finally, the weighting factor for the mixture, used in the RTE, is given by the product of the two individual weights:

$$a_{m,i} = a_{w,j} \times a_{c,k} \tag{4.41}$$

Such approach assumes that the spectra of the individual species are statistically uncorrelated. Including the transparent window, the weighting factor for the mixture must satisfy the relation:

$$\sum_{i=0}^{n_g} a_{m,i} = 1 \tag{4.42}$$

4.4 Summary

The most accurate radiative transfer prediction in participating media is made with the LBL spectral integration of the RTE. However, this method spends a high computational time since it is needed to solve the RTE for hundreds of thousands of spectral lines. The WSGG model came up as a possible alternative. The attractiveness of this method is its relatively simple formulation and implementation with satisfactory accuracy depending on the problem under analysis. The application of the WSGG model consists on first generating the participating gases correlations, which can be obtained for a mixture or for the individual species. The advantage of the individual correlations for each gas is that the radiative problems can be solved for variable partial pressure ratios along the spatial position. For a gas mixture, the combination of the individual correlations is made through the known superposition approach. In this work is proposed the reduced superposition method focused on the computational effort reduction. The superposition method is also used in the SLW model. This method, more complex and detailed, is based on the absorption line blackbody energy distribution function (ALBDF) calculated for each participating specie through its detailed spectrum. Thus, the ALBDFs can be used to calculate the weighting factors of the mixture.

5   RESULTS AND DISCUSSION

5.1   Analyze Between the LBL Solution and the WSGG and SLW Models

After describing the theory of the Gas Models of interest in this work, now it will be applied to the radiative transfer calculation in participating gases. In this chapter will be shown results considering two kinds of non-isothermal problems: homogeneous and non-homogeneous media. For each of them the solutions are carried out first for the individual species, and next for the mixture. The SLW and WSGG solutions for a one-dimensional gas layer are compared against the LBL benchmark solutions in order to evaluate the accuracy of these models.

5.1.1 Radiative Transfer in Non-isothermal, Homogeneous Media

The radiative heat transfer in non-isothermal homogeneous media is now investigated. The solutions are performed using the SLW and WSGG models for a one-dimensional gas layer bounded with two black walls, which are separated by one meter. The results are shown for the radiative heat flux and the heat source for which the LBL integration serves as the benchmark solution in the comparison. The molar concentrations of the gases are assumed to be constant and equal to 0.1 for carbon dioxide (CO_2), and 0.2 for water vapor (H_2O). In all cases the total pressure is 1 atm, and a spatial discretization of 200 points for the grid was used. Furthermore, the discrete ordinates method (DOM) [Cassol et al., 2014; Modest, 2013] was applied for the angular discretization: 40 directions were used for the LBL, 8 for the SLW, 8 for WSGG that uses the Cassol et al., 2014 coefficients and 30 directions for WSGG that uses the Dorigon et al., 2013 coefficients. Previous works show that these spatial and angular discretizations are enough to ensure the solutions independence. [Dorigon et al., 2013; Cassol et al., 2014; Brittes, 2015; Fonseca et al., 2018; Coelho and França, 2018]. For the WSGG model, 4 gray gases for each participating specie were used, as found in the literature. In the SLW formulation, 20 gray gases were adopted since above of this number the solutions does not vary significantly.

To evaluate the spectral models approached in this work, three temperature profiles

were adopted, described as follows:

$$T(x^*) = 400 + 1400\text{sin}^2(\pi x^*) \tag{5.1}$$

$$T(x^*) = 400 + 1400\text{sin}^2(2\pi x^*) \tag{5.2}$$

$$T(x^*) = \begin{cases} 800 + 920\text{sin}^2\left(2\pi x^*\right), & x^* \leq 0.25 \\ 400 + 1400\left\{1 - \text{sin}^{3/4}\left[\dfrac{2}{3}\pi(x^* - 0.25)\right]\right\}, & x^* > 0.25 \end{cases} \tag{5.3}$$

in which $x^* = x/L$, being x the local position, and L the distance between the walls. Figure 5.1 shows these temperature profiles. The cases discussed here are organized according to Table 5.1. The WSGG and SLW deviations with respect to the LBL
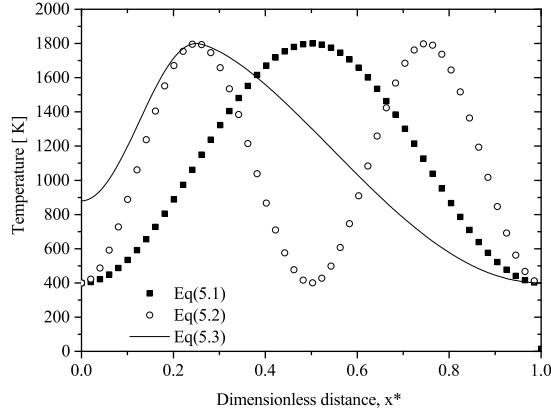
Figure 5.1 – Temperature profiles.

Table 5.1 – Homogeneous testes cases for molar concentration of $Y_{CO_2} = 0.1$ and $Y_{H_2O} = 0.2$.

Test Case	Temperature Profile
1	Eq.(5.1)
2	Eq.(5.2)
3	Eq.(5.3)

integration were computed for both the radiative heat flux, $q_R^{"}$, and the heat source, $-dq_R^{"}/dx$, as follow:

$$\delta(\%) = \frac{\left|q_{R,MODEL}^{"} - q_{R,LBL}^{"}\right|}{\text{max}\left|q_{R,LBL}^{"}\right|} \times 100\% \tag{5.4}$$

$$\zeta(\%) = \frac{\left|(-dq^{"}_{R,MODEL}/dx) - (-dq^{"}_{R,LBL}/dx)\right|}{\max\left|-dq^{"}_{R,MODEL}/dx\right|} \times 100\% \tag{5.5}$$

where δ and ζ are the local deviations in the computation of the radiative heat flux and the heat source, respectively. In Equations 5.4 and 5.5, $\max\left|q^{"}_{R,LBL}\right|$ and $\max\left|-dq^{"}_{R,LBL}/dx\right|$ are the maximum absolute values of the radiative heat flux and heat source for each case under analysis. Of special interest in the discussion will be the maximum deviations, δ_{max} and ζ_{max}, and the average deviations, δ_{avg} and ζ_{avg}, in the domain.

For the three cases presented in this section, two situations are considered. First, the problems are solved for individual species, and, next, for the mixture using both the WSGG and the SLW models. In the WSGG model, the solution for individual species is obtained with the Cassol et al., 2014 coefficients, while for the mixture is adopted both the Dorigon et al., 2013 ($p_w/p_c = 2$) and the Cassol et al., 2014 coefficients. In Case 1, the temperature profile varies symmetrically in the domain, with the temperature ranging from 400 K on the walls to 1800 K in the mid distance between the walls. In Figures 5.2-5.4 are shown the radiative heat flux and the heat source for a layer of CO_2, H_2O and H_2O/CO_2 mixture, respectively.

As can be seen in these figures, for all these problems the radiative heat flux is null in the middle of the domain due to the symmetry of the temperature profile. Since the radiative heat flux is directed from the higher temperature of the medium to the walls, the heat flux is positive for $x^* > 0.5$, and negative for $x^* < 0.5$. The radiative heat source has a peak at $x^* = 0.5$ where the temperature is at its maximum, and the negative sign means that the medium is losing energy due to radiation. For CO_2, the WSGG model presents a worst agreement with the LBL near to the walls for both the radiative heat flux and the heat source. The radiative heat flux of H_2O presents a behavior similar to that of CO_2, while the maximum radiative heat source deviation occurs in the mid distance between the walls, such as happens for the H_2O/CO_2 mixture. For the problems of Case 1, the radiative heat flux deviations for the SLW model has also its maximum value in the middle of the domain.

The SLW and WSGG maximum and average deviations with respect to LBL integration are shown in Table 5.2. For CO_2, with the WSGG model, the maximum and average deviations found for the radiative heat flux were of 11.53 % and 3.46 %, respectively. For the heat source the maximum deviation is 6.72 %, and 4.17 % for the average. When the SLW model is considered, it is seen (Table 5.2) that in average it has a better

(a)   (b)
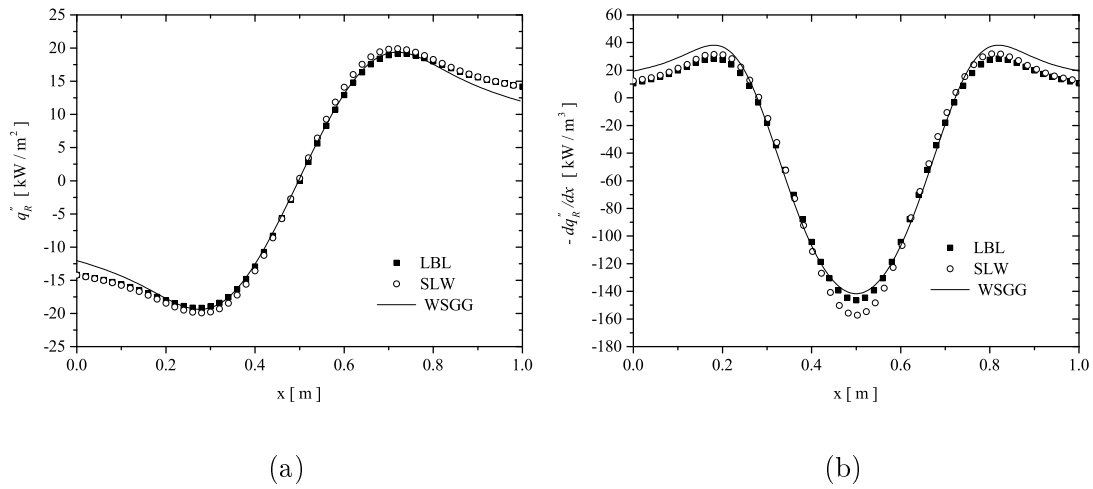
Figure 5.2 – Comparison of the solutions obtained by the LBL integration, SLW and WSGG models for a layer of CO_2 ($Y_{CO_2} = 0.1$), Case 1: (a) radiative heat flux, $q_R^{"}$, (b) radiative heat source, $-dq_R^{"}/dx$.

(a)   (b)
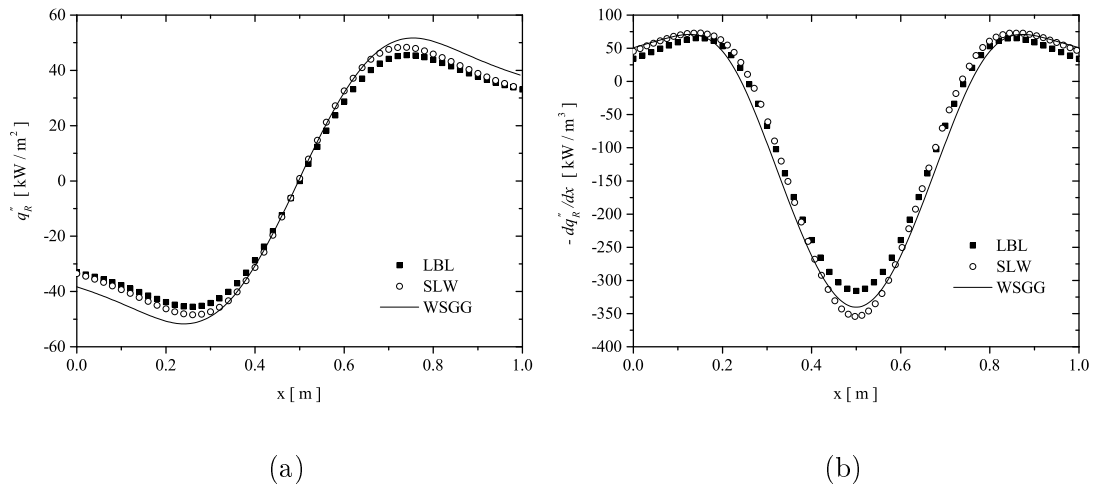
Figure 5.3 – Comparison of the solutions obtained by the LBL integration, SLW and WSGG models for a layer of H_2O ($Y_{H_2O} = 0.2$,), Case 1: (a) radiative heat flux, $q_R^{"}$, (b) radiative heat source, $-dq_R^{"}/dx$.

accuracy than WSGG, specially for the radiative heat flux. In the radiative heat source, the maximum deviation of 7.59 % occurs in the middle of the domain. When the participating gas is H_2O, the deviations increase significantly if compared to those of CO_2 for both the WSGG and the SLW models. However, surprisingly the WSGG maximum radiative heat source deviation is smaller than that for the SLW model for both the H_2O

(a)   (b)
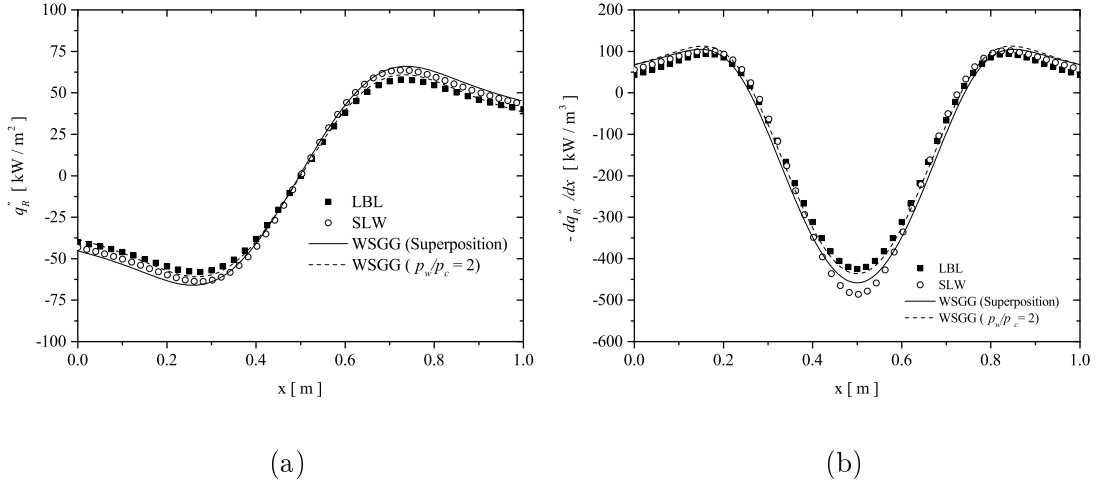
Figure 5.4 – Comparison of the solutions obtained by the LBL integration, SLW and WSGG models for a layer of H_2O/CO_2 mixture ($Y_{H_2O} = 0.2, Y_{CO_2} = 0.1$), Case 1: (a) radiative heat flux, $q_R^{''}$, (b) radiative heat source, $-dq_R^{''}/dx$.

and the CO_2.

The calculations for the H_2O/CO_2 mixture shows that the Dorigon et al., 2013 coefficients ($p_w/p_c = 2$) provides much better agreement with the LBL integration than the superposition methodology applied to both the WSGG and the SLW models. This happens because the superposition approach is a coupling method for the mixture from individual participating species coefficients, and it introduces approximations that are not found when the mixture is made before obtaining the coefficients. Besides that, using the WSGG coefficients for mixture, the RTE is solved only for 4 gray gases and one transparent window, while with the superposition method the RTE is solved 25 times in the WSGG model, and 441 times in the SLW model. Except for the maximum radiative heat source deviation of the mixture, the WSGG model employing the superposition method leads to higher deviations than SLW. Moreover, there is another interesting point to notice: the WSGG for H_2O/CO_2 ($p_w/p_c = 2$) mixture solution has a relevant smaller deviation if compared to the maximum deviations found for individual species.

The Cases 2 and 3 share some conclusions with Case 1 in such a way that only the deviations are shown in this section. The graphics for the radiative heat flux and the heat source can be seen in detail in the Appendix A. Tables 5.3 and 5.4 show the deviations for Cases 2 and 3, where it can be seen that, except for the WSGG heat source deviations

Table 5.2 – Maximum and average deviations of the SLW and WSGG solutions for the radiative heat flux, δ_{max} and δ_{avg}, and the radiative heat source, ζ_{max} and ζ_{avg}, for Case 1.

	$q_R^{''}$		$-dq_R^{''}/dx$	
SLW	$\delta_{max}(\%)$	$\delta_{avg}(\%)$	$\zeta_{max}(\%)$	$\zeta_{avg}(\%)$
CO_2	6.40	2.55	7.59	2.79
H_2O	8.79	4.73	12.28	4.31
H_2O/CO_2	11.48	7.77	14.48	4.38
WSGG	$\delta_{max}(\%)$	$\delta_{avg}(\%)$	$\zeta_{max}(\%)$	$\zeta_{avg}(\%)$
CO_2	11.53	3.46	6.72	4.17
H_2O	15.45	10.51	9.48	5.30
H_2O/CO_2 ($p_w/p_c = 2$)	5.09	2.88	5.72	3.43
H_2O/CO_2 (Superposition)	14.83	10.24	9.93	5.32

of Case 2, the CO_2 deviations are smaller than those of H_2O for both the WSGG and the SLW models, and, in average, the WSGG deviations found for the individual species are greater than those of SLW, as happens in Case 1. As can be noted, the superposition method applied to the WSGG model of Case 2 leads to deviations very closed to those of SLW, indicating that even with just 4 gray gases the WSGG model can be competitive depending on the case under study. For these two cases, the mixture with the Dorigon et al., 2013 coefficients ($p_w/p_c = 2$) also yields the smaller deviations if compared with the LBL benchmark solutions.

Table 5.3 – Maximum and average deviations of the SLW and WSGG solutions for the radiative heat flux, δ_{max} and δ_{avg}, and the radiative heat source, ζ_{max} and ζ_{avg}, for Case 2.

	$q_R^{''}$		$-dq_R^{''}/dx$	
SLW	$\delta_{max}(\%)$	$\delta_{avg}(\%)$	$\zeta_{max}(\%)$	$\zeta_{avg}(\%)$
CO_2	8.66	3.67	11.66	4.32
H_2O	9.54	4.72	16.37	6.53
H_2O/CO_2	12.95	6.18	15.67	5.66
WSGG	$\delta_{max}(\%)$	$\delta_{avg}(\%)$	$\zeta_{max}(\%)$	$\zeta_{avg}(\%)$
CO_2	12.64	5.00	17.53	6.37
H_2O	15.45	7.83	13.81	5.60
H_2O/CO_2 ($p_w/p_c = 2$)	8.31	3.34	13.34	4.77
H_2O/CO_2 (Superposition)	12.65	6.89	16.12	4.72

Table 5.4 – Maximum and average deviations of the SLW and WSGG solutions for the radiative heat flux, δ_{max} and δ_{avg}, and the radiative heat source, ζ_{max} and ζ_{avg}, for Case 3.

	$q_R^{''}$		$-dq_R^{''}/dx$	
SLW	$\delta_{max}(\%)$	$\delta_{avg}(\%)$	$\zeta_{max}(\%)$	$\zeta_{avg}(\%)$
CO_2	1.98	1.00	6.27	1.97
H_2O	5.39	3.06	13.95	3.35
H_2O/CO_2	8.51	5.87	14.46	3.35
WSGG	$\delta_{max}(\%)$	$\delta_{avg}(\%)$	$\zeta_{max}(\%)$	$\zeta_{avg}(\%)$
CO_2	5.06	1.74	8.50	3.65
H_2O	10.72	6.50	11.12	4.88
H_2O/CO_2 $(p_w/p_c = 2)$	4.89	2.77	6.84	2.85
H_2O/CO_2 (Superposition)	11.85	7.71	11.84	4.73

5.1.2 Radiative Transfer in Non-isothermal, Non-homogeneous Media

In real combustion systems the molar concentration of the participating gases is not homogeneous, which means that it varies in the spatial position. For this reason, it will be shown in this section some problems in which the media is non-isothermal and non-homogeneous. The molar concentration profiles adopted for the participating species are described by the following equations:

$$Y_{CO_2}(x^*) = 0.2\sin^2(\pi x^*) \tag{5.6}$$

$$Y_{CO_2}(x^*) = 0.2\sin^2(2\pi x^*) \tag{5.7}$$

$$Y_{CO_2}(x^*) = 0.1\cos^2(2\pi x^*) \tag{5.8}$$

$$Y_{H_2O}(x^*) = 0.2\sin^2(2\pi x^*) \tag{5.9}$$

in which $x^* = x/L$, being x the local position, and L the distance between the walls. Figure 5.5 presents the profiles of these concentration as well as those of temperature. The three test cases studied are organized in Table 5.5. All the computational parameters are the same as those defined for homogeneous media in the previous section.

The first two cases present a constant partial pressure ratio $(p_w/p_c = 2)$ over the domain, while for the Case 3 this ratio vary with the spatial coordinate. For Case 1, both the temperature and the molar concentration profiles present a double symmetry, with

(a)   (b)
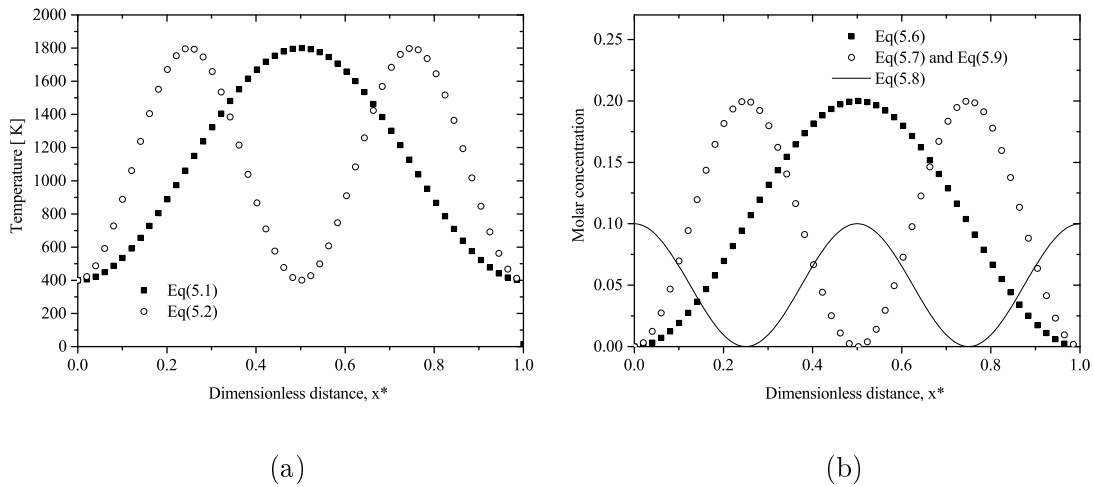
Figure 5.5 – Profiles of (a) temperature and (b) molar concentration of participating species.

Table 5.5 – Test cases considering non-homogeneous molar concentration of the participating species.

Test Case	Temperature Profile	Molar Concentration Profile	
		CO_2	H_2O
1	Eq.(5.2)	Eq.(5.7)	$2Y_{CO_2}$
2	Eq.(5.1)	Eq.(5.6)	$2Y_{CO_2}$
3	Eq.(5.1)	Eq.(5.8)	Eq.(5.9)

two points of maximum: $x^* = 0.25$ and $x^* = 0.75$. The maximum temperature for this case is 1800 K, while the minimum is 400 K and occurs in the walls and in the middle of the domain. Because of the symmetry of the profiles, the radiative heat flux is null in the half distance between the walls. Figures 5.6-5.8 shows the radiative heat flux and the heat source for a layer of CO_2, H_2O and H_2O/CO_2 mixture, respectively. For the H_2O and the H_2O/CO_2 mixture problems, the radiative heat flux presents higher deviations near the walls, in which there are low temperatures and molar concentrations. However, such behavior does not happens for CO_2. Furthermore, in all the problems solved for Case 1, the SLW model leads to the higher deviation of the radiative heat source in the regions of maximum temperature and molar concentration, which was expected.

Table 5.6 shows the deviations of the WSGG and SLW models with respect to the LBL benchmark solution, for individuals participating species and mixture of the Case

(a) (b)
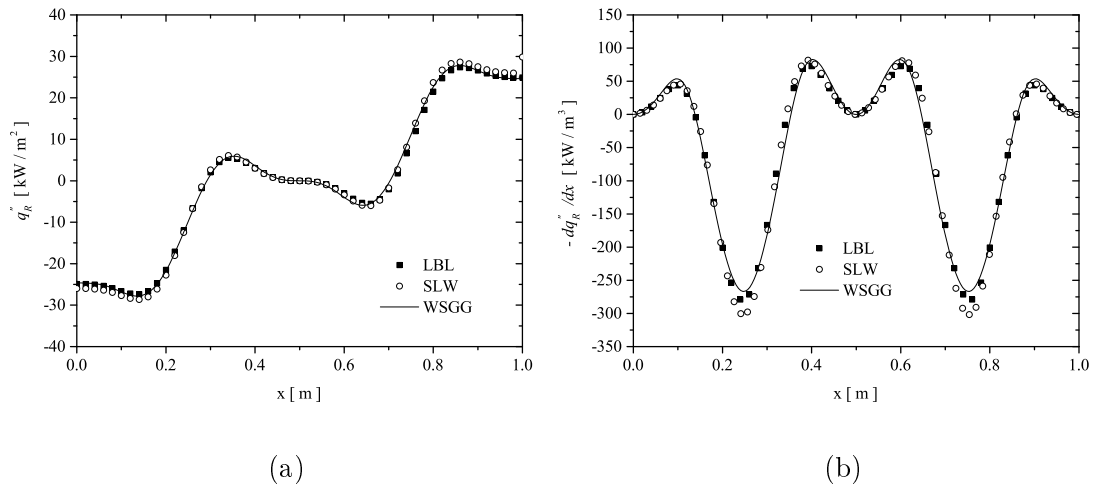
Figure 5.6 – Comparison of the solutions obtained by the LBL integration, SLW and WSGG models for a layer of CO_2, Case 1: (a) radiative heat flux, $q_R^{"}$, (b) radiative heat source, $-dq_R^{"}/dx$.

(a) (b)
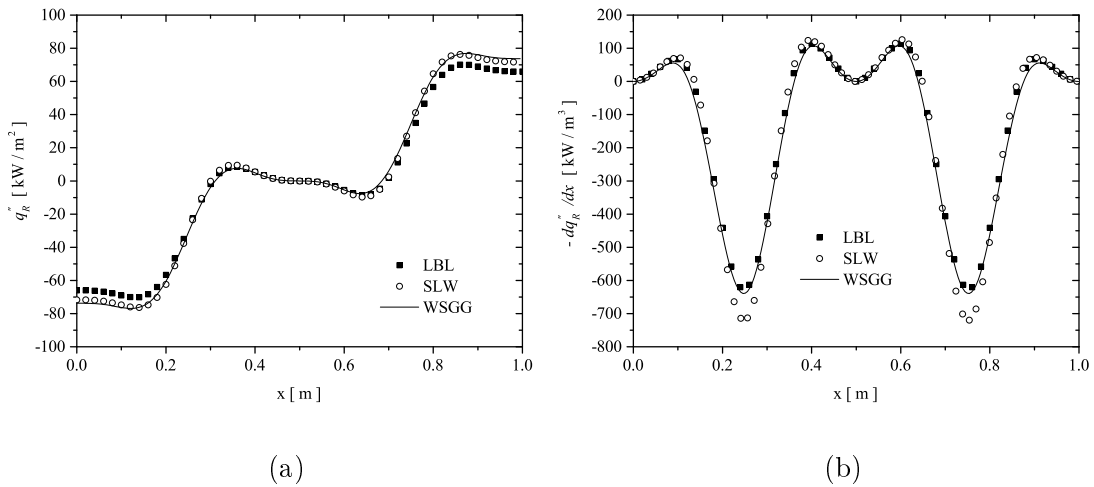
Figure 5.7 – Comparison of the solutions obtained by the LBL integration, SLW and WSGG models for a layer of H_2O, Case 1: (a) radiative heat flux, $q_R^{"}$, (b) radiative heat source, $-dq_R^{"}/dx$.

1. Considering the results of the SLW model, it can be seen that the H_2O, if compared to CO_2, provides the higher deviations. Besides that, the H_2O/CO_2 mixture deviations are greater than those found for individuals species, such as happens, in average, for the WSGG (superposition). Unlike SLW, the H_2O deviations for WSGG model has a higher value than those for CO_2 only for the radiative heat flux, while the maximum and average

(a)

(b)
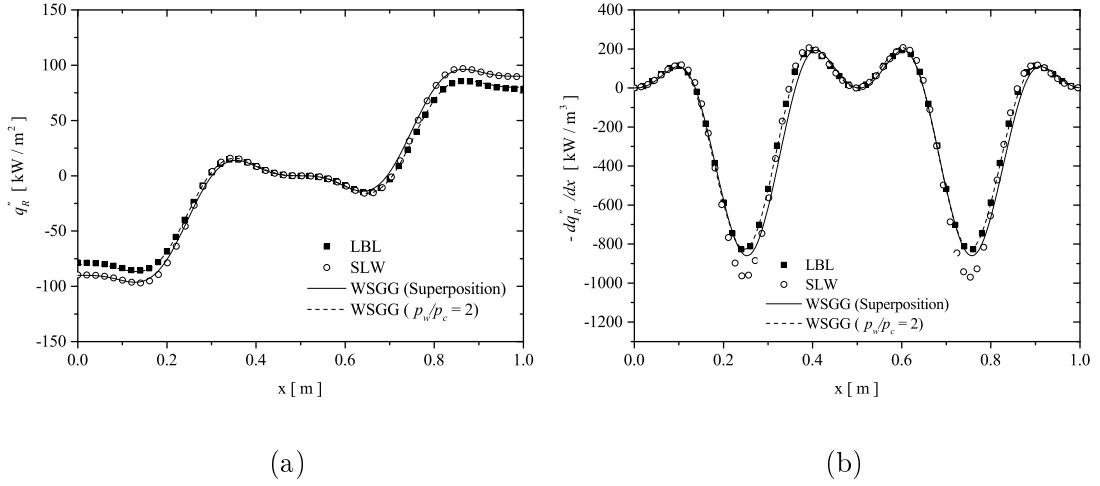
Figure 5.8 – Comparison of the solutions obtained by the LBL integration, SLW and WSGG models for a layer of H_2O/CO_2 mixture ($Y_{H_2O}/Y_{CO_2} = 0.2$), Case 1: (a) radiative heat flux, $q_R^{''}$, (b) radiative heat source, $-dq_R^{''}/dx$.

deviations for the radiative heat source are 8.81 % and 2.46 %, respectively. Moreover, it can be noted that the superposition methodology applied to the WSGG yields, in average, the smaller deviations than SLW, and it also is truth for the individual species. In the comparison of the WSGG and SLW radiative heat flux, it can be seen that the results are close to each other.

Table 5.6 – Maximum and average deviations of the SLW and WSGG solutions for the radiative heat flux, δ_{max} and δ_{avg}, and the radiative heat source, ζ_{max} and ζ_{avg}, for Case 1.

	$q_R^{''}$		$-dq_R^{''}/dx$	
SLW	$\delta_{max}(\%)$	$\delta_{avg}(\%)$	$\zeta_{max}(\%)$	$\zeta_{avg}(\%)$
CO_2	8.19	2.88	10.86	2.90
H_2O	11.45	4.78	16.21	3.85
H_2O/CO_2	15.52	6.97	17.98	4.16
WSGG	$\delta_{max}(\%)$	$\delta_{avg}(\%)$	$\zeta_{max}(\%)$	$\zeta_{avg}(\%)$
CO_2	7.02	1.87	15.13	3.69
H_2O	11.14	5.54	8.81	2.46
H_2O/CO_2 $(p_w/p_c = 2)$	3.62	1.19	6.44	1.57
H_2O/CO_2 (Superposition)	13.22	7.12	14.40	2.84

For Case 2, in general, when the problems are compared with each other, the con-

clusions have the same tendency of those derived from Case 1. Thus, only the computed deviation for the radiative heat flux and the heat source are shown in this section, and the graphics can be seen in detail in Appendix B. As can be observed in Table 5.7, except when it is used the Dorigon et al., 2013 coefficients, in average, the WSGG radiative heat flux deviations are close to those found employing the SLW model. Further, the WSGG radiative heat source maximum deviations for H_2O and H_2O/CO_2 (superposition) mixture are lower than those found employing the SLW model: for H_2O reaches 6.86 %, being 13.57 % in the SLW model; and for H_2O/CO_2 (superposition) this deviation is 13.54 %, while for the SLW model it is 18.44 %. Such results show that the WSGG might compete very well with the SLW, depending on the problem analyzed. It is very important for the thermal radiation field since the WSGG model present a formulation simpler to be implemented than SLW.

Table 5.7 – Maximum and average deviations of the SLW and WSGG solutions for the radiative heat flux, δ_{max} and δ_{avg}, and the radiative heat source, ζ_{max} and ζ_{avg}, for Case 2.

	$q_R^{"}$		$-dq_R^{"}/dx$	
SLW	$\delta_{max}(\%)$	$\delta_{avg}(\%)$	$\zeta_{max}(\%)$	$\zeta_{avg}(\%)$
CO_2	6.31	3.34	8.14	2.23
H_2O	9.89	7.14	13.57	2.97
H_2O/CO_2	14.22	11.38	18.44	3.99
WSGG	$\delta_{max}(\%)$	$\delta_{avg}(\%)$	$\zeta_{max}(\%)$	$\zeta_{avg}(\%)$
CO_2	7.50	2.89	8.98	3.54
H_2O	11.10	8.22	6.86	2.74
H_2O/CO_2 ($p_w/p_c = 2$)	2.13	0.71	1.58	0.72
H_2O/CO_2 (Superposition)	14.48	11.82	13.54	3.63

When the partial pressure ratio (p_w/p_c) is not constant over the domain, the disagreements between the WSGG and the SLW models are more pronounced. This behavior can be observed in Case 3 which was also solved for the individual species as well as for the mixture. The temperature and H_2O molar concentration profiles reach the maximum values at the positions $x^* = 0.25$ and $x^* = 0.75$. On the other hand, in these same locations, the CO_2 molar concentration has the lowest value, which allows for the variable partial pressure ratio p_w/p_c. The radiative heat flux and heat source for CO_2, H_2O,

and H_2O/CO_2 mixture are found in Figures 5.9-5.11, respectively. For the solution of the individual species, the radiative heat flux calculation obtained with WSGG model presents the worst results near the walls. The radiative heat source deviation for CO_2 has its maximum value in the middle of the domain where there is a peak of concentration, and a minimum of temperature; while for H_2O the location where there are the maximum deviations does not coincides with that of maximum temperature or molar concentration.

(a)   (b)
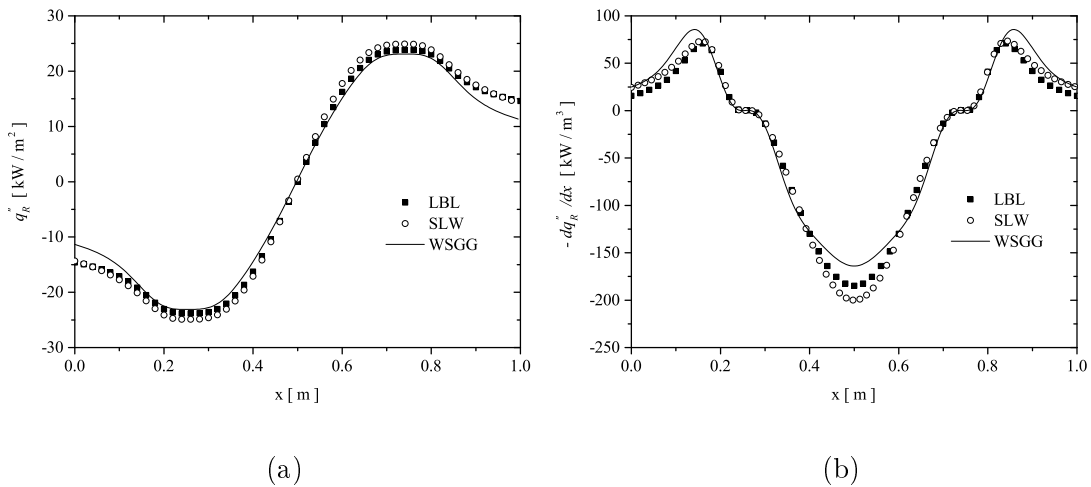
Figure 5.9 – Comparison of the solutions obtained by the LBL integration, SLW and WSGG models for a layer of CO_2, Case 3: (a) radiative heat flux, $q_R^{''}$, (b) radiative heat source, $-dq_R^{''}/dx$.

For all the problems of Case 3 it is seen that the SLW model is significantly more accurate than WSGG. It can also be verified in the deviations shown in Table 5.8. One interesting point to note is that the WSGG ($p_w/p_c = 2$) solution furnish the worst results for the radiative heat source, as found by Cassol et al., 2014. That is expected since the Dorigon et al., 2013 coefficients are generated under the conditions that the partial pressure ratio between the species is 2/1 in all positions in the medium, while in fact the concentration of H_2O is much smaller than that of CO_2 in the middle of the slab. However, among the solutions, such coefficients provides the best result for the radiative heat flux, having the advantage that it require the RTE to be solved only for four gray gases and one transparent window, while with the superposition method the RTE is solved 25 times in the WSGG model, and 441 times in the SLW model.

(a)   (b)
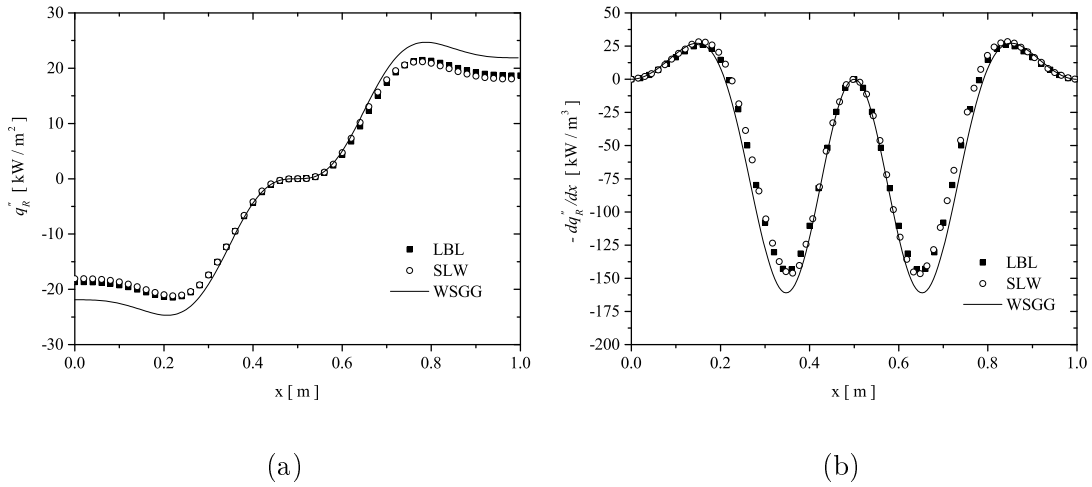
Figure 5.10 – Comparison of the solutions obtained by the LBL integration, SLW and WSGG models for a layer of H_2O, Case 3: (a) radiative heat flux, $q_R^{"}$, (b) radiative heat source, $-dq_R^{"}/dx$.

(a)   (b)
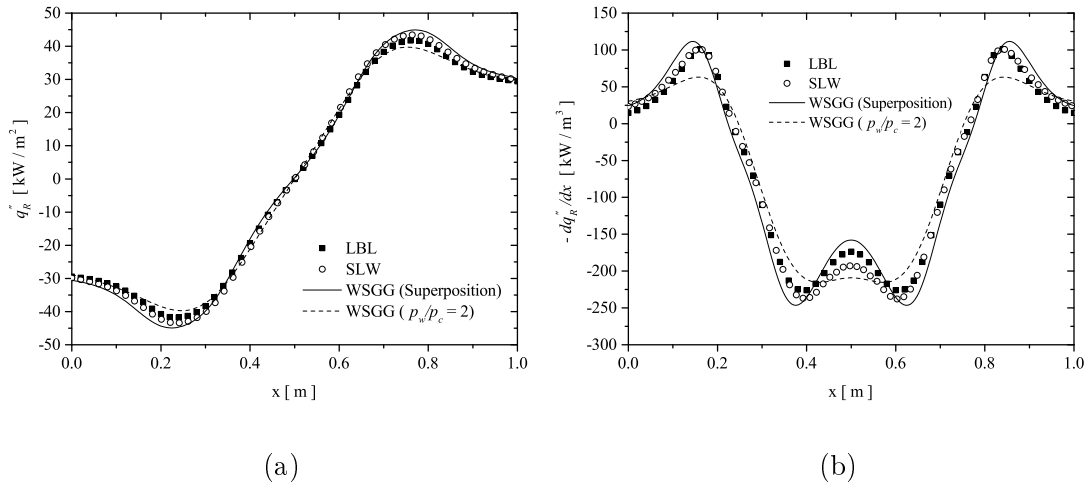
Figure 5.11 – Comparison of the solutions obtained by the LBL integration, SLW and WSGG models for a layer of H_2O/CO_2 mixture, Case 3: (a) radiative heat flux, $q_R^{"}$, (b) radiative heat source, $-dq_R^{"}/dx$.

As seen in the graphics, WSGG $(p_w/p_c = 2)$ overpredicted the absolute value of the radiative heat source in the half distance between the walls. The opposite effect takes place in the vicinity of $x^* = 0.2$ and 0.8, where the use of the WSGG $(p_w/p_c = 2)$ underpredicted the actual amount of H_2O, which is a more effective absorber-emitter than CO_2, leading to an underestimation of the absorption of radiation from the higher

temperature regions in the medium. Another observation is that, for the mixture made through the superposition method, the deviations found are very close to the maximum deviations found for the individual species, or even smaller, in both the SLW and the WSGG models. This behavior does not appears when the partial pressure ratio (p_w/p_c) is constant, for which the H_2O/CO_2 mixture deviations expressively increase if compared to those of individuals species.

Table 5.8 – Maximum and average deviations of the SLW and WSGG solutions for the radiative heat flux, δ_{max} and δ_{avg}, and the radiative heat source, ζ_{max} and ζ_{avg}, for Case 3.

	$q_R^{''}$		$-dq_R^{''}/dx$	
SLW	$\delta_{max}(\%)$	$\delta_{avg}(\%)$	$\zeta_{max}(\%)$	$\zeta_{avg}(\%)$
CO_2	6.35	3.37	8.34	3.02
H_2O	3.43	1.70	7.94	2.32
H_2O/CO_2	6.11	3.17	8.81	3.26
WSGG	$\delta_{max}(\%)$	$\delta_{avg}(\%)$	$\zeta_{max}(\%)$	$\zeta_{avg}(\%)$
CO_2	14.10	5.46	14.21	5.77
H_2O	16.03	9.82	14.79	4.85
H_2O/CO_2 ($p_w/p_c = 2$)	6.06	2.54	16.77	8.49
H_2O/CO_2 (Superposition)	9.58	4.41	14.48	7.08

5.1.3 Summary

The radiative heat transfer calculation was made in a one-dimensional gas layer. For this, both the WSGG and the SLW models were used. The results were compared against the LBL benchmark solutions in order to evaluate the accuracy of these models. The problems were solved for CO_2 and H_2O individually, and for H_2O/CO_2 mixtures considering a non-isothermal homogeneous or non-homogeneous media. In the WSGG model, the Cassol et al., 2014 coefficients were adopted for the individual participating species. These same coefficients were used for the mixture as well as to those of Dorigon et al., 2013. For both the homogeneous and the non-homogeneous media, when p_w/p_c ratio is constant, the results have shown that for both the WSGG and the SLW models, the H_2O deviations, in average, are higher than those found for CO_2. Furthermore, for homogeneous media, the WSGG deviations for individual species are significantly greater than those of SLW, except for the radiative heat source maximum deviation of H_2O;

while for mixtures, when the superposition approach is used, WSGG model can provide results as accurate as the SLW model depending on the problem under analysis. In all the cases where the partial pressure ratio is constant ($p_w/p_c = 0.2$) the Dorigon et al., 2013 coefficients provide the better agreement with the LBL solution. It happens because the superposition approach is a coupling method for the mixture from individual participating species coefficients, and it introduces same approximations that are not found when the mixture is made before obtaining the coefficients. On the other hand, in the case where the partial pressure ratio is not constant over the domain, the superposition method yields the lowest deviations for the radiative heat source. Besides that, in such condition, the deviations for the mixture are very close to the maximum deviations found for the individual species for both the WSGG and the SLW models, contrary to what happens for constant partial pressure ratio.

5.2   Application of the Proposed Reduced Superposition Method

Since the proposed reduced superposition method for the WSGG model was detailed in Chapter 4, now its accuracy will be evaluated in one-dimensional radiative transfer problems. Furthermore, it will be evaluated the consistency of this new proposition for the radiative transfer prediction in laminar diffusion flames.

5.2.1 Radiative Transfer in One-dimensional Problems

The first case is a non-isothermal non-homogeneous H_2O/CO_2 mixture. The temperature profile is that given by Equation 5.2, shown in Section 5.1.1. The CO_2 concentration profile (Y_{CO_2}) is described by Equation 5.7 in Section 5.1.2, being that $Y_{H_2O} = 2Y_{CO_2}$. Thus, the partial pressure ratio (p_w/p_c) between the species is constant through the domain and equal to 2.

For this case, the radiative heat flux and heat source were computed. Theses quantities were calculated using the WSGG model. Therefore, were adopted the standard superposition method [Cassol et al., 2014] and the reduced superposition method proposed in this work. The solutions obtained with these two approaches are compared against the LBL integration. As can be seen in Figure 5.12, there is no visible difference between the standard and the reduced superposition method solutions for both the radiative heat flux and the heat source. The disagreement between the solutions is only found when

the normalized deviations with respect to the LBL benchmark solutions are computed, as shown in Table 5.9. For the radiative heat flux, the maximum normalized deviation found with the standard and the reduced superposition method were 12.40 % and 12.33 %, respectively; accordingly, the maximum deviations for the radiative heat source were 13.22% and 12.38%.

(a)   (b)

Figure 5.12 – Comparison of the solutions obtained with the WSGG model, considering the standard superposition method and the proposed reduced superposition method, for a H_2O/CO_2 mixture. The solutions are also compared against the LBL integration for the (a) radiative heat flux, $q_R^{''}$ and (b) radiative heat source, $-dq_R^{''}/dx$, for temperature and CO_2 molar concentration given by Equations 5.2 and 5.7 with $p_w/p_c = 2$.

Table 5.9 – Maximum and average deviations of the WSGG solutions for the radiative heat flux, δ_{max} and δ_{avg}, and the radiative heat source, ζ_{max} and ζ_{avg}, considering the standard superposition method and the proposed reduced superposition method, for temperature and CO_2 molar concentration given by Equations 5.2 and 5.7 with $p_w/p_c = 2$.

WSGG	$q_R^{''}$		$-dq_R^{''}/dx$	
	$\delta_{max}(\%)$	$\delta_{avg}(\%)$	$\zeta_{max}(\%)$	$\zeta_{avg}(\%)$
Standard-Superposition	12.40	2.84	13.22	7.13
Reduced-Superposition	12.33	2.70	12.38	6.77

The next case is also a non-isothermal non-homogeneous media containing a H_2O/CO_2

gas layer. The temperature profile is given by Equation 5.1, in Section 5.1.1, and the molar concentration of CO_2 and H_2O are represented by Equations 5.8 and 5.9, receptively, in Section 5.1.2. Unlike first case, in this one the partial pressure ratio (p_w/p_c) between the participating species vary along the spatial position. The results for the radiative heat flux and heat source are shown in Figure 5.13, and again it can be seen that the standard and the reduced superposition method provide coincident solutions. When compared with the LBL solution, the deviations found are those presented in Table 5.10. For the radiative heat flux the maximum normalized deviation applying the standard and the reduced superposition method are 14.48% and 13.92%, respectively. Extending these calculations for the radiative heat source, the maximum deviation are, accordingly, 9.58% and 9.18%.

(a)   (b)

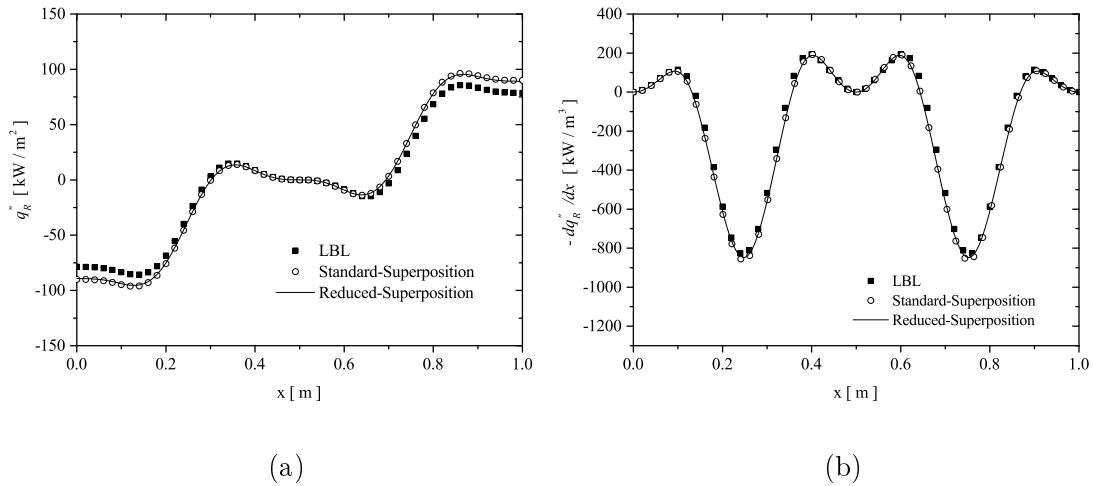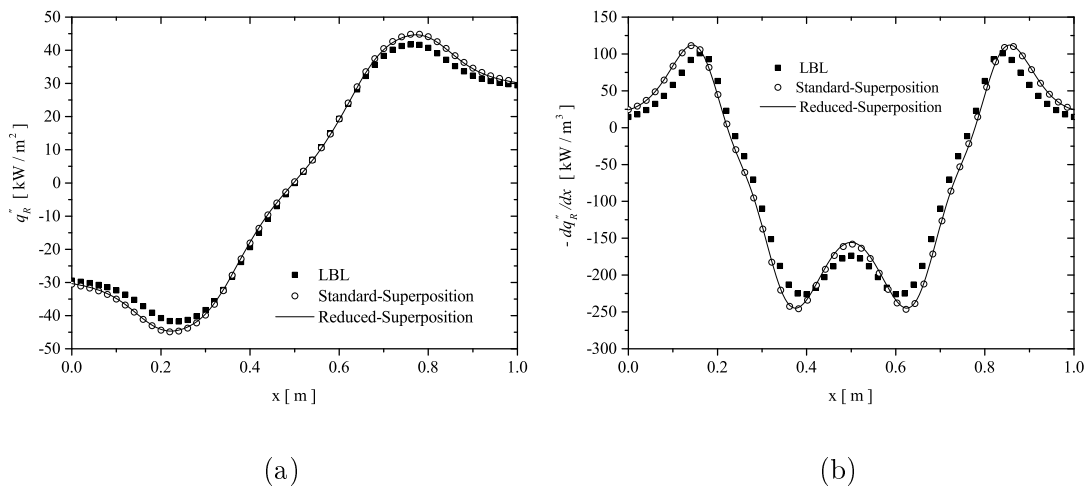Figure 5.13 – Comparison of the solutions obtained by the WSGG model, considering the standard superposition method and the proposed reduced superposition method, for a H_2O/CO_2 mixture. The solutions are also compared against the LBL integration for the (a) radiative heat flux, $q_R^{"}$ and (b) radiative heat source, $-dq_R^{"}/dx$. The temperature profile is given by Equation 5.1, and the molar concentration of CO_2 and H_2O represented by Equations 5.8 and 5.9, receptively.

The results presented in this section show the relevance of the proposed reduced superposition method for radiative transfer prediction in combustion gases. Considering the standard superposition method, for a H_2O/CO_2 mixture, the RTE must be solved 25 times. Employing the reduced superposition method this number is reduced to 13.

Table 5.10 − Maximum and average deviations of the WSGG solutions for the radiative heat flux, δ_{max} and δ_{avg}, and the radiative heat source, ζ_{max} and ζ_{avg}, considering the standard superposition method and the proposed reduced superposition method, for temperature profile given by Equation 5.1, and the molar concentration of CO_2 and H_2O represented by Equations 5.8 and 5.9, receptively.

	$q_R^{"}$		$-dq_R^{"}/dx$	
WSGG	$\delta_{max}(\%)$	$\delta_{avg}(\%)$	$\zeta_{max}(\%)$	$\zeta_{avg}(\%)$
Standard-Superposition	14.48	7.08	9.58	4.41
Reduced-Superposition	13.92	7.29	9.18	4.07

As already discussed in Chapter 4, this result is of great relevance when concerning computational effort. It gains even more importance when it is working with more than two participating species. In the case of three components, the RTE should be solved 125 times applying the standard superposition method. Since the combustion system modeling requires the consideration of even more components, the computational time increases significantly for the computation of the radiative transfer. Despite the proposed reduced superposition method working for one-dimensional problems, its validity also needs to be evaluated for the radiative transfer solution in combustion systems such as diffusion flames. Such discussion is the aim of the following section.

5.2.2 Evaluation of the Consistency of the Reduced Superposition Method in Diffusion Flames

The radiative transfer prediction using the WSGG model with the reduced superposition method was carried out for H_2O/CO_2 mixtures in one-dimensional domain in the previous section. However, it is important to verify the consistency of this new proposition in combustion systems, where the H_2O and the CO_2 are the main combustion products. For this, it was chosen a laminar diffusion flame. The diffusive term means that the fuel and the oxidant are not premixed.

The laminar diffusion flame has CH_4 as fuel, without dilution, and air as oxidant. For the evaluation of the consistency of the reduced superposition method it is necessary to know the fields of temperature, molar concentration of H_2O and CO_2, as well as the partial pressure ratio p_w/p_c between these species in the flame. As already discussed, the

partial pressures p_w and p_c are important for the absorption coefficient calculation for the gray gases. Moreover, the ratio between these partial pressures needs to be on scale with 1 ($p_w/p_c \sim 1$) over the domain for the proposed reduced superposition method to be valid. Otherwise, if p_w/p_c ratio is much larger or much smaller, the proposed reduced superposition method may not predict accurately the radiative transfer. In such case it is necessary to evaluate if the regions where it happens are important or not for the thermal radiation.

In Figure 5.14 it is shown the variables of interest in this analysis for the laminar flame. There is a symmetry axis at the right vertical edge. The flame was simulated in the ANSYS/Fluent 18, and the results are a courtesy of the colleague Luís Gustavo Pires Rodrigues. As can be observed in the p_w/p_c field, there are regions where this ratio is not on scale with 1. However, it is important to note that such regions are not relevant from the thermal radiation point of view. That is true because the radiative transfer is significant in the regions of high temperature and molar concentrations of the participating species. Thus, analyzing Figures 5.14 (a), (b) and (c), it can be seen that the regions of interest for the thermal radiation are not coincident with those of very high and very low p_w/p_c ratios. Thereby, even if the reduced superposition method does not work for such conditions, the regions where that happens do not have a relevant contribution in the radiative transfer calculation. Even if there are regions of high and low partial pressure ratios, in average this ratio are close to 2, which is on scale with 1. To verify that, the following expression can be used for the average partial pressure ratio computation in the flame:

$$\bar{r} = \frac{\displaystyle\int_V \alpha r dV}{\displaystyle\int_V \alpha dV} \tag{5.10}$$

in which α is given as $(p_w + p_c)T^4$, being T the local temperature; and r is the local partial pressure ratio (p_w/p_c). The integration is made over each finite volume. Solving this equation for the laminar flame, it yields $\bar{r} = 1.989$, which satisfy the conditions for the proposed reduced superposition to be valid.
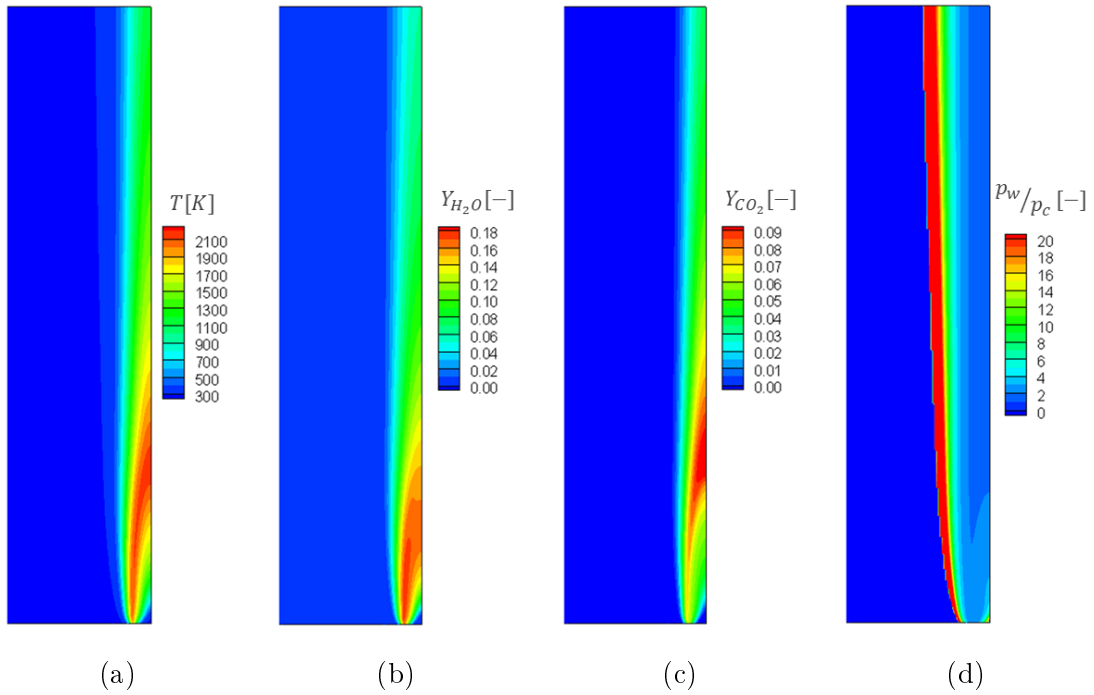
Figure 5.14 – Fields of (a) temperature, (b) H_2O and (c) CO_2 molar concentrations, and (d) the partial pressure ratio (p_w/p_c) for the laminar diffusion flame.

5.2.3 Summary

In this section was verified the accuracy and the consistency of the reduced superposition method proposed in this work. The radiative transfer prediction in one-dimensional domain was performed for non-isothermal and non-homogeneous problems. In such case it was considered both the constant and the non-constant partial pressure ratio (p_w/p_c) over the spatial position. The proposed methodology provided solutions as accurate as those found employing the standard superposition method, with the advantage that the number of times the RTE is solved was reduced by half. In addition, it was concluded that the reduced superposition method also is valid for the radiative transfer prediction in laminar diffusion flames. Although this method does not work for very high and very low p_w/p_c ratios, the regions where it happens in these flames are not important for the thermal radiation calculations.

6   CONCLUSIONS AND PERSPECTIVES

In this work, the radiative transfer was computed in one-dimensional problems employing both the WSGG and the SLW models. The results for the radiative heat flux and the heat source were compared against the LBL benchmark solution in order to evaluate the accuracy of these models. Therefore, its was considered non-isothermal homogeneous and non-homogeneous media with different temperature and concentration profiles of the participating species. The first step was to solve the problems for H_2O and CO_2 individually, and, next, for H_2O/CO_2 mixtures. The objective of doing that was to compare the accuracy of the WSGG and SLW models for several media conditions. Furthermore, the main challenge in the superposition method is the combination of participating gases since it requires increasing computational time as the components number increase. Thus, for the WSGG model, it was proposed a reduced superposition method capable of reducing the computational effort. Its accuracy was verified in one-dimensional radiative problems. Finally, the consistency of this new approach was proved in diffusion flames. The main conclusions of this study can be summarized as follow:

- In homogeneous media, analyzing the individual species solutions, the SLW model proved to be more accurate than WSGG. For both the WSGG and the SLW models, the H_2O normalized deviations found for the radiative heat flux and the heat source were expressively higher than those for CO_2. When the solution was carried out for H_2O/CO_2 mixtures, the deviations, in average, reached values close to those found for H_2O (maximum deviations between the individual species). Further, the superposition method applied to WSGG model, even with just four gray gases for each specie, led to results very close to those of SLW depending on the problem under analyze. It shows that despite the simple formulation, the WSGG model may compete very well with more sophisticated gas models in the solutions of thermal radiation problems. In all the test cases, for mixtures, the Dorigon et al., 2013 coefficients provided the best results, which make sense since such correlations were generated specifically for mixtures where the partial pressure ratio (p_w/p_c) is constant.

- When the media is non-homogeneous, for constant partial pressure ratio, in both the mixture and the individual species, the solutions lead to same conclusions that those derived from homogeneous media. However, if variable partial pressure ra-

tio is considered, the disagreements between the WSGG and the SLW models are more pronounced. The SLW model shown to be, in average, significantly more accurate than WSGG for both the mixture and the individual species. Moreover, when Dorigon et al., 2013 coefficients for mixture was applied provided the higher deviation for the radiative heat source, and the better results for the radiative heat flux. This result show that these coefficients may be a good option even when the partial pressure ratio is not constant, depending on the result of interest, having the advantage that it require the RTE to be solved only for four gray gases and one transparent window, while with the superposition method the RTE was solved 25 times in the WSGG model, and 441 times in the SLW model.

- The proposed reduced superposition method applied to the WSGG model led to solutions as good as those of the standard superposition method in the computation of the radiative transfer in one-dimensional problems for both constant and non-constant partial pressure ratio (p_w/p_c). Since the combination of participating species is the main challenge of the standard superposition method, this result is very important for the thermal radiation prediction from combustion gases due to the fact that the number of times need to solve the radiative transfer equation (RTE) is reduced by half. In combustion system, where the thermal radiation calculation need to be coupled with others complex mechanisms such as chemical kinetic and turbulence, this computational time reduction become of great relevance.

- The consistency of the reduced superposition method in methane diffusion laminar flames was certified. Since the proposition made in this work is valid when $p_w/p_c \sim$ 1, the fields of temperature, molar concentrations of H_2O and CO_2, and partial pressure ratio (p_w/p_c) were analyzed. Thereby, it was verified that the regions in the flame where p_w/p_c is not in scale with 1 are not important for thermal radiation. This phenomenon become relevant only in locations of high temperature and molar concentrations of the participating species, and in such regions the relation $p_w/p_c \sim$ 1 was satisfied.

The perspectives of this work are:

(i) It is important to extend the reduced superposition method to thermal radiation prediction in diffusion flames, and, thus, analyze the accuracy of this approach in

such conditions;

(ii) As realized for the WSGG model, the development of a new approach for optimization of the superposition method applied to SLW model is of great interest for the computational effort reduction;

(iii) Another perspective is to couple the optimized superposition method with an adequate approach to consider turbulence-radiation iterations (TRI) and soot formation in combustion processes.

BIBLIOGRAPHY

Al-Omari, S. A. B. On the sensitivity of soot and thermal radiation simulation results to the adopted PDF for temperature under highly sooting combustion conditions, **International Communications in Heat and Mass Transfer**, vol. 33, p. 1273–1280, 2006.

Andre, F., Solovjov, V., Lemonnier, D., and Webb, B. Comonotonic global spectral models of gas radiation in non-uniform media based on arbitrary probability measures, **Applied Mathematical Modelling**, vol. 50, p. 741–754, 2017.

Çayan, F. N. and Selçuk, N. A comparative study of modeling of radiative heat transfer using MOL solution of DOM with gray gas, wide-band correlated-k and spectral line-based weighted sum of gray gases models, **Numerical Heat Transfer**, vol. 52, p. 281–296, 2007.

Becher, V., Goanta, A., and Spliethoff, H. Validation of spectral gas radiation models under oxyfuel conditions – Part C: Validation of simplified models, **International Journal of Greenhouse Gas Control**, vol. 11, p. 34–51, 2012.

Bhuiyan, A. A. and Naser, J. Numerical modelling of oxy fuel combustion, the effect of radiative and convective heat transfer and burnout, **Fuel**, vol. 139, p. 268–284, 2015.

Bressloff, N. W. The influence of soot loading on weighted sum of gray gases solutions to the radiative transfer equation across mixtures of gases and soot, **International Journal of Heat and Mass Transfer**, vol. 42, p. 3469–3480, 1999.

Brittes, R., Centeno, F. R., Ziemniczak, A., and França, F. H. R. WSGG Model Correlations to Compute Nongray Radiation From Carbon Monoxide in Combustion Applications, **Journal of Heat Transfer**, vol. 139, p. 041202:1–7, 2017.

Brittes, R. S. **Desenvolvimento de um Novo Modelo para Integração Espectral da RTE em Problemas Não Homogêneos e Não Isotérmicos**. PhD thesis, Universidade Federal do Rio Grande do SUL, 2015.

Cassol, F., Brittes, R., Centeno, F. R., da Silva, C. V., and França, F. H. R. Evaluation of the gray gas model to compute radiative transfer in non-isothermal, non-homogeneous participating medium containing CO2, H2O and soot, **Journal of the Brazilian Society of Mechanical Sciences and Engineering**, vol. 37(1), p. 163–172, 2015.

Cassol, F., Brittes, R., França, F. H., and Ezekoye, O. A. Application of the weighted-sum-of-gray-gases model for media composed of arbitrary concentrations of H2O, {CO2} and soot, **International Journal of Heat and Mass Transfer**, vol. 79, p. 796 – 806, 2014.

Centeno, F. R., Brittes, R., França, F. H., and da Silva, C. V. Application of the WSGG model for the calculation of gas–soot radiation in a turbulent non-premixed

methane–air flame inside a cylindrical combustion chamber, **International Journal of Heat and Mass Transfer**, vol. 93, p. 742–753, 2016.

Centeno, F. R., Brittes, R., Rodrigues, L. G., Coelho, F. R., and França, F. H. Evaluation of the WSGG model against line-by-line calculation of thermal radiation in a non-gray sooting medium representing an axisymmetric laminar jet flame, **International Journal of Heat and Mass Transfer**, vol. 124, p. 475–483, 2018.

Centeno, F. R., Cassol, F., Vielmo, H. A., França, F. H. R., and Silva, C. V. Comparison of different WSGG correlations in the computation of thermal radiation in a 2D axisymmetric turbulent non-premixed methane–air flame, **Journal of the Brazilian Society of Mechanical Sciences and Engineering**, vol. 35, p. 419–430, 2013.

Centeno, F. R., Silva, C. V., and França, F. H. R. The influence of gas radiation on the thermal behavior of a 2D axisymmetric turbulent non-premixed methane–air flame, **Energy Conversion and Management**, vol. 79, p. 405–414, 2014.

Chu, H., Liu, F., and Zhou, H. Calculations of gas radiation heat transfer in a two-dimensional rectangular enclosure using the line-by-line approach and the statistical narrow-band correlated-k model, **International Journal of Heat and Mass Transfer**, vol. 59, p. 66–74, 2012.

Coelho, F. R. and França, F. H. R. WSGG correlations based on HITEMP2010 for gas mixtures of H_2O and CO_2 in high total pressure conditions, **International Journal of Heat and Mass Transfer**, vol. 127, p. 105–114, 2018.

Coelho, P. J. Numerical simulation of radiative heat transfer from non-gray gases in three-dimensional enclosures, **Journal of Quantitative Spectroscopy & Radiative Transfer**, vol. 74, p. 307–328, 2002.

Coelho, P. J. Turbulence–Radiation Interaction: From Theory to Application in Numerical Simulations, **Journal of Heat Transfer**, vol. 134, p. 1–13, 2012.

Consalvi, J. L. and Liu, F. Radiative heat transfer in the core of axisymmetric pool fires e I: Evaluation of approximate radiative property models, **International Journal of Heat and Mass Transfer**, vol. 84, p. 104–117, 2014.

Crnomarkovic, N., Sijercic, M., Belosevic, S., Tucakovic, D., and Zivanovic, T. Numerical investigation of processes in the lignite-fired furnace when simple gray gas and weighted sum of gray gases models are used, **International Journal Of Heat and Mass Transfer**, vol. 56, p. 197–205, 2013.

Demarco, R., Consalvi, J. L., Fuentes, A., and Melis, S. Assessment of radiative property models in non-gray sooting media, **International Journal of Heat and Mass Transfer**, vol. 50, p. 1672–1684, 2011.

Demarco, R. A. B. **Modelling thermal radiation and soot formation in buoyant diffusion flames**. PhD thesis, Universite de Provence, Aix-Marseille I, 2012.

Denison, M. K. and Webb, B. W. An absorption-line blackbody distribution function for efficient calculation of total gas radiative transfer, **Journal of Quantitative Spectroscopy & Radiative Transfer**, vol. 50, p. 499–510, 1993a.

Denison, M. K. and Webb, B. W. A spectral-line based weighted-sum-of-gray-gases model for arbitrary RTE solvers, **Journal of Heat Transfer**, vol. 115, p. 1004–1011, 1993b.

Denison, M. K. and Webb, B. W. Development and application of an absorption-line blackbody distribution function for CO_2, **International Journal of Heat and Mass Transfer**, vol. 38, p. 1813–1821, 1995a.

Denison, M. K. and Webb, B. W. The spectral line-based weighted sum-of-gray-gases model for H_2O/CO_2 mixtures, **Journal of Heat Transfer**, vol. 117, p. 788–792, 1995b.

Denison, M. K. and Webb, B. W. The spectral line-based weighted sum-of-gray-gases model in nonisothermal nonhomogeneous media, **Journal of Heat Transfer**, vol. 117, p. 359–365, 1995c.

Dorigon, L. J., Duciak, G., Brittes, R., Cassol, F., Galarça, M., and França, F. H. WSGG correlations based on HITEMP2010 for computation of thermal radiation in non-isothermal, non-homogeneous H2O/CO2 mixtures, **International Journal of Heat and Mass Transfer**, vol. 64, p. 863 – 873, 2013.

Edwards, D. K. and Balakrishnan, A. Thermal Radiation by Combustion gases, **International Journal of Heat and Mass Transfer**, vol. 16, p. 25–40, 1973.

Fischer, J., Gamache, R. R., Goldeman, A., Rothman, L. S., and Perrin, A. Total internal partition sums for molecular species in the 2000 edition of the HITRAN database, **Journal of Quantitative Spectroscopy & Radiative Transfer**, vol. 82, p. 401–412, 2003.

Fluent, A. **Fluent, ANSYS Academic Research, Release 18**, 2018.

Fonseca, R. C. and França, F. H. R. **Application of the weighted-sum-of-gray-gases model in enclosures with gray surfaces**. In *Proceedings of the 23rd International Congress of Mechanical Engineering*, 2015.

Fonseca, R. J. C., Fraga, G. C., Silva, R. B., and França, F. H. R. Application of the WSGG Model to Solve the Radiative Transfer in Gaseous Systems With Nongray Boundaries, **Journal of Heat Transfer**, vol. 140, p. 1–10, 2018.

Fraga, G., Centeno, F., Petry, A., and França, F. Evaluation and optimization-based modification of a model for the mean radiative emission in a turbulent non-reactive flow, **International Journal of Heat and Mass Transfer**, vol. 114, p. 664–674, 2017.

Galarça, M. M., Maurente, A., Vielmo, H. A., and França, F. H. R. **Correlations for the weighted-sum-of-gray-gases generated from the absorption-line blackbody distribution function**. In *Proceedings of the 12th Brazilian of Thermal Sciences and Engineering*, 2008.

Galarça, M. M., Mossi, A., and França, F. H. R. A modification of the cumulative wavenumber method to compute the radiative heat flux in non-uniform media, **Journal of Quantitative Spectroscopy & Radiative Transfer**, vol. 112, p. 384–393, 2011.

Garten, B., Hunger, F., Messig, D., Stelzner, B., Trimis, D., and Hasse, C. Detailed radiation modeling of a partial-oxidation flame, **International Journal of Thermal Sciences**, vol. 87, p. 68–84, 2015.

G.Clements, A., Porter, R., Pranzitelli, A., and Pourkashanian, M. Evaluation of FSK models for radiative heat transfer under oxyfuel conditions, **Journal of Quantitative Spectroscopy & Radiative Transfer**, vol. 151, p. 67–75, 2015.

Godson, W. L. The Evaluation of Infrared Radiation Fluxes Due to Atmospheric Water Vapor, **Quarterly Journal of Royal Meteorological Society**, vol. 79, p. 367–379, 1953.

Goody, R. M. A statistical model to water-vapor absorption, **Quarterly Journal of the Royal Meteorological Society**, vol. 78, p. 165–169, 1952.

Goody, W. L. and Yung, Y. L. **Atmospheric Radiation**. Clarendon Press, Oxford - United Kingdom, 1989.

Gordon, I. E., Rothman, L. S., Hill, C., Kochanov, R. V., Tana, Y., Bernath, P. F., Birk, M., Boudon, V., Campargue, A., Chance, K. V., Drouin, B. J., Flaud, J. M., Gamache, R. R., Hodges, J. T., Jacquemart, D., Perevalovm, V. I., Perrin, A., Shine, K. P., Smith, M. A. H., Tennyson, J., Toon, G. C., Tran, H., Tyuterev, V. G., Barbe, A., Császár, A. G., Devi, V. M., Furtenbacher, T., Harrison, J. J., Hartmann, J. M., Jolly, A., Johnson, T. J., Karman, T., Kleiner, I., Kyuberis, A. A., Loos, J., Lyulin, O. M., Massie, S. T., S. N. Mikhailenkom, N. M.-A., Müller, H. S. P., O. V. Naumenkom, A. V. Nikitinm, O. L. P., Rey, M., Rotger, M., Sharpe, S. W., Sung, K., Starikovam, E., Tashkunm, S. A., Auwera, J. V., Wagner, G., Wilzewski, J., Wcisło, P., Yuh, S., and Zak, E. J. The HITRAN2016 molecular spectroscopic database, **Journal of Quantitative Spectroscopy & Radiative Transfer**, vol. 203, p. 3–69, 2017.

Goutiere, V., Liu, F., and Charette, A. An assessment of real-gas modelling in 2D enclosures, **Journal of Quantitative Spectroscopy & Radiative Transfer**, vol. 64, p. 299–326, 2000.

Hottel, H. C. and Sarofim, A. F. **Radiative Transfer (McGraw-Hill Series in Mechanical Engineering)**. McGraw-Hill, 1967.

Howell, J. R. and Siegel, R. **Thermal Radiation heat transfer**. Taylor & Francis, 4*th* edition, 2002.

Howell, J. R., Siegel, R., and Mengüç, M. P. **Thermal Radiation heat transfer**. CRC Press, 5*th* edition, 2010.

Ismail, K. A. R. and Salinas, C. T. Application of a local-spectrum correlated model to modeling radiative transfer in a mixture of real gas media in bidimensional enclosures, **Numerical Heat Transfer**, vol. 47, p. 183–207, 2005.

Johansson, R., Leckner, B., Andersson, K., and Johnsson, F. Account for variations in the H2O to CO2 molar ratio when modeling gaseous radiative heat transfer with the weighted-sum-of-grey-gases model, **Combustion and Flame**, vol. 158, p. 893–901, 2011.

Kangwanpongpan, T., França, F. H., da Silva, R. C., Schneider, P. S., and Krautz, H. J. New correlations for the weighted-sum-of-gray-gases model in oxy-fuel conditions based on HITEMP 2010 database, **International Journal of Heat and Mass Transfer**, vol. 55, p. 7419–7433, 2012.

Krishnamoorthy, G. A new weighted-sum-of-gray-gases model for CO2–H2O gas mixtures, **International Communications in Heat and Mass Transfer**, vol. 37, p. 1182–1186, 2010.

Liu, F. and Smallwood, G. J. An efficient approach for the implementation of the SNB based correlated-k method and its evaluation, **Journal of Quantitative Spectroscopy & Radiative Transfer**, vol. 84, p. 465–475, 2004.

Ma, J., Li, B.-W., and Howell, J. R. Thermal radiation heat transfer in one- and two-dimensional enclosures using the spectral collocation method with full spectrum k-distribution model, **International Journal of Heat and Mass Transfer**, vol. 71, p. 35–43, 2014.

Maurente, A., Vielmo, H. A., and França, F. H. R. Comparison of the standard weighted-sum-of-gray-gases with the absorption-line blackbody distribution function for the computation of radiative heat transfer in H2O/CO2 mixtures, **Journal of Quantitative Spectroscopy & Radiative Transfer**, vol. 109, p. 1758–1770, 2008.

Mazumder, S. and Modest, M. F. Application of the Full Spectrum Correlated-k Distribution Approach to Modeling Non-Gray Radiation in Combustion Gases, **Combustion and Flame**, vol. 129, p. 416–438, 2002.

McClatchey, R. A., Benedict, W. S., Clough, S. A., Burch, D. E., Fox, K., Rothman, L. S., and Garing, J. S. AFCRL Atmospheric Absorption Line Parameters Compilation, **Technical Report**, vol. 434, p. AFCRL–TR–73–0096, 1973.

Modest, M. F. The Weighted-Sum-of-Gray-Gases Model for Arbitrary Solution Methods in Radiative Transfer, **Transactions of the ASME**, vol. 113, p. 650–656, 1991.

Modest, M. F. Narrow-band and full-spectrum k-distributions for radiative heat transfer—correlated-k vs. scaling approximation, **Journal of Quantitative Spectroscopy & Radiative Transfer**, vol. 76, p. 69–83, 2003a.

Modest, M. F. **Radiative heat transfer**. Academic press, $2th$ edition, 2003b.

Modest, M. F. **Radiative heat transfer**. Academic press, $3th$ edition, 2013.

Modest, M. F. and Haworth, D. C. **Radiative Heat Transfer in Turbulent Combustion Systems - Theory and Applications**. SpringerBriefs in Applied Sciences and Technology, New York, 2016.

Modest, M. F. and Riazzi, R. J. Assembly of full-spectrum k-distributions from a narrow-band database; efects of mixing gases, gases and nongray absorbing particles, and mixtures with nongray scatterers in nongray enclosures, **Journal of Quantitative Spectroscopy & Radiative Transfer**, vol. 90, p. 169–89, 2005.

Modest, M. F. and Zhang, H. **The full-spectrum correlated-k distribution and its relationship to the weighted-sum-of-gray-gases method**. In *Proceedings of 2000 IMECE*, 2000.

Modest, M. F. and Zhang, H. The Full-Spectrum Correlated-k Distribution for Thermal Radiation From Molecular Gas-Particulate Mixtures, **Transactions of the ASME**, vol. 124, p. 30–38, 2002.

Mossi, A., Galarça, M. M., Brittes, R., Vielmo, H. H., and França, F. H. R. Comparison of Spectral Models in the Computation of Radiative Heat Transfer in Participating Media Composed of Gases and Soot, **Journal of the Brazilian Society of Mechanical Sciences and Engineering**, vol. 34, p. 112–119, 2012.

Narayanan, P. and Trouvé, A. Radiation-driven flame weakening effects in sooting turbulent diffusion flames, **Proceedings of the Combustion Institute**, vol. 32, p. 1481–1489, 2009.

Pal, G. and Modest, M. F. A Narrow Band-Based Multiscale Multigroup Full-Spectrum k-Distribution Method for Radiative Transfer in Nonhomogeneous Gas-Soot Mixtures, **Transactions of the ASME**, vol. 132, p. 023307:1–9, 2010.

Pal, G., Modest, M. F., and Wang, L. Hybrid Full-Spectrum Correlated k-Distribution Method for Radiative Transfer in Nonhomogeneous Gas Mixtures, **Journal of Heat Transfer**, vol. 130, p. 082701:1–9, 2008.

Pearson, J. T. **The Development of Updated and Improved SLW Model Parameters and Its Application to Comprehensive Combustion Predictions**. PhD thesis, Brigham Young University, 2013.

Pearson, J. T., W., B. W., Solovjov, V. P., and Ma, J. Effect of total pressure on the absorption line blackbody distribution function and radiative transfer in H2O, CO2, and CO, **Journal of Quantitative Spectroscopy & Radiative Transfer**, vol. 143, p. 100–110, 2014a.

Pearson, J. T., W., B. W., Solovjov, V. P., and Ma, J. Efficient representation of the absorption line blackbody distribution function for H2O, CO2, and CO at variable temperature , mole fraction, and total pressure, **Journal of Quantitative Spectroscopy & Radiative Transfer**, vol. 138, p. 82–96, 2014b.

Pierrot, L., Rivière, P., Soufiani, A., and Taine, J. A fictitious-gas-based absorption distribution function global model for radiative transfer in hot gases, **Journal of Quantitative Spectroscopy & Radiative Transfer**, vol. 62, p. 609–624, 1999a.

Pierrot, L., Soufiani, A., and Taine, J. Accuracy of narrow-band and global models for radiative transfer in H2O, CO2, and H2O/CO2 mixtures at high temperature, **Journal of Quantitative Spectroscopy & Radiative Transfer**, vol. 62, p. 523–548, 1999b.

Rajhi, M., Ben-Mansour, R., Habib, M., Nemitallah, M., and Andersson, K. Evaluation of gas radiation models in CFD modeling of oxy-combustion, **Energy Conversion and Management**, vol. 81, p. 83–97, 2014.

Rivière, P., Soufiani, A., Perrin, M. Y., Riad, H., and Gleizes, A. Air mixture radiative property modeling in the temperature range 10,000-40,000 K, **Journal of Quantitative Spectroscopy & Radiative Transfer**, vol. 56, p. 29–45, 1996.

Rothman, L. S., Gamache, R. R., Goldamn, A., Brown, L. R., Toth, R. A., Pickett, H. M., Poynter, R. L., Flaud, J.-M., Camy-Peyret, C., Barbe, A., Husson, N., Rinsland, C. P., and Smith, M. A. H. The HITRAN database: 1986 edition, **Journal of Applied Optics**, vol. 26, p. 4058–4097, 1987.

Rothman, L. S., Gordon, I. E., Babikov, Y., Barde, A., Chris Benner, D., Bernath, P. F., Birk, M., Bizzocchi, L., Boudon, V., Brown, L. R., Campargue, A., Chance, K., Cohen, E. A., Coudert, L. H., Devi, V. M., Drouin, B. J., Fayt, A., Flaud, J. M., Gamache, R. R., Harrison, J. J., Hartmann, J. M., Hill, C., Hodges, J. T., Jacquemart, D., Jolly, A., Lamouroux, J., Le Roy, R. J., Li, G., Long, D. A., Lyulin, O. M., Mackie, C. J., Massie, S. T., Mikhailenko, S., Müller, H. S. P., Naumenko, O. V., Nikitin, A. V., Orphal, J., Perevalov, V., Perrin, A., Polovtseva, E. R., Richard, C., Smith, M. A. H., Starikova, E., Sung, K., Tashkun, S., Tennyson, J., Toon, G. C., Tyuterev, V. G., and Wagner, G. The HITRAN2012 molecular spectroscopic database, **Journal of Quantitative Spectroscopy & Radiative Transfer**, vol. 130, p. 4–50, 2013.

Rothman, L. S., Gordon, I. E., Barber, R. J., Dothe, H., Gamache, R. R., Goldman, A., Perevalov, V. I., Tashkun, S. A., and Tennyson, J. HITEMP, the high-temperature molecular spectroscopic database, **Journal of Quantitative Spectroscopy & Radiative Transfer**, vol. 111, p. 2139–2150, 2010.

Rothman, L. S., Rinsland, C. P., Goldman, A., Massie, S. T., Edwards, D. P., Flaud, J. M., Perrin, A., Camy-Peyret, C., Dana, V., Mandin, J. Y., Schroeder, J., Mccann, A., Gamache, R. R., Wattson, R. B., Yoshino, K., Chance, K. V., Jucks, K. W., Brown, L. R., Nemtchinov, V., and Varanasi, P. The HITRAN molecular spectroscopic database and Hawks (HITRAN Atmospheric Workstation): 1996 edition, **Journal of Quantitative Spectroscopy & Radiative Transfer**, vol. 60, p. 665–710, 1998.

Rothman, L. S., Wattson, R. B., Gamache, R. R., Schroeder, J., and McCann, A. **HITRAN WAWKS and HITEMP: High-temperature molecular database**. In *Proceedings of SPIE*, 1995.

Salinas, C. T. Fast approximate technique for the cumulative wavenumber model to modeling radiative transfer in a mixture of real gas media, **Journal of Quantitative Spectroscopy & Radiative Transfer**, vol. 109, p. 2078–2093, 2008.

Shiehnejadhesar, A., Mehrabian, R., Scharler, R., Goldin, G. M., and Obernberger, I. Development of a gas phase combustion model suitable for low and high turbulence conditions, **Fuel**, vol. 126, p. 177–187, 2014.

Siegel, R. and Howell, J. R. **Thermal Radiation heat transfer**. Hemisphere Publishing Corporation, *3th* edition, 1993.

Silva, C. V., França, F. H. R., and Vielmo, H. H. Analysis of turbulent, non-premixed combustion of natural gas in cylindrical chamber with and without radiation, **Combustion Science and Technology**, vol. 179, p. 1605–1630, 2007.

Smith, T. F., Al-Turki, A. M., Byun, K.-H., and Kim, T. K. Radiative and Conductive Transfer for a Gas/Soot Mixture Between Diffuse Parallel Plates, **Journal of Thermophysics**, vol. 1, p. 50–55, 1987.

Smith, T. F., Shen, Z. F., and Friedman, J. N. Evaluation of coefficients for the weighted sum of gray gases model, **Journal of Heat Transfer**, vol. 104, p. 602–608, 1982.

Solovjov, V. P., Andre, F., Lemonnier, D., and Webb, B. W. The Generalized SLW Model, **Journal of Physics: Conference Series**, vol. 676(012022), p. 1–36, 2016.

Solovjov, V. P., Andre, F., Lemonnier, D., and Webb, B. W. The rank correlated SLW model of gas radiation in non-uniform media, **Journal of Quantitative Spectroscopy & Radiative Transfer**, vol. 197, p. 26–44, 2017.

Solovjov, V. P., Andre, F., Lemonnier, D., and Webb, B. W. The Scaled SLW model of gas radiation in non-uniform media based on Planck-weighted moments of gas absorption cross-section, **Journal of Quantitative Spectroscopy & Radiative Transfer**, vol. 206, p. 198–212, 2018.

Solovjov, V. P., Lemonnier, D., and Webb, B. The SLW-1 model for efficient prediction of radiative transfer in high temperature gases, **Journal of Quantitative Spectroscopy & Radiative Transfer**, vol. 112, p. 1205–1212, 2011a.

Solovjov, V. P., Lemonnier, D., and Webb, B. The SLW-1 modeling of radiative heat transfer in nonisothermal nonhomogeneous gas mixture with soot, **Journal of heat Transfer**, vol. 133, p. 1–9, 2011b.

Solovjov, V. P., Lemonnier, D., and Webb, B. W. Efficient cumulative wavenumber model of radiative transfer in gaseous media bounded by non-gray walls, **Journal of Quantitative Spectroscopy & Radiative Transfer**, vol. 128, p. 2–9, 2013.

Solovjov, V. P., Lemonnier, D., and Webb, B. W. Extension of the exact SLW model to non-isothermal gaseous media, **Journal of Quantitative Spectroscopy & Radiative Transfer**, vol. 143, p. 83–91, 2014.

Solovjov, V. P. and Webb, B. W. **Radiative transfer model parameters for carbon monoxide at high temperature**. In *Proceedings of 11th IHTC*, 1998.

Solovjov, V. P. and Webb, B. W. SLW modeling of radiative transfer in multicomponent gas mixtures, **Journal of Quantitative Spectroscopy & Radiative Transfer**, vol. 65, p. 665–672, 2000.

Solovjov, V. P. and Webb, B. W. An efficient method for modeling radiative transfer in multicomponent gas mixtures with soot, **Journal of Heat Transfer**, vol. 123(3), p. 450–457, 2001.

Solovjov, V. P. and Webb, B. W. A local-spectrum correlated model for radiative transfer in non-uniform gas media, **Journal of Quantitative Spectroscopy & Radiative Transfer**, vol. 73, p. 361–373, 2002.

Solovjov, V. P. and Webb, B. W. The cumulative wavenumber method for modeling radiative transfer in gas mixtures with soot, **Journal of Quantitative Spectroscopy & Radiative Transfer**, vol. 93, p. 273–287, 2005.

Solovjov, V. P. and Webb, B. W. Multilayer modeling of radiative transfer by SLW and CW methods in non-isothermal gaseous medium, **Journal of Quantitative Spectroscopy & Radiative Transfer**, vol. 109, p. 245–257, 2008.

Solovjov, V. P. and Webb, B. W. **The SLW model: exact limit and relationship to other global methos**. In *Proceedings of the ASME 2009 Heat Transfer Summer Conference*, 2009.

Solovjov, V. P. and Webb, B. W. Application of CW local correction approach to SLW modeling of radiative transfer in non-isothermal gaseous media, **Journal of Quantitative Spectroscopy & Radiative Transfer**, vol. 111, p. 318–324, 2010.

Trivic, D. N. 3-D radiation modeling of nongray gases–particles mixture by two different numerical methods, **International Journal of Heat and Mass Transfer**, vol. 70, p. 298–312, 2014.

Wang, A. and Modest, M. F. Importance of Combined Lorentz- Doppler Broadening in High- Temperature Radiative Heat Transfer Applications, **Transactions of the ASME**, vol. 126, p. 858–861, 2004.

Wang, L. and Modest, M. F. Narrow-Band Based Multiscale Full-Spectrum k-Distribution Method for Radiative Transfer in Inhomogeneous Gas Mixtures, **Transactions of the ASME**, vol. 127, p. 740–748, 2005.

Webb, B. W., Solovjov, V. P., and Andre, F. An exploration of the influence of spectral model parameters on the accuracy of the rank correlated SLW model, **Journal of Quantitative Spectroscopy & Radiative Transfer**, vol. 218, p. 161–170, 2018.

Xue, H., Ho, J. C., and Cheng, Y. M. Comparison of different combustion models in enclosure fire simulation, **Fire Safety Journal**, vol. 36, p. 37–54, 2001.

Zhang, H. and Modest, M. F. Multi-scale full-spectrum correlated-k distribution for radiative heat transfer in inhomogeneous gas mixtures, **Journal of Quantitative Spectroscopy & Radiative Transfer**, vol. 73, p. 349–360, 2002.

Zhang, H. and Modest, M. F. Multi-group full-spectrum k-distribution database for water vapor mixtures in radiative transfer calculations, **International Journal of Heat and Mass Transfer**, vol. 46, p. 3593–3603, 2003.

Zhang, J., Ito, T., Ito, S., Riechelmann, D., and Fujimori, T. Numerical investigation of oxy-coal combustion in a large-scale furnace: Non-gray effect of gas and role of particle radiation, **Fuel**, vol. 139, p. 87–93, 2015.

Ziemniczak, A., Brittes, R., Centeno, F. R., and França, F. H. R. **Generation of new correlations for the weighted-sum-of-gray-gases model for carbon monoxide**. In *23rd ABCM International Congress of Mechanical Engineering*, 2015.

APPENDIX A – Homogeneous media - Radiative Heat Flux and Heat Source for Cases 2 and 3

Figures A.1, A.2, and A.3 presents the radiative heat flux and the heat source for a layer of CO_2, H_2O and H_2O/CO_2 mixture, respectively, for Case 2 discussed in section 6.1.1. For this case, the temperature profile presents a double symmetric, with two points of maximum: $x^* = 0.25$ and $x^* = 0.75$. The maximum temperature for this case is 1800 K, while the minimum is 400 K and occur in the walls and in the mid distance of the domain. Because of the symmetry of the profiles, the radiative heat flux is null in mid distance between the walls, reaching the highest absolute values at $x^* = 0.125$ and $x^* = 0.825$, where the temperature gradient is maximum. The maximum absolutes values of the radiative heat source occurs in the regions where the temperature profile has its peak; and the heat source is positive in the cold regions of the medium, indicating net gain of radiation from the hot regions. For both the individual and the mixture problems, the WSGG radiative heat flux presents higher deviations near to the walls, where there are low temperatures. Furthermore, in all the problems, the SLW model leads to the maximum deviation of the radiative heat source in the regions of maximum temperature. In the H_2O/CO_2 mixture problem the WSGG radiative heat flux deviations shows to be very close to those of the SLW model.

(a)   (b)

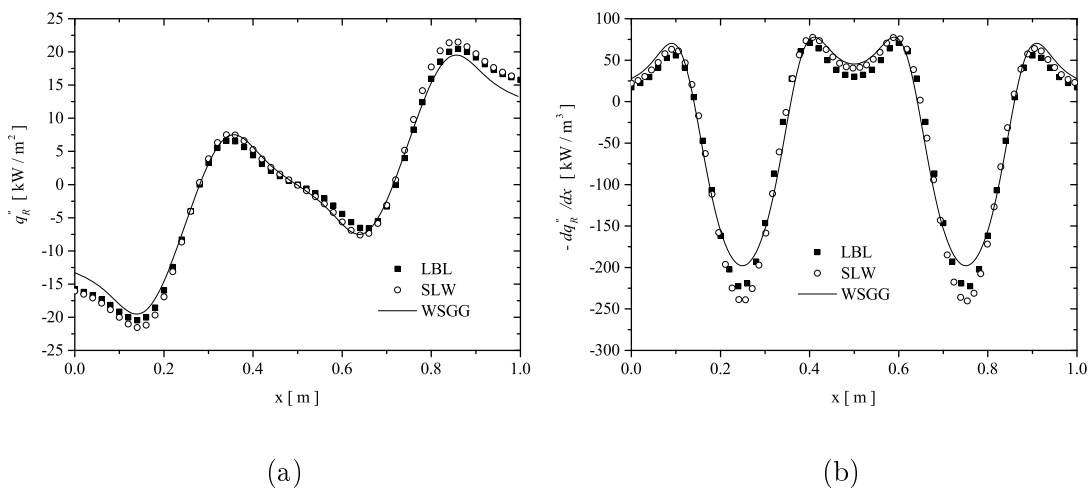Figure A.1 – Comparison of the solutions obtained by the LBL integration, SLW and WSGG models for a layer of CO_2 ($Y_{CO_2} = 0.1$), Case 2: (a) radiative heat flux, $q_R^"$, (b) radiative heat source, $-dq_R^"/dx$.

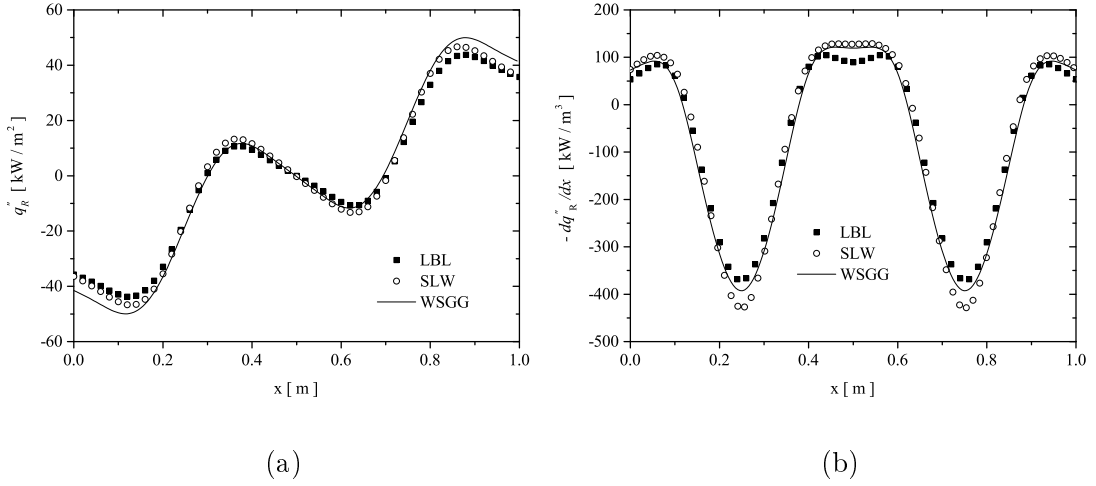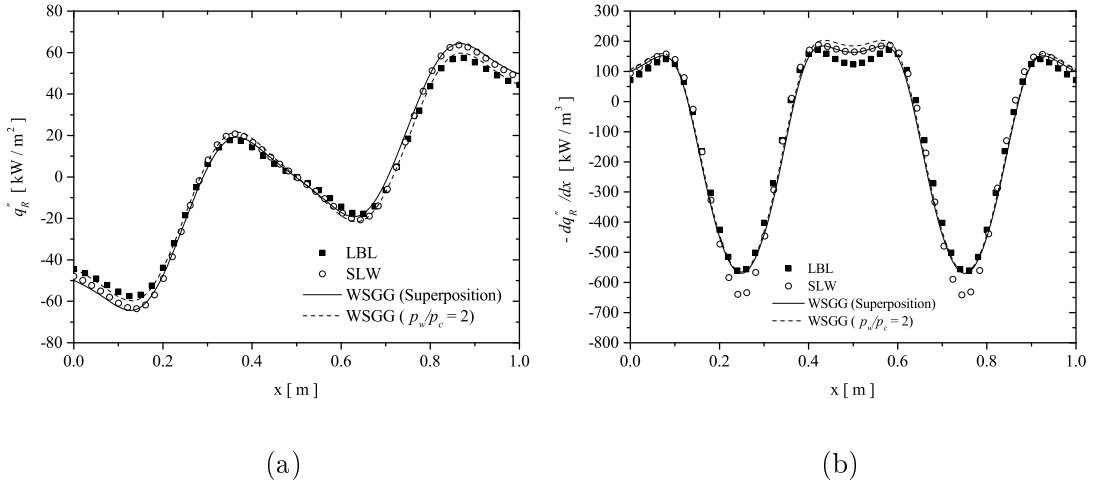(a)   (b)

Figure A.2 – Comparison of the solutions obtained by the LBL integration, SLW and WSGG models for a layer of H_2O ($Y_{H_2O} = 0.2,$), Case 2: (a) radiative heat flux, $q_R^{''}$, (b) radiative heat source, $-dq_R^{''}/dx$.

(a)   (b)

Figure A.3 – Comparison of the solutions obtained by the LBL integration, SLW and WSGG models for a layer of H_2O/CO_2 mixture ($Y_{H_2O} = 0.2, Y_{CO_2} = 0.1$), Case 2: (a) radiative heat flux, $q_R^{''}$, (b) radiative heat source, $-dq_R^{''}/dx$.

In Figures A.4, A.5, and A.6 are showed the radiative heat flux and the heat source for a layer of CO_2, H_2O and H_2O/CO_2 mixture, respectively, for Case 3 discussed in section 6.1.1. Contrarily to cases 1 and 2, the temperature profile is not symmetric, reaching its peak at $x^* = 0.25$. The maximum temperature is still 1800 K as with the other cases, but the walls temperatures are no longer the same value: at $x^* = 0$, $T = 880$

K, and $x^* = 1$, $T = 400$ K. As can be seen, for all problems, since the temperature profile is no longer symmetric, the point in which the heat flux is null was no longer in the mid distance between the walls. Moreover, for the radiative heat source, the maximum for all problems took place in $x^* = 0.25$, which is where the temperature of the participating species is at its peaks. For x^* larger than about 0.6, where there is the lower temperature of the domain, the radiative heat source does not have steep variations. Analyzing the deviations, except for H_2O/CO_2 ($p_w/p_c = 2$) mixture, the problems solved with the WSGG model provided the worts results than the SLW model if compared to the LBL benchmark computation. When the results for radiative heat source is verified, it is seen that such behavior change in some cases: for H_2O, the WSGG maximum deviation is 11.12 %, while for SLW achieve 13.95 %; for H_2O/CO_2 mixture, using the superposition approach, the WSGG maximum deviation is 11.84 %, and for the SLW is 14.46 %. This interesting fact shows that the WSGG model can compete in a satisfactory way with the more sophisticated SLW model.
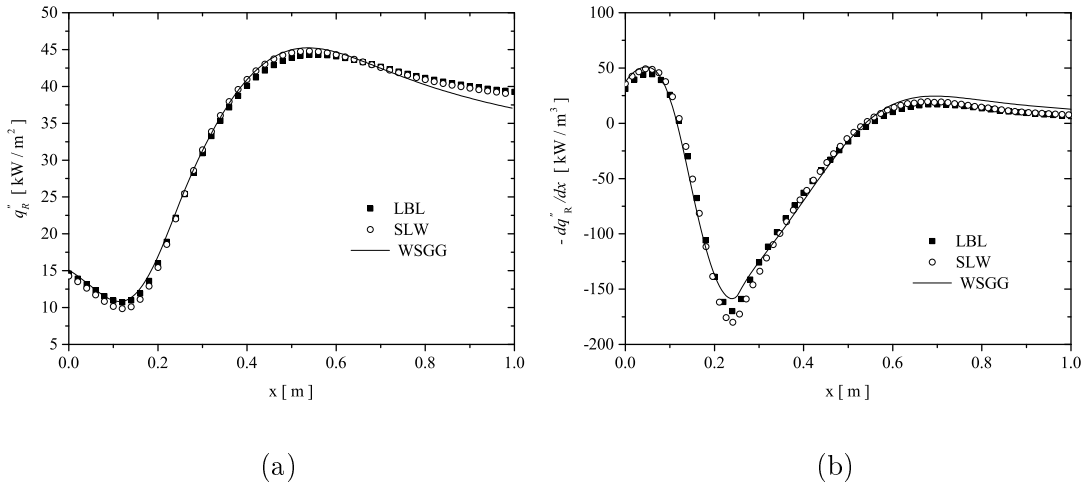

(a)   (b)

Figure A.4 – Comparison of the solutions obtained by the LBL integration, SLW and WSGG models for a layer of CO_2 ($Y_{CO_2} = 0.1$), Case 3: (a) radiative heat flux, $q_R^{''}$, (b) radiative heat source, $-dq_R^{''}/dx$.
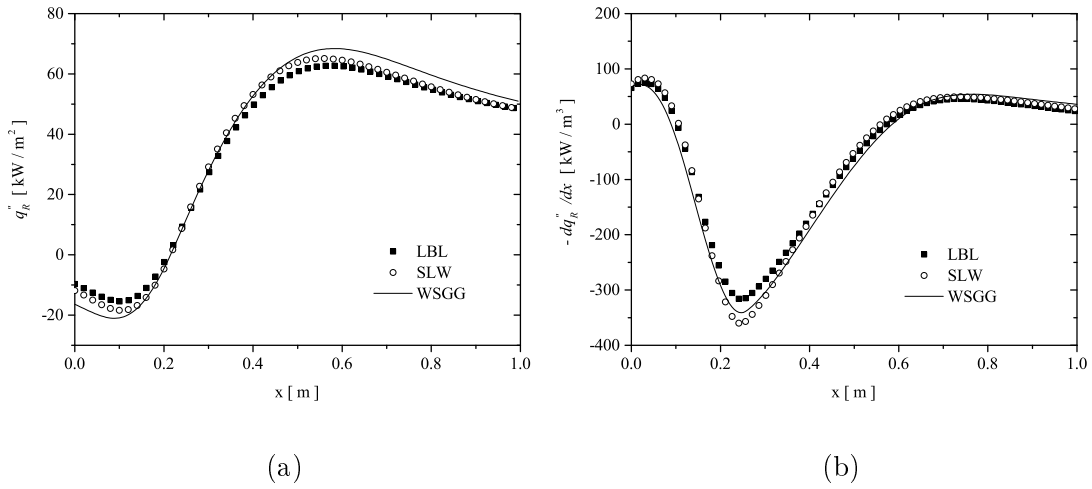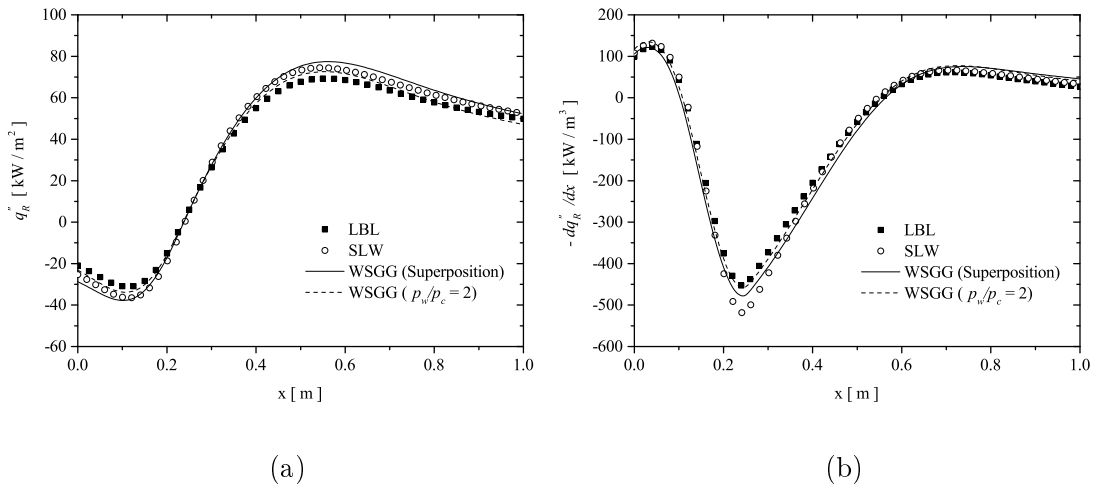
(a)   (b)

Figure A.5 – Comparison of the solutions obtained by the LBL integration, SLW and WSGG models for a layer of H_2O ($Y_{H_2O} = 0.2$,), Case 3: (a) radiative heat flux, $q_R^{"}$, (b) radiative heat source, $-dq_R^{"}/dx$.

(a)   (b)

Figure A.6 – Comparison of the solutions obtained by the LBL integration, SLW and WSGG models for a layer of H_2O/CO_2 mixture ($Y_{H_2O} = 0.2, Y_{CO_2} = 0.1$), Case 3: (a) radiative heat flux, $q_R^{"}$, (b) radiative heat source, $-dq_R^{"}/dx$.

APPENDIX B – Non-homogeneous media - Radiative Heat Flux and Heat Source for Case 2

Figures B.1, B.2, and B.3 present the radiative heat flux and the heat source for a layer of CO_2, H_2O and H_2O/CO_2 mixture, respectively, in non-homogeneous media, for Case 2 discussed in section 6.1.2. The results of the radiative heat flux for the WSGG model are very close to those of the SLW model for all the problems, and it is null in the half distance between the walls where the temperature and concentration profiles have their peak. The maximum deviations found for the radiative heat flux are also at $x^* = 0.5$ for both the individual and the mixture problems.
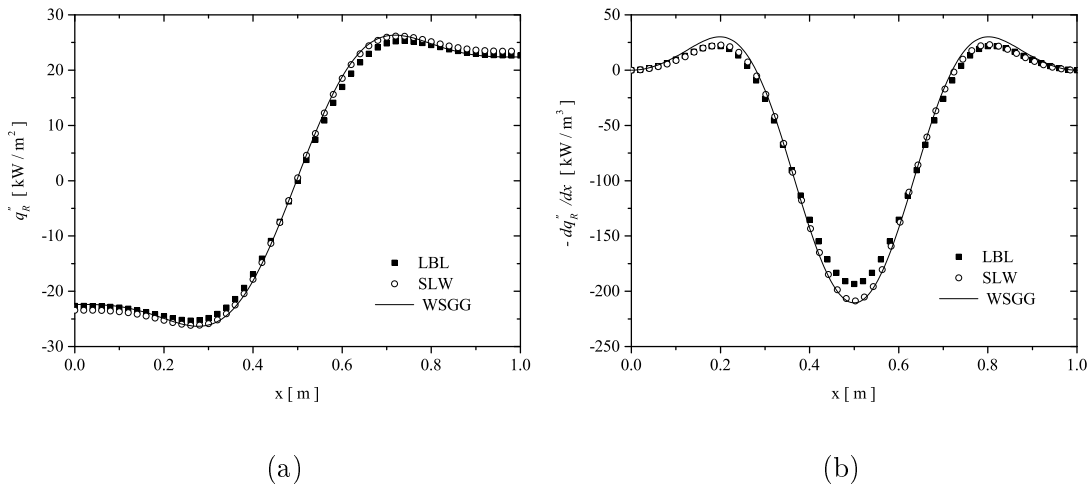

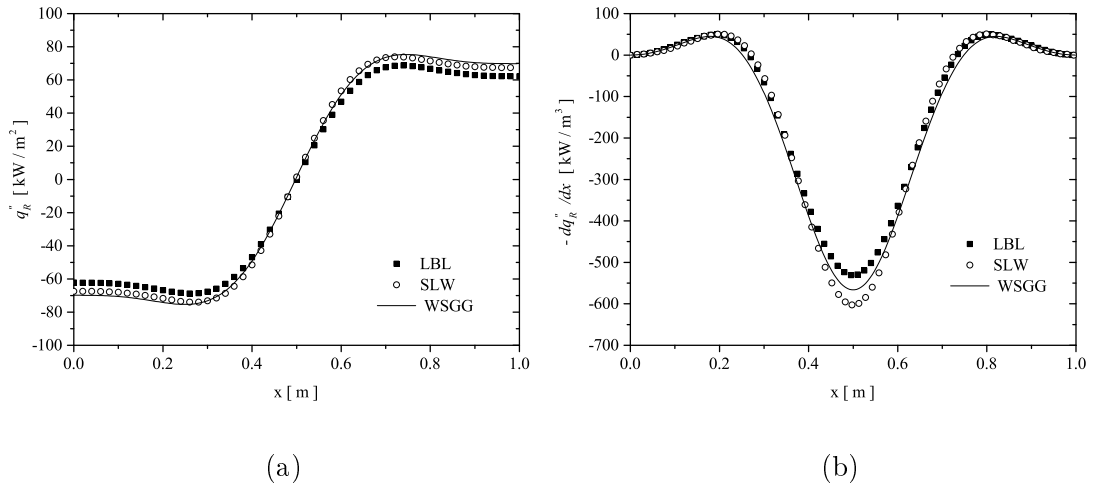(a)   (b)

Figure B.1 – Comparison of the solutions obtained by the LBL integration, SLW and WSGG models for a layer of CO_2, Case 2: (a) radiative heat flux, $q_R^{"}$, (b) radiative heat source, $-dq_R^{"}/dx$.

(a)   (b)

Figure B.2 – Comparison of the solutions obtained by the LBL integration, SLW and WSGG models for a layer of H_2O, Case 2: (a) radiative heat flux, $q_R^{"}$, (b) radiative heat source, $-dq_R^{"}/dx$.
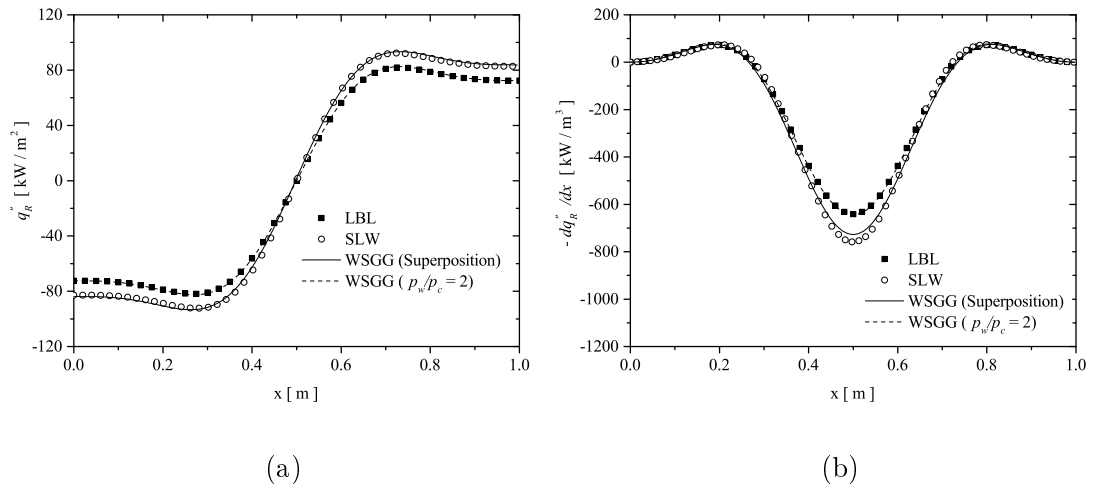

(a)   (b)

Figure B.3 – Comparison of the solutions obtained by the LBL integration, SLW and WSGG models for a layer of H_2O/CO_2 mixture ($Y_{H_2O}/Y_{CO_2} = 0.2$), Case 2: (a) radiative heat flux, $q_R^{"}$, (b) radiative heat source, $-dq_R^{"}/dx$.